

**Methodical developments for
hydrodynamic
scanning electrochemical microscopy**



Dissertation

zur Erlangung des Doktorgrades der Naturwissenschaften (Dr. rer. nat.)

der Fakultät für Chemie und Pharmazie

der Universität Regensburg

vorgelegt von

Timo Raith

aus Untertraubenbach

im Jahr 2020

Die vorgelegte Dissertation entstand in der Zeit von Januar 2017 bis Dezember 2019 am Institut für Analytische Chemie, Chemo- und Biosensorik der naturwissenschaftlichen Fakultät IV - Chemie und Pharmazie - der Universität Regensburg.

Die Arbeit wurde angeleitet von Prof. Dr. Frank-Michael Matysik.

Promotionsgesuch eingereicht am: 16.01.2020

Tag der mündlichen Prüfung: 26.06.2020

Prüfungsausschuss:

Vorsitzender: Prof. Dr. Rainer Müller

Erstgutachter: Prof. Dr. Frank-Michael Matysik

Zweitgutachter: Prof. Dr. Gerd-Uwe Flechsig

Drittprüfer: PD Dr. Hans-Heiner Gorris

Danksagung

An dieser Stelle möchte ich mich bei allen Personen bedanken, die mich auf dem Weg zur Promotion begleitet und unterstützt haben.

Mein Dank gilt hierbei in gleichem Maße:

Herrn Prof. Dr. Frank-Michael Matysik für die Anleitung der Arbeit, sowie die stetige Unterstützung und wertvolle Diskussionen.

Herrn Prof. Dr. Gerd-Uwe Flechsig für die Tätigkeit als Zweitgutachter.

Herrn PD Dr. Hans-Heiner Gorris für die Tätigkeit als Drittprüfer.

Herrn Prof. Dr. Rainer Müller für den Vorsitz des Prüfungsausschusses.

Der Studienstiftung des Deutschen Volkes für die finanzielle Unterstützung.

Meinen Arbeitskollegen für sämtliche Diskussionen und die einzigartige Arbeitsatmosphäre.

Insbesondere Dr. Christian Iffelsberger, Dr. Patrick Hanekamp und Stefan Wert – unser Team SECM.

Insbesondere Thomas Herl, der mich seit meiner Masterarbeit begleitet und durch wertvolle Diskussionen sowie graphische Zuarbeit unterstützt hat.

Meinen Freunden, insbesondere Markus Tautz, für die Unterstützung und den stetigen Ansporn.

Meiner Familie Gabriele Raith, Werner Raith, Fabian Raith, Florian Raith und Nina Feirer für den stetigen Rückhalt.

Table of contents

Table of contents	I
List of publications	III
Conference contributions	IX
Supervised students	XI
Supervised lab courses.....	XII
Awards & honors.....	XIII
Declaration of collaboration	XIV
List of abbreviations	XV
1. Introduction	1
2. Theoretical background	8
2.1 Voltammetry	8
2.1.1 Introduction to voltammetry	8
2.1.2 Voltammetric behavior of macroelectrodes and ultramicroelectrodes	9
2.1.3 Cyclic voltammetry and amperometry	13
2.1.4 Mass transfer and hydrodynamic effects	15
2.2 Scanning electrochemical microscopy	18
2.2.1 Setup of the scanning electrochemical microscope	18
2.2.2 Probes for scanning electrochemical microscopy.....	19
2.2.3 Operational modes of scanning electrochemical microscopy.....	20
2.2.4 Forced convection in scanning electrochemical microscopy	25
3. Experimental	32
3.1 Software, instrumentation, materials, chemicals	32
3.2 Electrochemical mediators	34
3.3 Fabrication of ultramicroelectrodes	35
3.4 Scanning electrochemical microscopy setup	36
3.5 Electrochemical flow cells	37

4. Results and discussion	41
4.1 Development and characterization of electrochemical flow cells for hydrodynamic scanning electrochemical microscopy.....	41
4.1.1 Introduction.....	42
4.1.2 Results and discussion.....	43
4.1.3 Conclusion.....	49
4.1.4 Experimental.....	49
4.2 Impacts of forced convection generated via high precision stirring on scanning electrochemical microscopy experiments in feedback mode	56
4.2.1 Introduction.....	57
4.2.2 Experimental.....	59
4.2.3 Results and discussion.....	62
4.2.4 Conclusion.....	69
4.2.5 Supporting information.....	71
4.3 Enhanced resolution of generator-collector studies of enzymatic structures by means of hydrodynamic scanning electrochemical microscopy	76
4.3.1 Introduction.....	77
4.3.2 Experimental.....	78
4.3.3 Results and discussion.....	82
4.3.4 Conclusion.....	87
5. Summary.....	93
6. Zusammenfassung in deutscher Sprache	95

List of publications

Peer-reviewed articles

2018 **Development and characterization of electrochemical flow cells for hydrodynamic scanning electrochemical microscopy**

Timo Raith, Stefan Wert, Christian Iffelsberger, Frank-Michael Matysik

Monatshefte für Chemie - Chemical Monthly 149 (2018) 1671–1677

Abstract

In the frame of this contribution, two electrochemical flow cells developed for scanning electrochemical microscopy (SECM) are presented. Forced convection was generated by a flow of the mediator solution through the flow cells. A description of the mandatory design aspects of the experimental flow cell setups is included. Using a macroscopic working electrode as a substrate electrode, forced convection leads to the formation of a stable diffusion layer during amperometric experiments in contrast to a growing diffusion layer in quiescent solution. To characterize the effects of forced convection, the diffusion layer around a platinum substrate electrode integrated into the cells was investigated utilizing chronoamperometric measurements and hydrodynamic SECM imaging in amperometric substrate generation-tip collection (SG/TC) mode. Both methods proved the stability and the time-independency of the diffusion layer. Mathematical simulations using COMSOL Multiphysics were computed to investigate the flow profile generated by the flowing mediator solution in the relevant region close to the substrate electrode. In summary, two different electrochemical flow cells for SECM were developed and characterized. Both cell designs enabled steady-state diffusion layer characteristics at a macroscopic substrate electrode offering interesting possibilities such as time-independent measurements in the context of the SG/TC mode.

2018 **Detection and imaging of reactive oxygen species associated with the electrochemical oxygen evolution by hydrodynamic scanning electrochemical microscopy**

Christian Iffelsberger, Timo Raith, Preety Vatsyayan, Vlastimil Vyskočil, Frank-Michael Matysik

Electrochimica Acta 281 (2018) 494-501

Abstract

Hydrodynamic scanning electrochemical microscopy (SECM) was applied for the characterization of Pt and boron-doped diamond (BDD) macroelectrodes operated in a potential region producing reactive oxygen species (ROS) during oxygen evolution reaction (OER). Forced convection introduced by highprecision stirring enabled the formation of a stable diffusion layer of electrochemically produced species and tip-substrate voltammetry was used for the detection of different ROS species produced during OER at BDD. Hydrodynamic SECM imaging in substrate generation/tip collection mode revealed local differences in the production of the ROS species across the BDD electrode surface.

2018 **New Electrochemical Flow-Cell Configuration Integrated into a Three-Dimensional Microfluidic Platform: Improving Analytical Application in the Presence of Air Bubbles**

Magno Aparecido Gonçalves Trindade, Cauê Alves Martins, Lucio Angnes, Thomas Herl, Timo Raith, Frank-Michael Matysik

Analytical Chemistry 90 (2018) 10917-10926

Abstract

A newly configured electrochemical flow cell to be used for (end-channel) amperometric detection in a microfluidic device is presented. The design was assembled to place the reference electrode in a separated compartment, isolated from the flow in the microchannel, while the working and counter electrodes remain in direct contact with both compartments. Moreover, a three-dimensional coil-shaped microfluidic device was fabricated using a nonconventional protocol. Both devices working in association enabled us to solve the drawback caused by the discrete injection when the automatic micropipette was used. The high performance of the proposed electrochemical flow cell was demonstrated after in situ modifying the surface of the platinum working electrode with surfactant (e.g., using Tween 20 at 0.10%). As the reference electrode remained out of contact with the flowing solution, there was no trouble by air bubble formation (generated by accidental insertion or by presence of surfactants) throughout the measurements. This device was characterized regarding its analytical performance by evaluating the amperometric detection of acetaminophen, enabling determination from 6.60 to 66.0 $\mu\text{mol L}^{-1}$. This issue is important since at high concentration (e.g., as assessed in clinical analysis) the acetaminophen is known to passivate the working electrode surfaces by electrogenerated products, impairing the accuracy of the electrochemical measurements.

2019 **Impacts of Forced Convection Generated via High Precision Stirring on Scanning Electrochemical Microscopy Experiments in Feedback Mode**

Timo Raith, Christian Iffelsberger, Preeti Vatsyayan, Frank-Michael Matysik

Electroanalysis 31 (2019) 273-281

Abstract

In this study, the effects of forced convection on scanning electrochemical microscopy (SECM) experiments in feedback mode using ferrocenemethanol as redox mediator are presented. Forced convection, which enhances the mass transfer inside the system, was generated via an electrical high precision stirrer integrated into the SECM setup. A thin-film interdigitated array electrode serving as model substrate was investigated with probe scan curves in z-direction and SECM imaging in constant-height mode utilizing ultramicroelectrodes (UME) with diameters (d_{probe}) of 25 μm and 12.5 μm . It was found that forced convection increased the overall current during SECM imaging without distorting distinctive features of the imaged structure when working with a 25 μm UME at substrate-to-tip distances of 14 μm and 11 μm . Furthermore, the electrochemical contrast was improved under hydrodynamic conditions for a substrate-to-tip distance of 11 μm and scan rates of 5 $\mu\text{m s}^{-1}$, 10 $\mu\text{m s}^{-1}$, 20 $\mu\text{m s}^{-1}$ and 40 $\mu\text{m s}^{-1}$. When further decreasing the gap between the UME and the substrate to 9 μm , almost no effects of the forced convection were observed. Consequently, for a 25 μm UME, forced convection led to higher currents and improved performance during SECM experiments in feedback mode at substrate-to-tip distances of 14 μm and 11 μm , whereas no effects were observed for a 12.5 μm UME at a distance of 8 μm .

2019 **Material contrast studies of conductive thin films on semiconductor substrates using scanning electrochemical microscopy**

Patrick Hanekamp, Timo Raith, Christian Iffelsberger, Tobias Zankl, Werner Robl, Frank-Michael Matysik

Journal of Applied Electrochemistry 49 (2019) 455-463

Abstract

In this paper, a mediator-free scanning electrochemical microscopy (SECM) imaging concept is presented, which is capable of generating high electrochemical contrast and high spatial resolution between two conductive materials. The methodical approach is based on the hydrogen evolution reaction which shows potential dependent material selectivity. Various conductive thin films deposited on silicon substrates were studied. The investigated materials included copper, ruthenium, platinum, tantalum nitride, and titanium nitride. The hydrogen evolution was studied with chronoamperometry ($E_{\text{substrate}} = 1 \text{ V vs. Ag/AgCl/3 M KCl}$) to characterize the material selectivity of this reaction for the above-listed thin films. SECM imaging in the substrate generation-tip collection (SG/TC) mode was carried out and applied to study the boundary regions of thin copper films in combination with the aforementioned thin film materials. In addition, the spatial resolution of hydrogen based SG/TC SECM imaging was characterized using lithographically fabricated platinum/copper structures as test substrates. For comparison, the common feedback mode was also applied for SECM imaging of the conducting thin film combinations. It was found that only the hydrogen based SG/TC mode enabled SECM imaging with clear material contrast between different conductive materials which was not possible in the feedback mode.

2020 **Enhanced resolution of generator-collector studies of enzymatic structures by means of hydrodynamic scanning electrochemical microscopy**

Timo Raith, Anna Kröninger, Matthias J. Mickert, Hans H. Gorris and Frank-Michael Matysik

Talanta DOI: 10.1016/j.talanta.2020.120844

Abstract

In this report, the effects of forced convection on scanning electrochemical microscopy (SECM) studies of enzymes in the context of the generator-collector mode (G/C mode) were investigated. Forced convection was generated via an electrical high precision stirrer integrated into the electrochemical cell. Circular spots of glucose oxidase were immobilized on a gold support serving as model substrate. The diffusion layer of enzymatically generated H₂O₂ was characterized recording probe scan curves (PSCs) in z-direction. Furthermore, the enzyme-modified surfaces were investigated via constant-height SECM imaging in feedback mode and in G/C mode. For methodical comparison all sets of experiments were performed in quiescent solution (conventional approach) and with forced convection, respectively. In contrast to a growing diffusion layer without forced convection by applying forced convection, a constant diffusion layer of produced H₂O₂ was observed. Hence, via hydrodynamic SECM time-independent SECM images within a reasonable time scale of SECM measurements in G/C mode were enabled and their resolution was enhanced.

Non-peer-reviewed articles

2017 **Trends in der elektrochemischen Rastermikroskopie**

Christian Iffelsberger, Timo J. Raith, Patrick J. Hanekamp, Preety Vatsayayan und Frank- Michael Matysik

chrom+food FORUM 4 (2017) 20-22

Conference contributions

Oral Presentations

2017 **11. Interdisziplinäres Doktorandenseminar**, 12.-14.03.2017, Berlin, Germany

Forced convection in scanning electrochemical microscopy

2017 **13th International Students Conference Modern Analytical Chemistry**, 21.22.-09.2017, Prague, Czech Republic

Forced convection in scanning electrochemical microscopy introduced by an electrochemical flow cell

2018 **1st Cross-Border Seminar on Electroanalytical Chemistry**, 04.-06.04.2018, Furth im Wald, Germany

Scanning electrochemical microscopy with forced convection

2018 **17th International Conference on Electroanalysis (ESEAC)**, 03.-07.06.2018, Rhodes Island, Greece

Forced convection in scanning electrochemical microscopy

2018 **Electrochemistry 2018**, 24.-26.09.2018, Ulm, Germany

Methodical developments of hydrodynamic scanning electrochemical microscopy

2019 **ANAKON 2019**, 25.-28.03.2019, Münster, Germany

Generation of forced convection in the context of scanning electrochemical microscopy

2019 **2nd Cross-Border Seminar on Electroanalytical Chemistry**, 10.-12.04.2019,
České Budějovice, Czech Republic

*Impacts of Forced Convection Generated via High Precision Stirring on
Scanning Electrochemical Microscopy Experiments in Feedback Mode*

2019 **7th Regional Symposium on Electrochemistry for South-East Europe**, 25.-
30.05.2019, Split, Croatia

Hydrodynamic scanning electrochemical microscopy

Poster Presentations

2017 **ANAKON 2017**, 03.-06.04.2017, Tübingen, Germany

*Forced convection in scanning electrochemical microscopy introduced by an
electrochemical flow cell*

2018 **International conference on ion analysis**, 09.-13.09.2018, Berlin, Germany

*Formation of a stable diffusion layer of an electrochemically generated ion via
forced convection in the context of scanning electrochemical microscopy*

2019 **ANAKON 2019**, 25.-28.03.2019, Münster, Germany

*Avoiding transient signals via forced convection in the generator/collector mode
of scanning electrochemical microscopy*

Supervised students

- 2017 **Untersuchung zur hydrodynamischen elektrochemischen Rastermikroskopie**
- Michael Biendl - bachelor thesis in cooperation with Ostbayerische Technische Hochschule Regensburg
- 2017-2018 **Development and optimization of an electrochemical flow cell configuration for hydrodynamic scanning electrochemical microscopy**
- Stefan Wert - master thesis
- 2018 **Charakterisierung verschiedener Messparameter in der elektrochemischen Rastermikroskopie**
- Jonas Fuchs - bachelor thesis
- 2019 **Scanning electrochemical microscopy studies of enzymes**
- Anna Kröninger – research internship

Supervised lab courses

- 2017 - 2019 „**Praktikum Chemie wässriger Lösungen Analytischer Teil**“ for chemistry students of the 2nd semester
- 2017 „**Praktikum Pharmazeutische Bioanalytik**“ for chemistry students of the 5th semester
- 2017 „**Praktikum Chemie in der Medizin**“ for medicine students of the 1st semester
- 2018 „**Chemiecamp**“ for pupils
- 2018/2019 „**Bioanalytical Lab**“ for chemistry, biochemistry and medical chemistry students of the 8th semester

Awards & honors

- 2017 – 2019 Funding of doctoral studies by **Studienstiftung des deutschen Volkes**
- 2017 Price for the second best presentation awarded by **Gesellschaft Deutscher Chemiker** in the frame of the *11. Interdisziplinären Doktorandenseminar* in Berlin, Germany
- 2018 Price for the second best presentation awarded by **Gesellschaft Deutscher Chemiker** in the frame of the *1st Cross-Border Seminar on Electroanalytical Chemistry* in Furth im Wald, Germany
- 2018 Funding of conference participation at *17th International Conference on Electroanalysis (ESEAC) on Rhodes Island, Greece* by **Internationales Promotionsprogramm der Universität Regensburg**
- 2019 Price for the third best presentation awarded by **Gesellschaft Deutscher Chemiker** in the frame of the *2nd Cross-Border Seminar on Electroanalytical Chemistry* in České Budějovice, Czech Republic
- 2019 **Opening keynote lecture** of the Electroanalytical Chemistry session in the frame of the *ANAKON 2019* in Münster, Germany

Declaration of collaboration

The research presented within this thesis was partly obtained in cooperation with other scientists. In accordance with § 8 Abs. 1 Satz 2 Punkt 7 of the *Ordnung zum Erwerb des akademischen Grades eines Doktors der Naturwissenschaften (Dr. rer. nat.) an der Universität Regensburg vom 18. Juni 2009*, these collaborations are described within this section.

4.1. Development and characterization of electrochemical flow cells for hydrodynamic scanning electrochemical microscopy

Conceptual design and writing was done by the author. The first generation cell prototype was developed by the author. Following the ideas of the author, the second generation cell prototype was developed during the master thesis of Stefan Wert, which was supervised by the author. Hence, all experiments concerning the first prototype were conducted by the author, whereas all experiments concerning the second prototype were conducted by Stefan Wert. The artwork was partly established in collaboration with Thomas Herl. Dr. Christian Iffelsberger was involved in discussions. The project was supervised by Prof. Dr. Frank-Michael Matysik.

4.2. Impacts of Forced Convection Generated via High Precision Stirring on Scanning Electrochemical Microscopy Experiments in Feedback Mode

Conceptual design and writing was done by the author. The experimental work was performed by the author. Dr. Christian Iffelsberger and Dr. Preeti Vatsyayan were involved in discussions. The artwork was partly established in collaboration with Thomas Herl. The project was supervised by Prof. Dr. Frank-Michael Matysik.

4.3. Enhanced resolution of generator-collector studies of enzymatic structures by means of hydrodynamic scanning electrochemical microscopy

Conceptual design and writing was done by the author. SECM measurements were performed by the author and Anna Kröninger during her research internship, which was supervised by the author. The immobilization of the enzymes was performed in collaboration with Matthias Mickert and PD Dr. Hans-Heiner Gorris. The artwork was partly established in collaboration with Thomas Herl. The project was supervised by Prof. Dr. Frank-Michael Matysik.

List of abbreviations

In the following, a general overview in alphabetical order on commonly used abbreviations is given. Any specialized expressions are described in the individual chapters within the results section.

Abbreviation	Full name	Unit
AFM	atomic force microscopy	
c	concentration	mol l ⁻¹
CE	counter electrode	
D	diffusion coefficient	cm ² s ⁻¹
d _{inner}	inner diameter	m
d _{outer}	outer diameter	m
E	potential	V
e ⁻	electron	
EDC	N-(3-dimethylaminopropyl)-N'-ethylcarbodiimide hydrochloride	
F	faraday constant	A s mol ⁻¹
FcMeOH	ferrocenemethanol	
f _{rot}	stirrer rotation frequency	s ⁻¹
HPLC	high performance liquid chromatography	
I or i	current	A
J	flux	mol cm ⁻² s ⁻¹
L	normalized distance	
NHS	N-hydroxysuccinimide	
PEEK	polyether ether ketone	
PAC	probe approach curve	

PSC	probe scan curve	
R	universal gas constant and resistance	$\text{J mol}^{-1} \text{K}^{-1}$ Ω
r	radius	m
RE	reference electrode	
RG	RG value	
SECM	scanning electrochemical microscopy or scanning electrochemical microscope	
SG/TC	substrate generation-tip collection	
SICM	scanning ion conductance microscopy	
SPM	scanning probe microscopy	
T	temperature	K
t	time	s
TG/SC	tip generation-substrate collection	
UME	ultramicroelectrode	
WE	working electrode	
δ	diffusion layer thickness	μm
Φ	electric field potential	V

1. Introduction

In the late 1980s, a new representative of the scanning probe techniques was introduced to the science community: scanning electrochemical microscopy (SECM) [1,2]. Numerous developments regarding different measuring modes [2–8], instrumental aspects [9–15] and target substrates [16–23] were established which led to the SECM evolving into a powerful and versatile technique with a vast field of applications ranging from corrosion science [24,25] to biological systems [26–30]. Around 15 years after its introduction, developments regarding the technique itself slowly started to remain static and a shift of research focus to coupling of the SECM with other methods such as scanning ion conductance microscopy (SICM) [31–33], atomic force microscopy (AFM) [34–36] or fluorescence microscopy [37,38] was observable. Nevertheless, refining and improving an original technique within fundamental research always remains equally important.

One new development concerning this topic, as introduced by the Matysik group, was the integration of an electrical high precision stirrer into the electrochemical SECM cell and thus the generation of forced convection within the SECM system. Generation of hydrodynamics via forced convection in form of flow systems, rotating electrodes or sonication is a well-established approach in electroanalytical chemistry to enhance the mass transfer inside the system and generally speaking the performance of the measurement technique. Nevertheless, in literature only a few publications can be found concerning the topic of forced convection in SECM [39–44]. What all of these publications have in common is that the convection was generated intrinsically via fast scan movement of the probe and usually it was suggested that this has to be avoided.

Until the beginning of 2017, no publication treating the external generation of forced convection within the SECM system could be found which seems surprising keeping in mind the fact that SECM belongs to electroanalytical chemistry and forced convection plays such a traditional and important role within this field. In 2017, a pioneering study published by the Matysik group [45] showed that forced convection can be generated within the SECM system in a controlled manner. Its effects were characterized and advantages of the newly established hydrodynamic SECM system concerning measurements in amperometric substrate generation-tip collection (SG/TC) mode were presented.

The objective of this thesis was to expand this new research field of forced convection in scanning electrochemical microscopy based on three categories:

- Methodical developments to diversify the possibilities of generating forced convection within the SECM system
- Fundamental research to characterize the effects of forced convection concerning different SECM operating modes
- Transfer of the hydrodynamic SECM system from fundamental research to the field of applications

References

- [1] A.J. Bard, F.R.F. Fan, J. Kwak, O. Lev, Scanning Electrochemical Microscopy. Introduction and Principles, *Anal. Chem.* 61 (1989) 132–138. doi:10.1021/ac00177a011.
- [2] R.C. Engstrom, C.M. Pharr, Scanning electrochemical microscopy, *Anal. Chem.* 61 (1989) 1099A-1104A. doi:10.1021/ac00194a002.
- [3] A.J. Bard, F.F. Fan, J. Kwak, O. Lev, Scanning Electrochemical Microscopy. Introduction and Principles, 138 (1989) 132–138.
- [4] F. Zhou, P.R. Unwin, A.J. Bard, Scanning electrochemical microscopy. 16. Study of second-order homogeneous chemical reactions via the feedback and generation/collection modes, *J. Phys. Chem.* 96 (1992) 4917–4924. doi:10.1021/j100191a036.
- [5] K. Eckhard, X. Chen, F. Turcu, W. Schuhmann, Redox competition mode of scanning electrochemical microscopy (RC-SECM) for visualisation of local catalytic activity, *Phys. Chem. Chem. Phys.* 8 (2006) 5359–5365. doi:10.1039/b609511a.
- [6] S. Meltzer, D. Mandler, Microwriting of Gold Patterns with the Scanning Electrochemical Microscope, *J. Electrochem. Soc.* 142 (1995) 82–85. doi:10.1149/1.2044252.
- [7] Y.M. Wu, F.R.F. Fan, A.J. Bard, High Resolution Deposition of Polyaniline on Pt with the Scanning Electrochemical Microscope, *J. Electrochem. Soc.* 136 (1989) 885–886. doi:10.1149/1.2096765.
- [8] E.E.D.M. El-Giar, D.O. Wipf, Microparticle-based iridium oxide ultramicroelectrodes for pH sensing and imaging, *J. Electroanal. Chem.* 609 (2007) 147–154. doi:10.1016/j.jelechem.2007.06.022.
- [9] C.G. Zoski, Ultramicroelectrodes: Design, fabrication, and characterization, *Electroanalysis*. 14 (2002) 1041–1051. doi:10.1002/1521-4109(200208)14:15/16<1041::AID-ELAN1041>3.0.CO;2-8.
- [10] D. Schäfer, A. Puschhof, W. Schuhmann, Scanning electrochemical microscopy at variable temperatures, *Phys. Chem. Chem. Phys.* 15 (2013) 5215–5223. doi:10.1039/c3cp43520b.
- [11] M.A. O'Connell, A.J. Wain, Combined electrochemical-topographical imaging: A critical review, *Anal. Methods*. 7 (2015) 6983–6999. doi:10.1039/c5ay00557d.

- [12] K. McKelvey, M.A. Edwards, P.R. Unwin, Intermittent contact-scanning electrochemical microscopy (IC-SECM): A new approach for tip positioning and simultaneous imaging of interfacial topography and activity, *Anal. Chem.* 82 (2010) 6334–6337. doi:10.1021/ac101099e.
- [13] M. Gębala, W. Schuhmann, F. La Mantia, A new AC-SECM mode: On the way to high-resolution local impedance measurements in SECM, *Electrochem. Commun.* 13 (2011) 689–693. doi:10.1016/j.elecom.2011.04.010.
- [14] C. Cougnon, K. Bauer-Espindola, D.S. Fabre, J. Mauzeroll, Development of a phase-controlled constant-distance scanning electrochemical microscope, *Anal. Chem.* 81 (2009) 3654–3659. doi:10.1021/ac802211u.
- [15] C. Kranz, Recent advancements in nanoelectrodes and nanopipettes used in combined scanning electrochemical microscopy techniques., *Analyst.* 139 (2014) 336–52. doi:10.1039/c3an01651j.
- [16] C. Lee, J. Kwak, A.J. Bard, Application of scanning electrochemical microscopy to biological samples, *Proc. Natl. Acad. Sci. U. S. A.* 87 (1990) 1740–1743. doi:10.1073/pnas.87.5.1740.
- [17] L. Li, C. Bu, Y. Zhang, J. Du, X. Lu, X. Liu, Composite system based on biomolecules-functionalized multiwalled carbon nanotube and ionic liquid: Electrochemistry and electrocatalysis of tryptophane, *Electrochim. Acta.* 58 (2011) 105–111. doi:10.1016/j.electacta.2011.08.097.
- [18] V. Alizadeh, M.F. Mousavi, M.A. Mehrgardi, S.H. Kazemi, H. Sharghi, Electron transfer kinetics of cytochrome c immobilized on a phenolic terminated thiol self assembled monolayer determined by scanning electrochemical microscopy, *Electrochim. Acta.* 56 (2011) 6224–6229. doi:10.1016/j.electacta.2011.03.029.
- [19] P. Bertoncillo, Advances on scanning electrochemical microscopy (SECM) for energy, *Energy Environ. Sci.* 3 (2010) 1620–1633. doi:10.1039/c0ee00046a.
- [20] T. Yasukawa, T. Kaya, T. Matsue, Characterization and imaging of single cells with scanning electrochemical microscopy, *Electroanalysis.* 12 (2000) 653–659. doi:10.1002/1521-4109(200005)12:9<653::AID-ELAN653>3.0.CO;2-S.
- [21] K. Yamashita, M. Takagi, K. Uchida, H. Kondo, S. Takenaka, Visualization of DNA microarrays by scanning electrochemical microscopy (SECM), *Analyst.* 126 (2001) 1210–1211. doi:10.1039/b105097b.

- [22] D.T. Pierce, P.R. Unwin, A.J. Bard, Scanning electrochemical microscopy. 17. Studies of enzyme-mediator kinetics for membrane- and surface-immobilized glucose oxidase, *Anal. Chem.* 64 (1992) 1795–1804. doi:10.1021/ac00041a011.
- [23] D. Mandler, A.J. Bard, Scanning Electrochemical Microscopy: The Application of the Feedback Mode for High Resolution Copper Etching, *J. Electrochem. Soc.* 136 (1989) 3143–3144. doi:10.1149/1.2096416.
- [24] L. Niu, Y. Yin, W. Guo, M. Lu, R. Qin, S. Chen, Application of scanning electrochemical microscope in the study of corrosion of metals, *J. Mater. Sci.* 44 (2009) 4511–4521. doi:10.1007/s10853-009-3654-x.
- [25] P. Dauphin-Ducharme, J. Mauzeroll, Surface Analytical Methods Applied to Magnesium Corrosion, *Anal. Chem.* 87 (2015) 7499–7509. doi:10.1021/ac504576g.
- [26] A.J. Bard, X. Li, W. Zhan, Chemically imaging living cells by scanning electrochemical microscopy, *Biosens. Bioelectron.* 22 (2006) 461–472. doi:10.1016/j.bios.2006.04.028.
- [27] G. Wittstock, Modification and characterization of artificially patterned enzymatically active surfaces by scanning electrochemical microscopy, *Fresenius. J. Anal. Chem.* 370 (2002) 303–315. doi:10.1007/s002160100795.
- [28] A. Hamzehloei, S. Zahra Bathaie, M.F. Mousavi, Probing redox reaction of azurin protein immobilized on hydroxyl-terminated self-assembled monolayers with different lengths, *J. Electroanal. Chem.* 755 (2015) 27–38. doi:10.1016/j.jelechem.2015.07.005.
- [29] M.E. Abdelhamid, S. Piantavigna, A.M. Bond, B. Graham, L. Spiccia, L.L. Martin, A.P. O'Mullane, An SECM study on the influence of cationic, membrane-active peptides on a gold-supported self-assembled monolayer, *Electrochem. Commun.* 51 (2015) 11–14. doi:10.1016/j.elecom.2014.11.018.
- [30] A.J. Bard, F.R.F. Fan, D.T. Pierce, P.R. Unwin, D.O. Wipf, F. Zhou, Chemical imaging of surfaces with the scanning electrochemical microscope, *Science* (80). 254 (1991) 68–74. doi:10.1126/science.254.5028.68.
- [31] Y. Takahashi, A.I. Shevchuk, P. Novak, Y. Murakami, H. Shiku, Y.E. Korchev, T. Matsue, Simultaneous noncontact topography and electrochemical imaging by SECM/SICM featuring ion current feedback regulation, *J. Am. Chem. Soc.* 132 (2010) 10118–10126. doi:10.1021/ja1029478.
- [32] D.J. Comstock, J.W. Elam, M.J. Pellin, M.C. Hersam, Integrated ultramicroelectrode-nanopipet probe for concurrent scanning electrochemical microscopy and scanning ion conductance microscopy, *Anal. Chem.* 82 (2010) 1270–1276. doi:10.1021/ac902224q.

- [33] C.A. Morris, C.C. Chen, L.A. Baker, Transport of redox probes through single pores measured by scanning electrochemical-scanning ion conductance microscopy (SECM-SICM), *Analyst*. 137 (2012) 2933–2938. doi:10.1039/c2an16178h.
- [34] K. Leonhardt, A. Avdic, A. Lugstein, I. Pobelov, T. Wandlowski, M. Wu, B. Gollas, G. Denuault, Atomic force microscopy-scanning electrochemical microscopy: Influence of tip geometry and insulation defects on diffusion controlled currents at conical electrodes, *Anal. Chem.* 83 (2011) 2971–2977. doi:10.1021/ac103083y.
- [35] M. Salomo, S.E. Pust, G. Wittstock, E. Oesterschulze, Integrated cantilever probes for SECM/AFM characterization of surfaces, *Microelectron. Eng.* 87 (2010) 1537–1539. doi:10.1016/j.mee.2009.11.032.
- [36] J. Wiedemair, J.S. Moon, F. Reinauer, B. Mizaikoff, C. Kranz, Ion beam induced deposition of platinum carbon composite electrodes for combined atomic force microscopy-scanning electrochemical microscopy, *Electrochem. Commun.* 12 (2010) 989–991. doi:10.1016/j.elecom.2010.05.008.
- [37] S.E. Salamifar, R.Y. Lai, Use of combined scanning electrochemical and fluorescence microscopy for detection of reactive oxygen species in prostate cancer cells, *Anal. Chem.* 85 (2013) 9417–9421. doi:10.1021/ac402367f.
- [38] C. Renault, K. Marchuk, H.S. Ahn, E.J. Titus, J. Kim, K.A. Willets, A.J. Bard, Observation of nanometer-sized electro-active defects in insulating layers by fluorescence microscopy and electrochemistry, *Anal. Chem.* 87 (2015) 5730–5737. doi:10.1021/acs.analchem.5b00898.
- [39] P.A. Kottke, A.G. Fedorov, Advective and transient effects in combined AFM/SECM operation, *J. Electroanal. Chem.* 583 (2005) 221-231. doi:10.1016/j.jelechem.2005.06.017.
- [40] R. Cornut, S. Poirier, J. Mauzeroll, Forced convection during feedback approach curve measurements in scanning electrochemical microscopy: Maximal displacement velocity with a microdisk, *Anal. Chem.* 84 (2012) 3531–3537. doi:10.1021/ac203047d.
- [41] C. a Nkuku, R.J. LeSuer, Electrochemistry in deep eutectic solvents., *J. Phys. Chem. B.* 111 (2007) 13271–13277. doi:10.1021/jp075794j.
- [42] S. Kuss, D. Trinh, J. Mauzeroll, High-Speed Scanning Electrochemical Microscopy Method for Substrate Kinetic Determination: Application to Live Cell Imaging in Human Cancer, *Anal. Chem.* 87 (2015) 8102–8106. doi:10.1021/acs.analchem.5b01269.

- [43] S. Kuss, C. Kuss, D. Trinh, S.B. Schougaard, J. Mauzeroll, Forced convection during scanning electrochemical microscopy imaging over living cells: Effect of topographies and kinetics on the microelectrode current, *Electrochim. Acta.* 110 (2013) 42–48. doi:10.1016/j.electacta.2013.03.149.
- [44] M.A. Edwards, A.L. Whitworth, P.R. Unwin, Quantitative analysis and application of tip position modulation-scanning electrochemical microscopy, *Anal. Chem.* 83 (2011) 1977–1984. doi:10.1021/ac102680v.
- [45] C. Iffelsberger, P. Vatsyayan, F. Matysik, Scanning Electrochemical Microscopy with Forced Convection Introduced by High-Precision Stirring, *Anal. Chem.* 89 (2017) 1658–1664. doi:10.1021/acs.analchem.6b03764.

2. Theoretical background

2.1 Voltammetry

2.1.1 Introduction to voltammetry

Voltammetry is based on the measurement of the current I flowing through an electrochemical cell in dependence of the potential E . As presented schematically in Figure 2.1, voltammetric measurements are usually performed in a three-electrode setup [1,2].

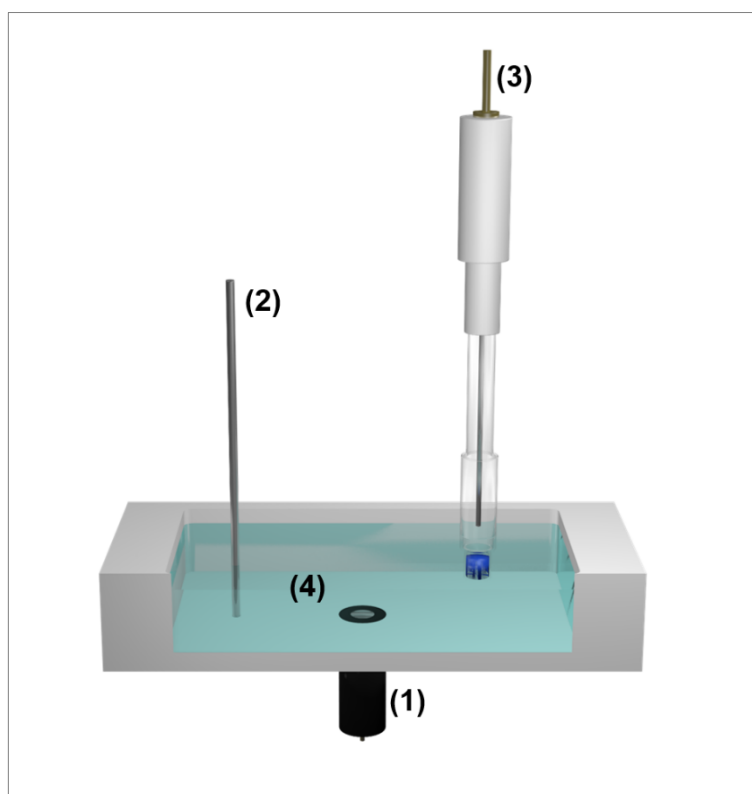


Figure 2.1: Schematic representation of the experimental setup for electrochemical experiments. Working electrode WE (1), counter electrode CE (2) and reference electrode RE (3) are immersed into the electrolyte solution (4) containing a redox active species. All electrodes are connected to a potentiostat for potential control and current read-out.

A reference electrode (RE), a counter electrode (CE) and a working electrode (WE) are immersed into the electrolyte solution usually containing an electrochemically active species. All electrodes are connected to a potentiostat enabling potential control and current read-out. The potential applied to the working electrode is adjusted versus the reference electrode. Measuring this reference potential should be currentless as otherwise part of the applied potential is lost due to the resistance R_{sol} of the solution. Considering this so-called ohmic

potential drop, the potential E_{eff} which is effectively applied to the working electrode is differing from the initial potential E according to:

$$E_{eff} = E - E_{sol} = E - R_{sol} \cdot I \quad (1)$$

This potential E_{eff} leads to a current flow between working electrode and counter electrode. Two contributions add up to the measured current I :

$$I = I_C + I_F \quad (2)$$

The capacitive current I_C results from the charging process of the electrical double layer formed at the electrode when a potential is applied, whereas the Faradaic current I_F results from the conversion of a redox active species present in the electrolyte solution. Consequently, only the Faradaic current delivers qualitative and quantitative information about the investigated system meaning that a large ratio I_F/I_C is desired. As both currents are superimposed, pulsed techniques or very small electrodes can be applied to increase this ratio [3-5]. These so-called ultramicroelectrodes (UMEs) exhibit a negligible contribution of the capacitive current I_C to the overall current leading to large I_F/I_C ratios and thus increased accessibility of analytical information. Furthermore, since UMEs exhibit a high current density but low currents in the range of nanoampere or even less, the ohmic drop can be neglected. According to equation 1, the effectively applied potential E_{eff} equals the initial potential E in this case. Hence, utilizing UMEs electrochemical systems can be operated in a two-electrode setup without a reference electrode. Nevertheless, the voltammetric behavior of UMEs differs strongly from conventional macroscopic electrodes.

2.1.2 Voltammetric behavior of macroelectrodes and ultramicroelectrodes

The electrochemical conversion of a redox active species at the working electrode resulting in the Faradaic current I_F is composed of three major steps. The mass transfer of the species from the bulk solution to the electrode surface, the transfer of electrons between electrode and species and the mass transfer away from the electrode. Comparing these steps, electrochemical reactions are reversible if the electron transfer is faster than the mass transfer and irreversible vice versa [6].

The mass transfer which is defined as flux J_i of a species i is composed of diffusion, migration and convection. In the case of one dimension, the flux J_i in x-direction is defined by the Nernst-

Planck equation with the three terms on the right representing the contributions of diffusion, migration and convection [1,6].

$$J_i(x) = -D_i \cdot \frac{\partial c_i(x)}{\partial x} - \frac{z \cdot F}{RT} \cdot D_i \cdot c_i \frac{\partial \Phi(x)}{\partial x} + c_i \cdot v(x) \quad (3)$$

D_i describes the diffusion coefficient of the species i , c_i its concentration, z the number of transferred electrons, R the universal gas constant, T the temperature, ϕ the electric field potential and v the velocity. The concentration gradient of the electroactive species that is formed when the electrochemical reaction is started and the species is consumed at the electrode is described by the change in concentration along the x-dimension $\partial c_i/\partial x$.

Usually, when designing an electrochemical experiment, migration and convection are suppressed by the addition of an inert supporting electrolyte and the absence of a convective source. In this case, the diffusion resulting from the concentration gradient is the predominant contribution to the mass transfer of the analyte species leading to a simplified form of equation 3 known as Fick's first law.

$$-J_i(x) = D_i \cdot \frac{\partial c_i(x)}{\partial x} \quad (4)$$

Diffusion in turn is composed of linear and radial diffusion. As presented in Figure 2.2, the ratio of these contributions is dependent on the geometry and the size of the electrode where the electrochemical reaction takes place.

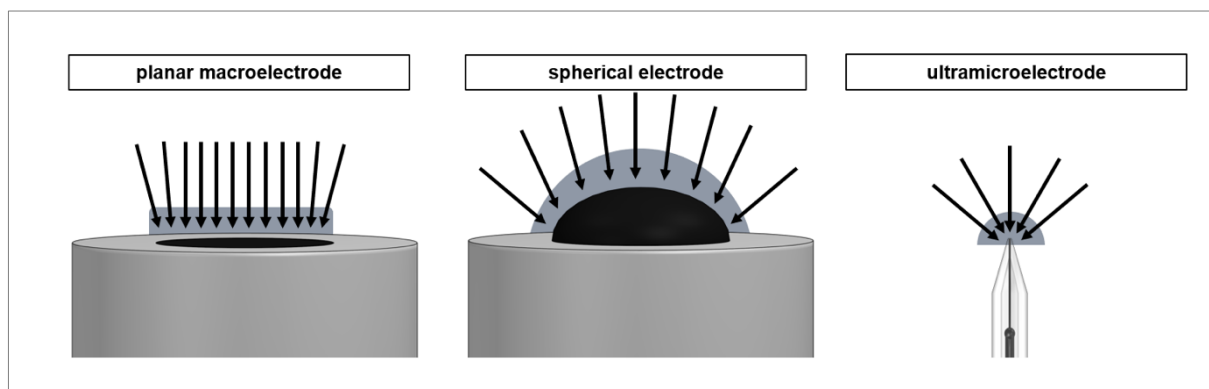


Figure 2.2: Schematic representation of a linear diffusion field occurring during electrochemical reactions at planar macroelectrodes in comparison to a spherical diffusion field occurring at spherical electrodes and ultramicroelectrodes adapted from [7].

Hence, based on the electrode characteristics different forms of Fick's second law which describes the variation of concentration with time due to diffusion have to be considered. For

planar macroelectrodes the flux towards the surface is controlled by linear diffusion as the radial diffusion on the edges of the electrodes is negligible:

$$\frac{\partial c_i(x, t)}{\partial t} = D_i \cdot \left(\frac{\partial^2 c_i(x, t)}{\partial x^2} \right) \quad (5)$$

Solving equation 5 delivers the Cottrell equation for the diffusion-limited current I_{planar} measured at a planar macroelectrode in presence of a redox active species with initial concentration c_i^0 when a potential is applied. The other parameters represent the electrode area A and the the number of transferred electrons z .

$$I_{planar}(t) = z \cdot F \cdot A \cdot \sqrt{\frac{D_i}{\pi \cdot t}} \cdot c_i^0 \quad (6)$$

If the electrode is rather spherical than planar, radial diffusion is the predominant contribution leading to a spherical diffusion field and thus a different form of Fick's second law [4,8]:

$$\frac{\partial c_i(x, t)}{\partial t} = D_i \cdot \left(\frac{\partial^2 c_i(x, t)}{\partial r^2} + \frac{2}{r} \cdot \frac{\partial c_i(x, t)}{\partial r} \right) \quad (7)$$

Solving equation 7 delivers the equation for the current $I_{spherical}$ measured at a spherical electrode.

$$I_{spherical}(t) = z \cdot F \cdot A \cdot D_i \left(\frac{1}{\sqrt{D_i \cdot \pi \cdot t}} + \frac{1}{r_e} \right) \cdot c_i^0 \quad (8)$$

In comparison to planar macroelectrodes, equation 8 contains a time-independent component $1/r_e$ with r_e being the radius of the electrode. Increasing the electrode radius, the time-independent component becomes negligible leading to a transition of equation 8 into the Cottrell equation for planar electrodes.

Decreasing the radius, however, UMEs are obtained exhibiting at least one dimension smaller than 25 μm . For a disk UME representing the most important practical UME geometry Fick's second law for two dimensions is given by

$$\frac{\partial c_i(r, z, t)}{\partial t} = D_i \cdot \left(\frac{\partial^2 c_i(r, z, t)}{\partial r^2} + \frac{1}{r} \cdot \frac{\partial c_i(r, z, t)}{\partial r} + \frac{\partial^2 c_i(r, z, t)}{\partial z^2} \right) \quad (9)$$

where r describes the radial position and z the linear displacement normal to the plane of the electrode. Solving Fick's second law and applying further simplifications delivers the equation for the steady-state current I_{UME} measured late in the experiment at a disk UME with an insulating mantle of infinite thickness [4,9].

$$I_{UME} = 4 \cdot z \cdot F \cdot D_i \cdot c_i^0 \cdot r \quad (10)$$

Disk UMEs exhibit a time-independent current corresponding to a hemispherical diffusion field with a constant diffusion layer. In comparison to an insulating mantle of infinite thickness, an additional geometrical factor $\beta(RG)$ has to be considered if the mantle is finite:

$$I_{UME} = 4 \cdot z \cdot F \cdot D_i \cdot c_i^0 \cdot r \cdot \beta(RG) \quad (11)$$

This factor $\beta(RG)$ describes the flux from behind the electrode surface and is defined as

$$\beta(RG) = 1 + \frac{0.23}{(RG^3 - 0.81)^{0.36}} \quad (12)$$

with RG being defined as the ratio between radius of the insulating mantle r_g and radius of the active electrode area r .

Consequently, different equations have to be considered due to the different diffusional contributions resulting in different behavior of macroelectrodes and UMEs during electrochemical experiments such as cyclic voltammetry or amperometry [7,10].

2.1.3 Cyclic voltammetry and amperometry

Cyclic voltammetry (CV) is a frequently applied voltammetric measurement technique to obtain information about the electrochemical properties of an analyte [6]. Figure 2.3 delivers an overview of the technique's most important characteristics.

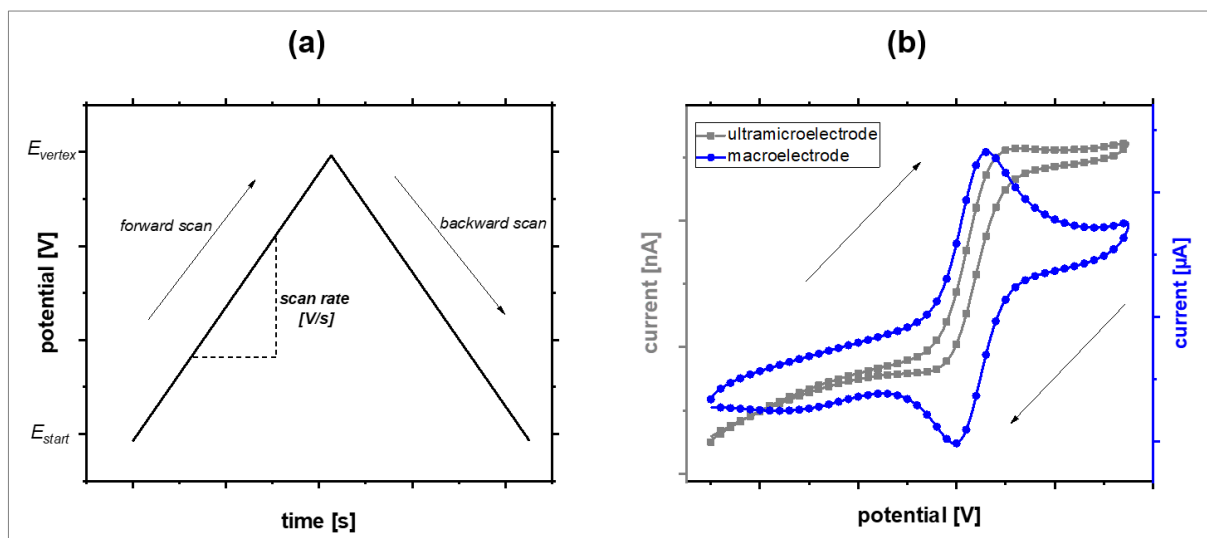


Figure 2.3: (a) Time-dependent potential change during cyclic voltammetry. (b) Typical current response of a macroelectrode and an UME during cyclic voltammetry in presence of a reversibly convertible redox active species exhibiting a one electron transfer.

As can be seen in Figure 2.3 (a), the starting potential E_{start} applied to the working electrode is linearly increased during the forward scan and decreased again during the backward scan upon reaching a certain turning point E_{vertex} . This so-called scan cycle can be repeated arbitrarily. The current I is recorded throughout the cycle delivering the typical current-potential (I - E) curves known as cyclic voltammograms (also abbreviated as CV).

The shape of these curves strongly depends on both the characteristics of the analyte as well as the dimensions of the working electrode. Figure 2.3 (b) compares I - E curves obtained for a diffusion limited reaction during cyclic voltammetry in presence of a reversibly oxidizable and reducible species exhibiting a one electron transfer utilizing a macroelectrode and an UME. A peak-shaped curve is observed for a macroelectrode due to the current decrease according to the Cottrell equation (equation 6). Furthermore, forward and backward scans show hysteresis due to the rather high contribution of capacitive currents. An s-shaped curve exhibiting a steady-state current with very small hysteresis is observed for an UME due to the lack of a time-dependent component in the valid equation (equation 10) and the small contribution of capacitive currents.

Similar differences can be observed during amperometric measurements [6]. In comparison to cyclic voltammetry, the potential applied to the working electrode is kept constant during amperometry as can be seen in Figure 2.4 (a).

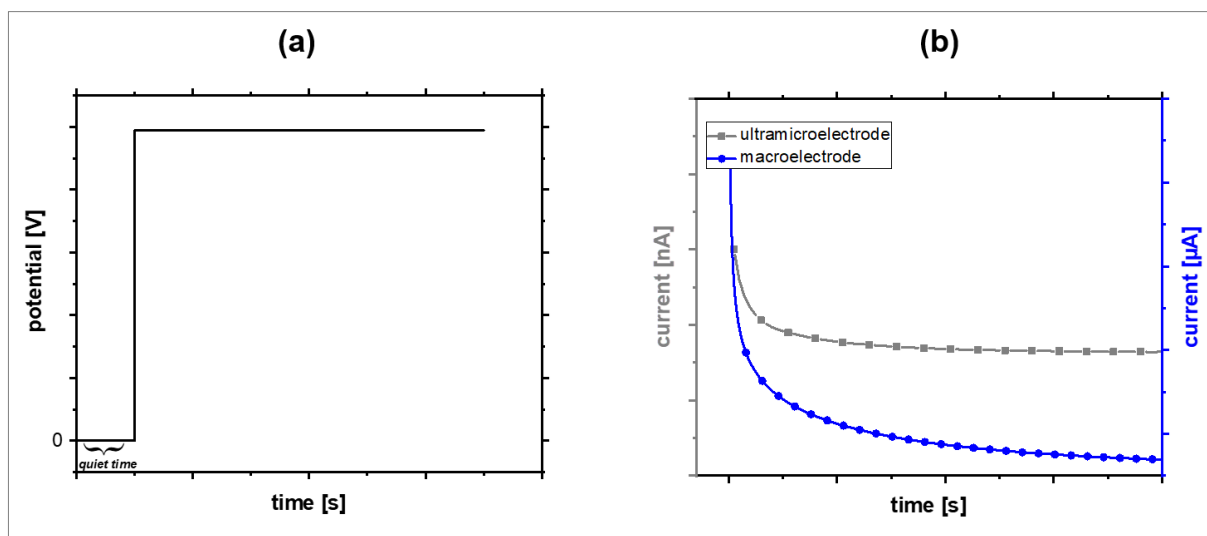


Figure 2.4: (a) Time-dependent potential change during chronoamperometry. (b) Typical current response of a macroelectrode and an UME during chronoamperometry in presence of a redox active species.

Figure 2.4 (b) compares the time-dependent current for a diffusion limited reaction recorded with a macroelectrode and an UME when a constant potential is applied. Similar to cyclic voltammetry, a constant current is observed for the UME whereas the current decreases for the macroelectrode due to its Cottrellian behavior.

Consequently, the different behavior of macroelectrodes and UMEs during cyclic voltammetry and amperometry can be attributed to the different sizes of the electrodes and thus the different diffusional characteristics as described in section 2.1.2. Nevertheless, the voltammetric behavior of the electrodes in dependence of their size is only valid if migration and convection are excluded and mass transfer is governed solely by diffusion.

2.1.4 Mass transfer and hydrodynamic effects

When forced convection is generated within an electrochemical system rather than being excluded, hydrodynamic effects on the mass transfer have to be considered [1,6,10]. For instance, forced convection can be generated by stirring the electrolyte solution [11], by flow systems [10,12], by sonication [13] or by rotating electrodes [14,15]. Figure 2.5 schematically sums up the processes at a macroscopic electrode during electrochemical reactions in quiescent solution and with forced convection.

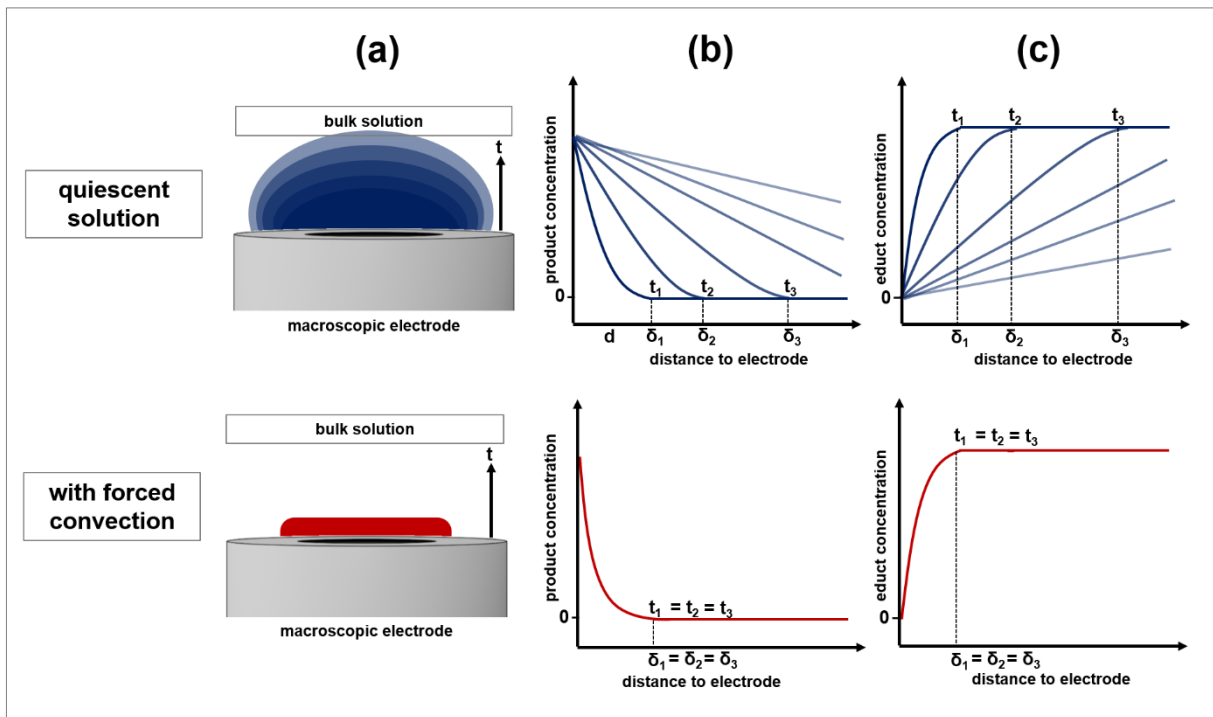


Figure 2.5: Schematic representation of the time-dependency t of the diffusion layer δ of the product species generated during an electrochemical reaction at a macroelectrode (a) and the corresponding change of the product concentration profile (b). The time-dependency t of the concentration profile δ of the species that is consumed during the electrochemical reaction at the electrode is shown in (c). All characteristics are depicted in quiescent solution (top) and with forced convection (bottom)^{adapted from [2]}.

As depicted in part (a) of Figure 2.5 a time-dependent growing diffusion layer of the product species generated during an electrochemical reaction is observed in comparison to a stable diffusion layer with forced convection applied to the system. Looking at the concentration profile of the product species in part (b) it is visible that its concentration in the region close to the electrode increases with ongoing reaction time in quiescent solution whereas a constant profile is obtained with forced convection. Analogous, in part (c) the same observations can be made for the concentration profile of the species that is consumed during the electrochemical reaction but with its concentration being depleted in the region close to the electrode. Furthermore, with forced convection thinner diffusion layers are formed resulting in increased

currents due to steeper concentration gradients and hence an increased mass transfer. The increase in mass transfer can be adjusted by varying the intensity of the convection. Thus, an additional parameter can be optimized concerning the kinetics of the system that is to be studied.

The theoretical treatment of convective systems involves solving a hydrodynamic problem like determining the flow velocity of the solution as a function of the intensity of the convection before solving the electrochemical one. The simplest treatment is based on a diffusion layer approach meaning that within the diffusion layer close to the electrode surface the convection can be neglected and the mass transfer is governed solely by diffusion. Outside the diffusion layer a constant concentration of all analyte species is to be expected due to the convection. A more complex approach is the convective-diffusion equation where only the contribution of migration can be excluded from the Nernst-Planck equation (equation 3). Deriving the valid equations of so-called hydrodynamic electrodes requires both modelling as well as simplifying assumptions and strongly depends on the characteristics of the hydrodynamic system [10].

Figure 2.6 representatively sums up the effects of forced convection on an amperometric experiment utilizing a planar macroelectrode.

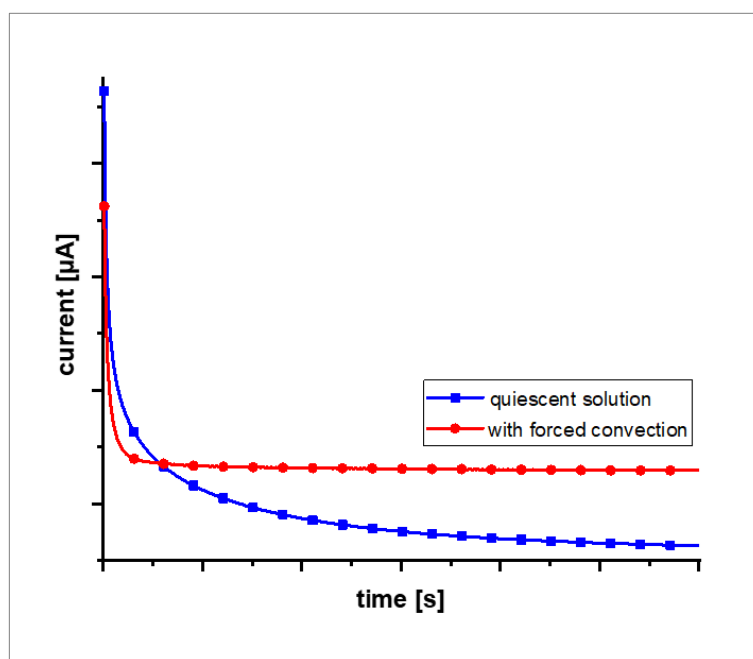


Figure 2.6: Typical current response of a macroelectrode during chronoamperometry in presence of a redox active species in quiescent solution and with forced convection applied to the system.

A decreasing current is observed in quiescent solution due to the time-dependent growth of the diffusion layers. During this growth the concentration gradient of the species that is consumed flattens causing the mass transfer towards the surface to slow down. The resulting decrease in current can be calculated using the Cottrell equation (equation 6) for a

macroelectrode described in section 2.1.2. With forced convection, however, constant diffusion layers are formed resulting in a steady-state current response similar to UMEs with increased currents due to the increased mass transfer.

Consequently, time-independent diffusion layers of both the product species as well as the species that is consumed are formed during electrochemical reactions with forced convection in contrast to growing diffusion layers without forced convection effecting the electrochemical response of macroelectrodes. Concerning UMEs, the interference of convection is negligible due to their high current density.

2.2 Scanning electrochemical microscopy

Scanning electrochemical microscopy is a versatile analytical method for the characterization of a vast field of substrates ranging from inorganic surfaces to biological samples [9,16-22]. The technique was introduced concurrently by the Bard [23] and Engstrom [24] research groups as a representative of the field of scanning probe microscopy (SPM). In general, in scanning probe microscopy information is generated via processes taking place at a probe while being scanned across a surface. Other representatives include atomic force microscopy and scanning tunneling microscopy. Throughout the years, various instrumental developments and coupling of the SECM with other SPM techniques were established leading to a wide variety of experimental parameters and operational modes. The following sections deliver an overview of the most important aspects fundamental for the research conducted within this thesis.

2.2.1 Setup of the scanning electrochemical microscope

The individual components of the experimental setup for scanning electrochemical microscopy are depicted schematically in Figure 2.7.

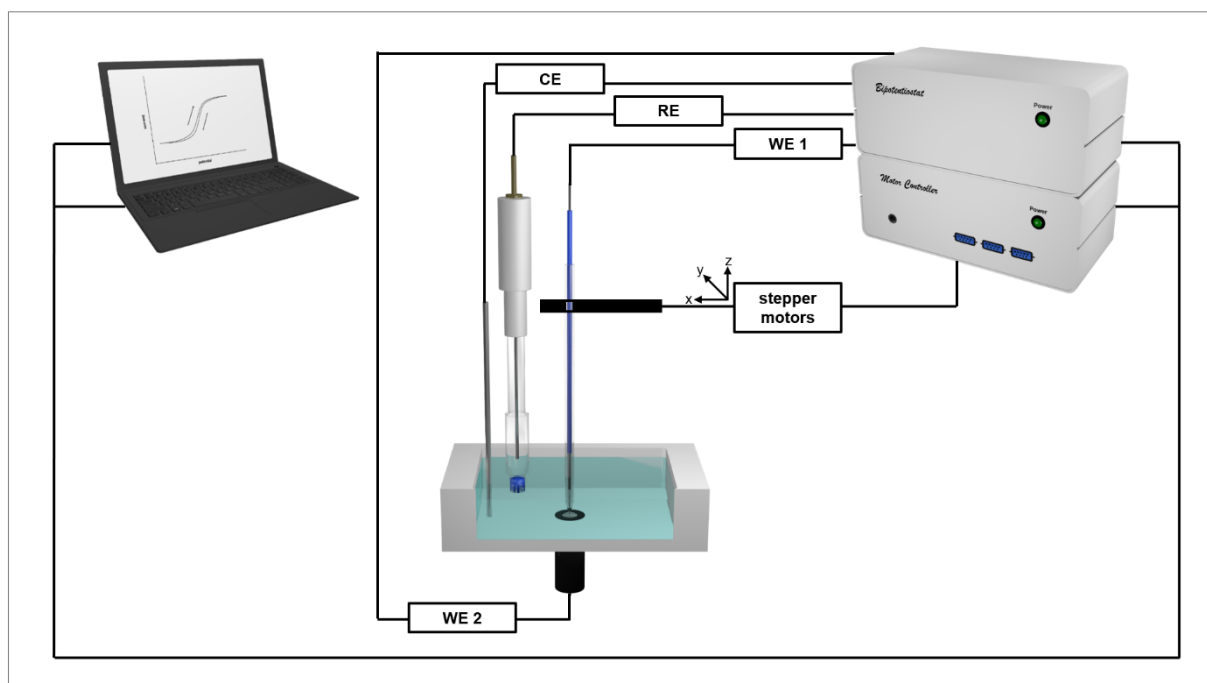


Figure 2.7: Schematic representation of the experimental setup for scanning electrochemical microscopy. Both working electrodes (WE 1, WE 2), as well as reference electrode (RE) and counter electrode (CE) are immersed into the electrolyte solution containing a redox active species. All electrodes are connected to a bipotentiostat. Additionally, WE 1 is connected to stepper motors enabling scan movement of the electrode^{adapted from [9]}.

As described in section 2.1.1 the electrochemical cell consists of a reference electrode, a counter electrode and a working electrode. The substrate of interest is mounted within the cell according to the desired application and is operated as a second working electrode for some SECM modes. In this case, it is referred to as substrate electrode. All electrodes are connected to a bipotentiostat and immersed into the electrolyte solution which usually contains a redox active species. The choice of this so-called redox mediator is dependent on the experimental conditions meaning that aspects like solubility, stability and electron transfer characteristics have to be considered [21]. Its conversion at the working electrode which is employed as probe in SECM generates information about the system of interest. The probe is connected to stepper motors enabling its scan movement during measurements. Hence, its precise positioning and mapping of surfaces is facilitated. Usually, disk UMEs with a radius smaller than 25 μm are employed as SECM probes.

2.2.2 Probes for scanning electrochemical microscopy

The most important characteristics of these UMEs influencing the conducted experiments are illustrated schematically in Figure 2.8.

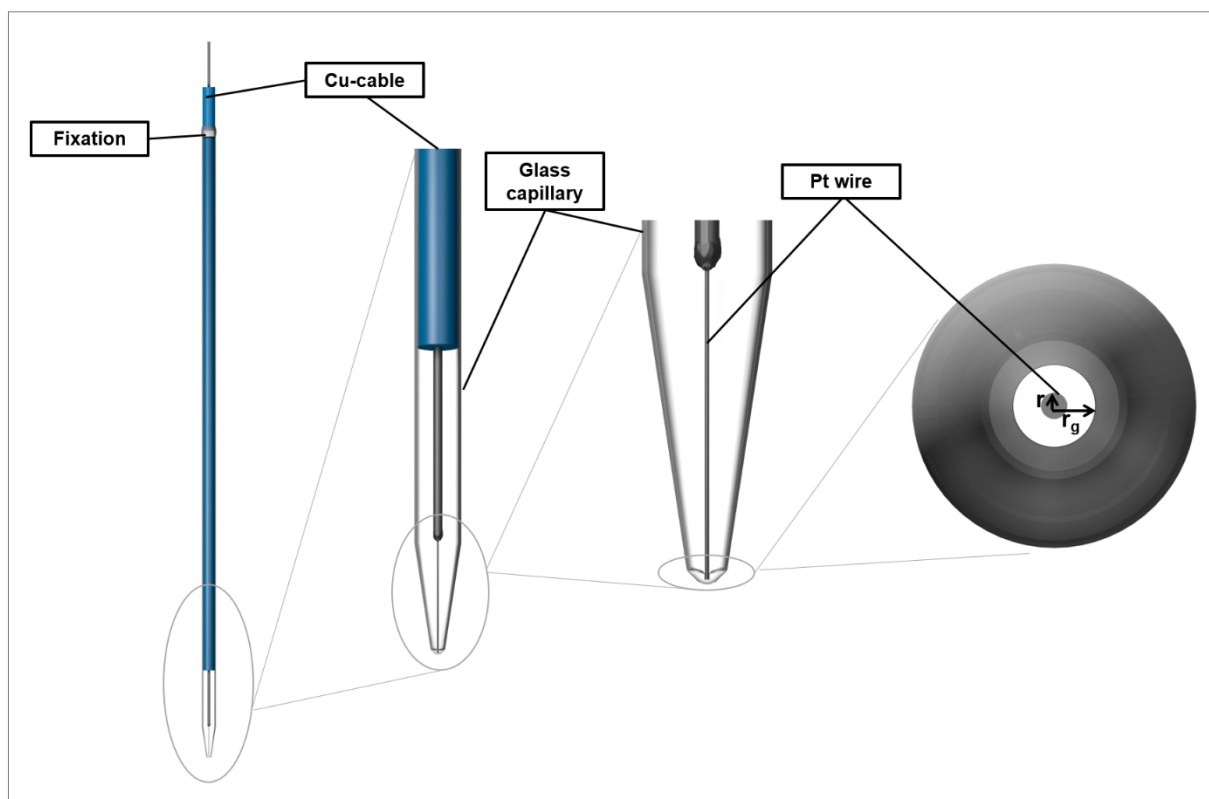


Figure 2.8: Schematic representation of an UME used as working electrode in scanning electrochemical microscopy^{adapted from [25]}.

Different electrode materials such as platinum [26] or silver [27] and different protocols can be applied for the fabrication of the electrodes [7,28]. Usually, they consist of a cable with a wire exhibiting a radius of 25 μm or smaller soldered to its end. This electrode body is inserted into a pulled glass capillary for isolation purposes and for increasing mechanical stability. A common protocol is to seal the capillary via melting and expose the wire manually via polishing. The dimensions of the UME are defined by the radius r of the active electrode area and the radius r_g of the isolating glass mantle. As briefly mentioned in section 2.1.2 the ratio r_g/r between these radii is defined as the RG value.

$$RG = \frac{r_g}{r} \quad (13)$$

The RG value can be determined optically or via so-called probe approach curves – a measurement principle that will be introduced in section 2.2.3. Knowing the RG value, equation 11 can be used to calculate the radius of the active electrode area from the steady-state current obtained from cyclic voltammograms recorded with the corresponding electrodes. Moreover, the hysteresis within the CVs delivers information about the sealing quality of the electrodes. A good sealing results in a smaller contribution of capacitive currents I_C indicated by a less pronounced hysteresis.

Achievable resolution and general performance of all operational modes in SECM strongly depend on the characteristics of the employed UMEs. Thus, their comprehensive characterization is mandatory for data evaluation and comparison of obtained results.

2.2.3 Operational modes of scanning electrochemical microscopy

The SECM was operated in amperometric mode for all conducted experiments meaning that a constant potential was applied to the UME and the Faradaic current resulting from the conversion of the redox mediator was recorded as measurement signal. The amperometric mode can be divided into the subcategories of feedback mode and generator-collector mode [9,21,29].

Feedback mode

Experiments in feedback mode are usually carried out in a two- or three-electrode setup with the UME as working electrode, a counter electrode and optionally an additional reference electrode. Applications of the feedback mode include the possibility to resolve material contrast

between conducting and isolating surfaces [30]. The different behavior of the Faradaic current recorded over both surfaces can be exemplified when investigating so-called probe approach curves (PACs) as depicted in Figure 2.9. Recording PACs is a measurement principle in which the UME is approached vertically to the surface and the current is monitored throughout this approach. To improve comparability of the obtained PACs with respect to different UME dimensions, both the current as well as the distance are normalized for data presentation. The current I is normalized to the current I_∞ recorded in bulk solution, whereas the distance d is normalized to the radius r_{UME} of the UME [9].

$$I_L = \frac{I}{I_\infty} \quad (14)$$

$$L = \frac{d}{r_{UME}} \quad (15)$$

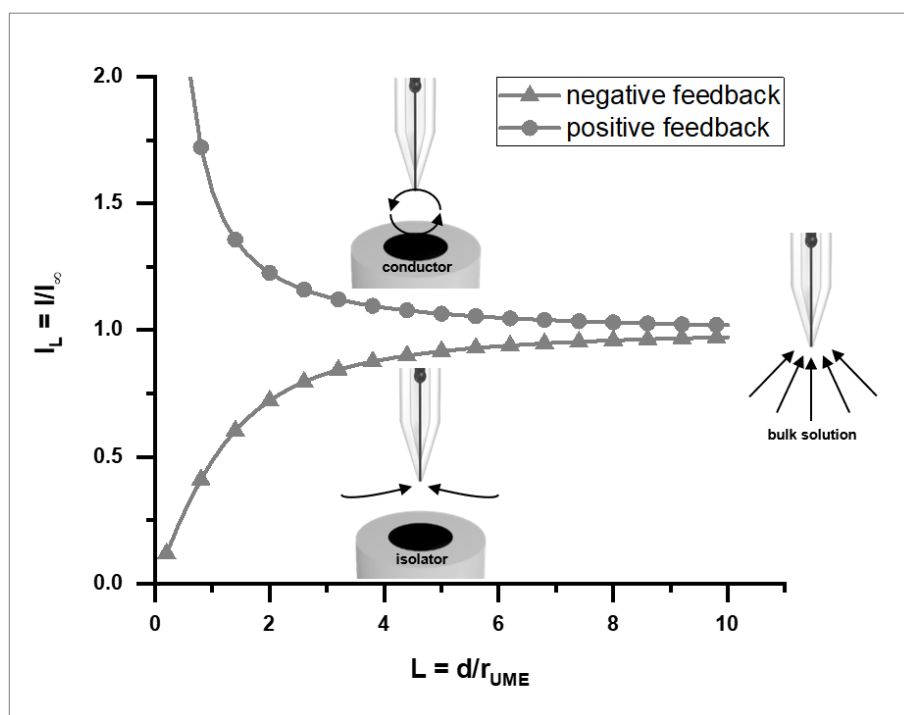


Figure 2.9: Schematic representation of the distance-dependent current response of an UME while approaching a conductor (positive feedback) and an isolator (negative feedback)^{adapted from [9]}.

Starting in the bulk solution, a constant current response is obtained for approach curves over conducting and isolating material due to the hemispherical diffusion field of the redox mediator formed at the UME. When approaching an isolator, the current decreases due to blocking effects of both the substrate as well as the isolating glass mantle of the UME leading to a hindered diffusion of the mediator towards the electrode. Approaching a conductor, the

diffusion of the mediator is also hindered by the substrate, nevertheless, a so-called feedback loop is established due to the ability of the conducting surface to transfer electrons. Thus, the reversibly oxidizable and reducible mediator species that is converted at the UME can be regenerated at the surface of the substrate. This leads to a local increase of mediator concentration in the gap between UME and substrate and thus to an increased current response. The current increase above conductors is referred to as positive feedback, the current decrease above isolators as negative feedback. In general, the influence of the surface on the current is observed starting at distances smaller than five times the radius of the UME. Both positive and negative feedback effects will increase with decreasing distance between substrate and tip of the UME.

Different theoretical models were designed to describe the current recorded throughout the approach curves dependent on the RG value of the UME and the substrate-to-tip distance L . A simplified form [31] for the positive feedback approach is defined by

$$I_{positive}(L, RG) = A + \frac{B}{L} + C \cdot \exp\left(\frac{D}{L}\right) \quad (16)$$

whereas parameters A , B , C , D can be obtained from literature in dependence of the RG value. As this equation is only valid for RG values ranging from 1.1 to 10 a more complex correlation [32] has to be used if the RG value is outside this frame:

$$I_{positive}(L, RG) = \alpha + \frac{\pi}{4 \cdot \beta \cdot \arctan(L)} + \left(1 - \alpha - \frac{1}{2 \cdot \beta}\right) \cdot \frac{2}{\pi} \cdot \arctan(L) \quad (17)$$

with α and β being defined as a function of RG:

$$\alpha(RG) = \ln(2) + \ln(2) \cdot \left(1 - \frac{2}{\pi} \cdot \arccos\left(\frac{1}{RG}\right)\right) - \ln(2) \cdot \left(1 - \left(\frac{2}{\pi} \cdot \arccos\left(\frac{1}{RG}\right)\right)^2\right) \quad (18)$$

$$\beta(RG) = 1 + 0.639 \cdot \left(1 - \frac{2}{\pi} \cdot \arccos\left(\frac{1}{RG}\right)\right) - 0.186 \cdot \left(1 - \left(\frac{2}{\pi} \cdot \arccos\left(\frac{1}{RG}\right)\right)^2\right) \quad (19)$$

Negative feedback approaches can be described by [33]:

$$I_{negative}(L, RG) = \frac{\frac{2.08}{RG^{0.358}} \cdot \left(L - \frac{0.145}{RG}\right) + 1.585}{\frac{2.08}{RG^{0.358}} \cdot (L + 0.0023 \cdot RG) + 1.57 + \frac{\ln(RG)}{L} + \frac{2}{\pi \cdot RG} \cdot \ln\left(1 + \frac{\pi \cdot RG}{2 \cdot L}\right)} \quad (20)$$

As these equations depend on the RG value introduced in section 2.2.2, an experimentally recorded PAC can be used to determine this value by fitting the theoretical model.

Generator-collector mode

Investigating conducting substrates offers the possibility of applying a potential to them. They can be utilized as a second working electrode enabling additional operational modes. Operating the SECM in generator-collector (G/C) mode the redox active mediator species is generated in-situ at the substrate or the UME, respectively [9,21]. Figure 2.10 illustrates the two different G/C mode principles.

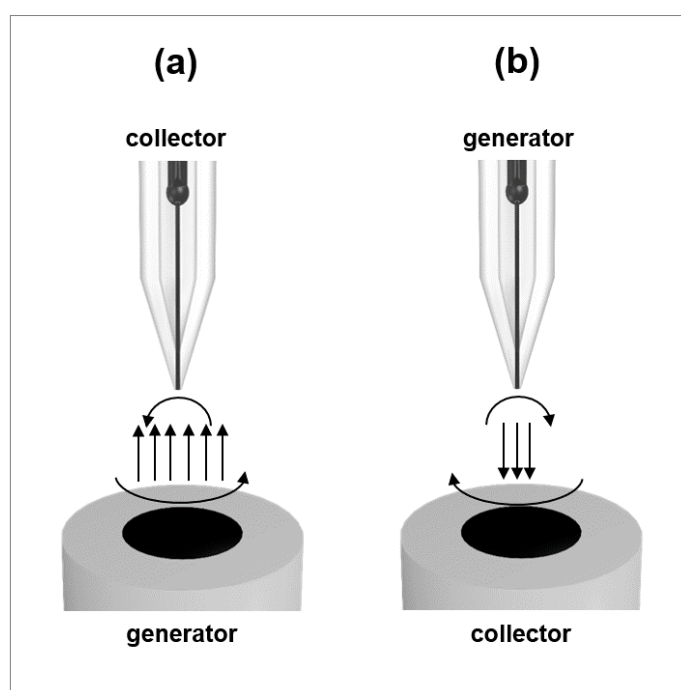


Figure 2.10: Schematic representation of the substrate generation/tip collection mode (a) and the tip generation/substrate collection mode (b) adapted from [34].

In the amperometric substrate generation-tip collection (SG/TC) mode the mediator species is generated electrochemically at the substrate electrode and detected at UME after diffusing through the substrate-tip gap. Analogously, the principle is vice versa in tip generation-substrate collection (TG/SC) mode. Both modes are usually applied to investigate concentration profiles and chemical fluxes or to modify surfaces [21]. Furthermore, in comparison to the amperometric generator-collector mode, also chemical reactions occurring at the substrate or the UME can be deployed to generate the mediator species. As described in section 2.1.4 challenges of the SG/TC mode include the time-dependent growth of the diffusion layer of the mediator species generated at larger substrates and hence a lack of steady-state resulting in a rising background signal.

SECM imaging

Both the feedback mode as well as the generator-collector mode cannot only be applied to study local processes but also to scan a certain area of the substrate and thus create images of its surface. Operating the SECM in the conventional setup, two different imaging principles summed up in Figure 2.11 have to be distinguished.

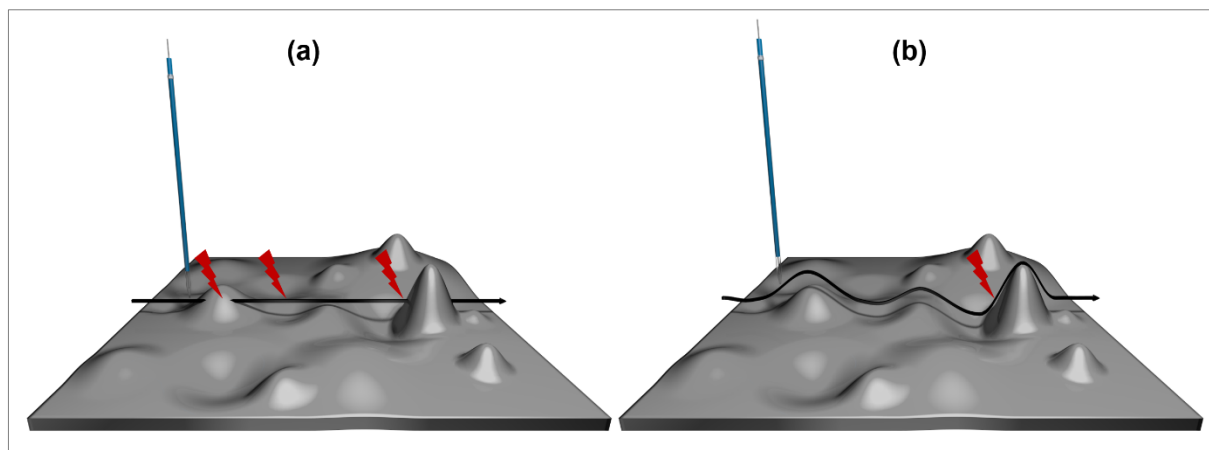


Figure 2.11: Schematic representation of the constant-height (a) and the constant-distance (b) imaging modes of scanning electrochemical microscopy^{adapted from [35]}.

In constant-height mode, the z-position of the UME is kept constant during the scan, whereas in constant-distance mode the distance between UME and the surface is kept constant [9]. The distance control is performed by adjusting the z-position of the UME in dependence of the measured signal. Both imaging principles are struggling with rough topography. In constant-height mode the probe can either crash at local peaks of the surface, whereas information about surface valleys can be lost. Constant-distance mode is less prone to topography, nevertheless, limitations at too rough topographic changes occur due to the response time of the adjustment process. As SECM signals depend on both the substrate-to-tip distance as well as the electrochemical activity of the surface obtaining information about these two characteristics independently is not possible utilizing solely SECM imaging.

2.2.4 Forced convection in scanning electrochemical microscopy

Almost all literature regarding the topic of forced convection in scanning electrochemical microscopy is only broaching the issue of generating convection internally due to too fast scan movement of the UME during imaging or recording of approach curves [36-39]. Mostly, it is suggested that exceeding certain threshold values depending on the characteristics of the UME has to be avoided as all theoretical models applied in SECM are based on purely diffusive currents. Nevertheless, as visualized in Figure 2.12 the effects of forced convection discussed in section 2.1.4 can offer various advantages for SECM experiments especially in SG/TC mode.

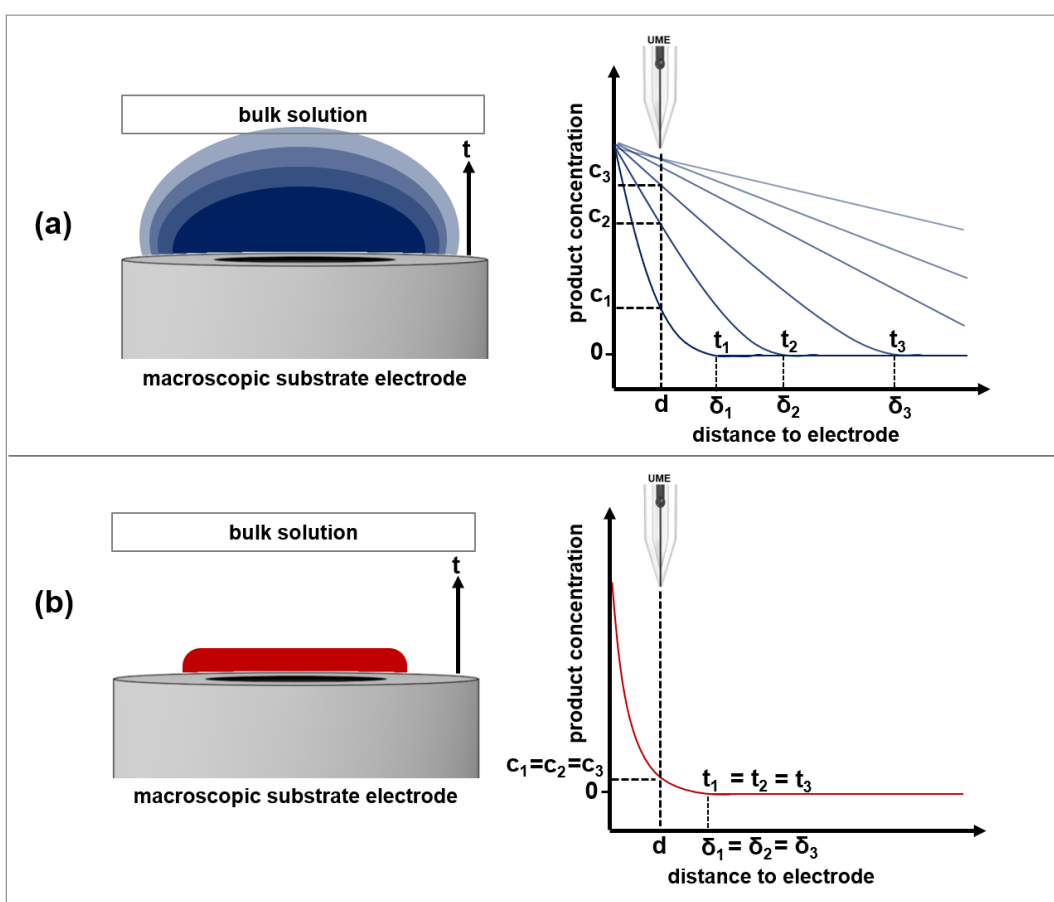


Figure 2.12: Schematic representation of the time-dependent growth t of the diffusion layer δ of the product species generated during an electrochemical reaction at a macroelectrode and the corresponding concentration profile c in quiescent solution (a) and with forced convection applied to the system (b). The UME is placed in a fixed distance d within the diffusion layer of the product species for SECM experiments in SG/TC mode.

As described in section 2.2.3, the UME is placed in a fixed distance from the substrate electrode and scanned across the surface during constant-height imaging in SG/TC mode. In part (a) of Figure 2.12, it can be seen that the concentrations detected at the UME are changing with ongoing reaction time due to the growth of the diffusion layer in quiescent solution. With

forced convection, however, a constant concentration of the product species is detected corresponding to a constant diffusion layer. Figure 2.13 illustrates the consequences of these considerations via repetitive SECM images recorded in SG/TC mode within the diffusion layer of a macroscopic substrate electrode.

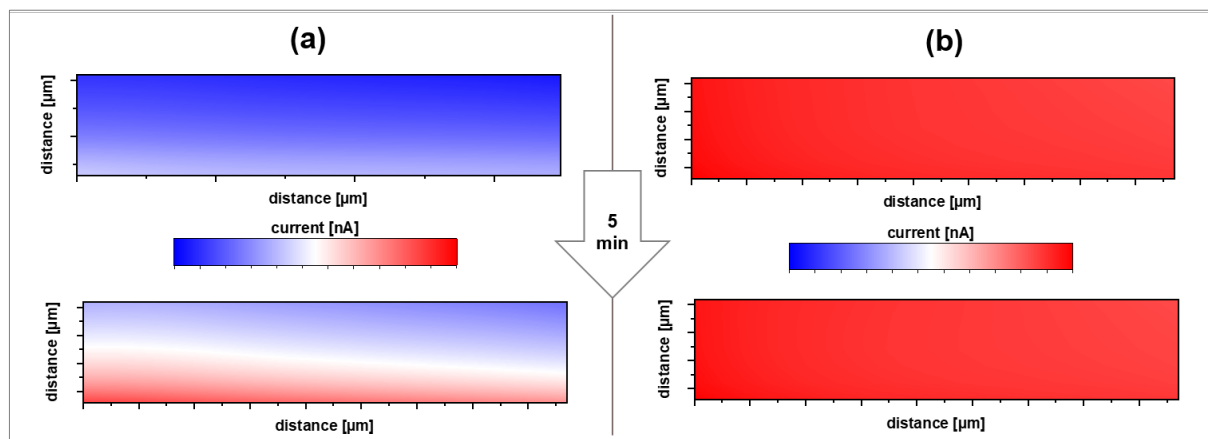


Figure 2.13: Repetitive SECM images in SG/TC mode recorded within the diffusion layer of a macroscopic substrate electrode in quiescent solution (a) and with forced convection applied to the system (b) adapted from [11,40].

In quiescent solution the measured current changes throughout the individual measurements and also differs between the images corresponding to a growing diffusion layer and thus the changing concentration of the product species. With forced convection applied to the system, constant signals are obtained due to constant diffusion layers. Consequently, images in SG/TC mode with macroscopic substrate electrodes exhibit time-dependency which makes it hard to obtain reproducible results. As shown by our group the application of forced convection is a feasible approach to address these problems. Within a pioneering study published in 2017 a constant convective environment was successfully established within the SECM electrolyte via stirring the solution. The setup which was developed to enable integrating an electrical high precision stirrer into the SECM system is presented in Figure 2.14.

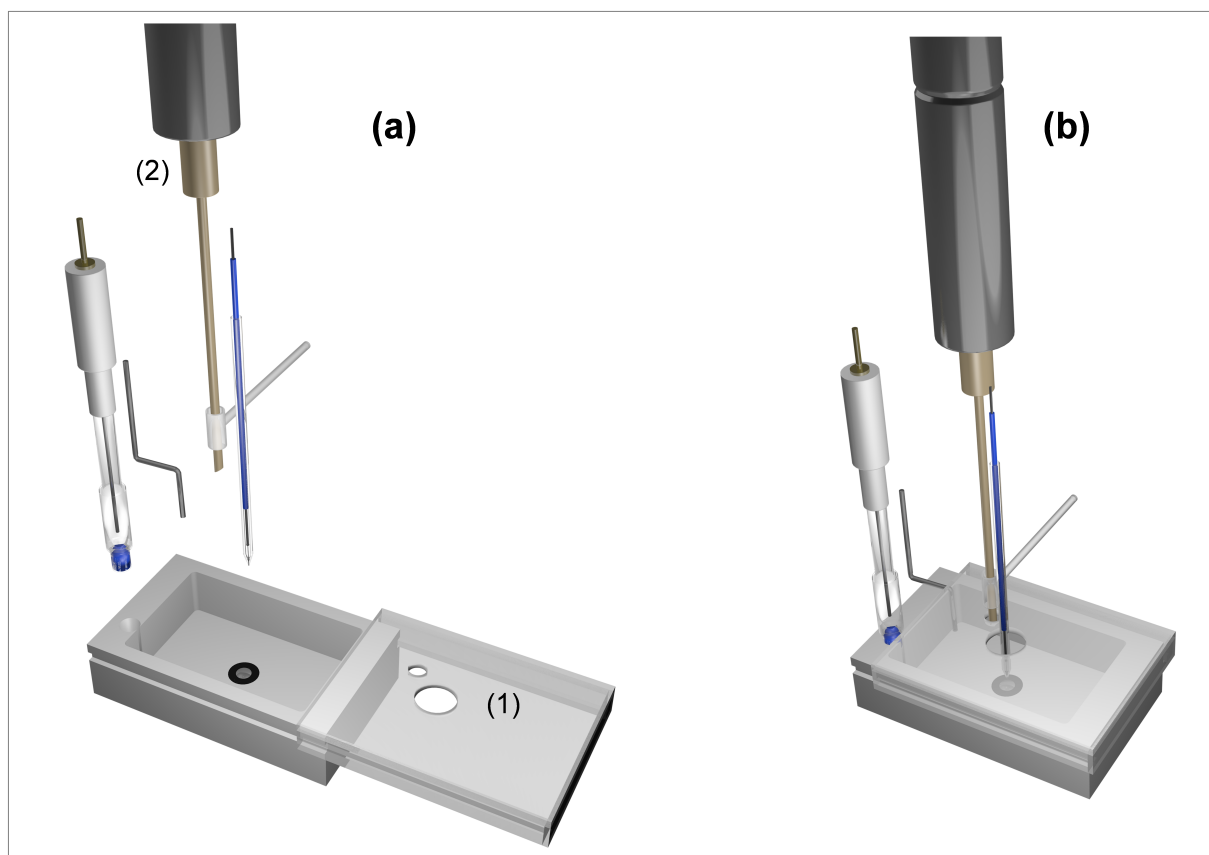


Figure 2.14: Schematic representation of the individual components of the experimental setup for hydrodynamic SECM experiments (a). A 3D-printed mask (1) was fabricated to ensure reproducible positioning of the high precision stirrer (2) within the electrochemical cell. The assembled experimental setup is shown in (b)^{adapted from [11]}.

The diffusion characteristics at a macroscopic substrate electrode were investigated utilizing chronoamperometric measurements, probe scan curves and SECM imaging in SG/TC mode with forced convection applied to the system. Constant diffusion layers were observed under conditions of forced convection enabling time-independent measurements in SG/TC mode and opening up a vast field of applications [11]. Based on these findings the new research field of forced convection in scanning electrochemical microscopy was expanded within this thesis. Further insights on relevant literature concerning forced convection are given in the individual projects of the results section.

References

- [1] A. Bard, L. Faulkner, *Electrochemical methods: fundamentals and applications*, John Wiley&Sons, INC., 2001.
- [2] G. Henze, *Polarographie und Voltammetrie: Grundlagen und analytische Praxis*, Springer, 2001.
- [3] J. Wang, *Analytical Electrochemistry*, John Wiley&Sons, INC., 2006.
- [4] J.L.D. M. Irene Montenegro, M. Arlete Queirós, *Microelectrodes: Theory and Applications*, Springer Science & Business Media, 2012.
- [5] M. Otto, *Analytische Chemie*, WILEY-VCH, 2006.
- [6] R.G. Compton, C.E. Banks, *Understanding Voltammetry*, Imperial College Press, 2011.
- [7] C.G. Zoski, *Handbook of Electrochemistry*, Elsevier B.V., 2007.
- [8] K. Stulík, C. Amatore, K. Holub, V. Marecek, W. Kutner, *Microelectrodes. Definitions, characterization, and applications (Technical report)*, *Pure Appl. Chem.* 72 (2000) 1483–1492. doi:10.1351/pac200072081483.
- [9] A.J. Bard, M.V. Mirkin, *Scanning Electrochemical Microscopy Second Edition*, 2012.
- [10] C.M.A. Brett, A.M.O. Brett, *Electrochemistry: principles, methods and applications*, Oxford Science Publications, 1994.
- [11] C. Iffelsberger, P. Vatsyayan, F. Matysik, *Scanning Electrochemical Microscopy with Forced Convection Introduced by High-Precision Stirring*, *Anal. Chem.* 89 (2017) 1658–1664. doi:10.1021/acs.analchem.6b03764.
- [12] D.J. Pike, N. Kapur, P.A. Millner, D.I. Stewart, W. Yorkshire, W. Yorkshire, W. Yorkshire, *Flow Cell Design for Effective Biosensing*, (2013) 58–70. doi:10.3390/s130100058.
- [13] C.E. Banks, R.G. Compton, A.C. Fisher, I.E. Henley, *The transport limited currents at insonated electrodes*, *Phys. Chem. Chem. Phys.* 6 (2004) 3147. doi:10.1039/b403751k.
- [14] I. Fried, P.J. Elving, *The Rotating Disk Electrode Effect of Rates of Rotation and Polarization*, *Anal. Chem.* 37 (1965) 803–806. doi:10.1021/ac60226a007.
- [15] C.E. Banks, A.O. Simm, R. Bowler, K. Dawes, R.G. Compton, *Hydrodynamic Electrochemistry: Design for a High-Speed Rotating Disk Electrode*, *Anal. Chem.* 77 (2005) 1928–1930. doi:10.1021/ac048259d.

- [16] M. V. Mirkin, B.R. Horrocks, Electroanalytical measurements using the scanning electrochemical microscope, *Anal. Chim. Acta.* 406 (2000) 119–146. doi:10.1016/S0003-2670(99)00630-3.
- [17] P. Sun, F.O. Laforge, M. V. Mirkin, Scanning electrochemical microscopy in the 21st century, *Phys. Chem. Chem. Phys.* 9 (2007) 802–823. doi:10.1039/B612259K.
- [18] G. Wittstock, M. Burchardt, S.E. Pust, Y. Shen, C. Zhao, Scanning Electrochemical Microscopy for Direct Imaging of Reaction Rates, *Angew. Chemie Int. Ed.* 46 (2007) 1584–1617. doi:10.1002/anie.200602750.
- [19] S. Amemiya, A.J. Bard, F.-R.F. Fan, M. V. Mirkin, P.R. Unwin, Scanning Electrochemical Microscopy, *Annu. Rev. Anal. Chem.* 1 (2008) 95–131. doi:10.1146/annurev.anchem.1.031207.112938.
- [20] C.G. Zoski, Review—Advances in Scanning Electrochemical Microscopy (SECM), *J. Electrochem. Soc.* 163 (2016) H3088–H3100. doi:10.1149/2.0141604jes.
- [21] D. Polcari, P. Dauphin-Ducharme, J. Mauzeroll, Scanning Electrochemical Microscopy: A Comprehensive Review of Experimental Parameters from 1989 to 2015, *Chem. Rev.* 116 (2016) 13234–13278. doi:10.1021/acs.chemrev.6b00067.
- [22] J. Izquierdo, P. Knittel, C. Kranz, Scanning electrochemical microscopy: an analytical perspective, *Anal. Bioanal. Chem.* 410 (2018) 307–324. doi:10.1007/s00216-017-0742-7.
- [23] A.J. Bard, F.F. Fan, J. Kwak, O. Lev, Scanning Electrochemical Microscopy. Introduction and Principles, 138 (1989) 132–138.
- [24] R.C. Engstrom, C.M. Pharr, Scanning electrochemical microscopy, *Anal. Chem.* 61 (1989) 1099A-1104A. doi:10.1021/ac00194a002.
- [25] S. Bergner, Untersuchungen von Zellmonoschichten mittels Elektrochemischer Rastermikroskopie, 2013. <http://epub.uni-regensburg.de/28606> (accessed June 1, 2014).
- [26] C. Lee, C.J. Miller, A.J. Bard, Scanning Electrochemical Microscopy: Preparation of Submicrometer Electrodes, *Anal. Chem.* 63 (1991) 78–83. doi:10.1021/ac00001a016.
- [27] J.-M. Noël, J. Velmurugan, E. Gökmelçse, M. V. Mirkin, Fabrication, characterization, and chemical etching of Ag nanoelectrodes, *J. Solid State Electrochem.* 17 (2013) 385–389. doi:10.1007/s10008-012-1849-6.

- [28] C.G. Zoski, Ultramicroelectrodes: Design, fabrication, and characterization, *Electroanalysis*. 14 (2002) 1041–1051. doi:10.1002/1521-4109(200208)14:15/16<1041::AID-ELAN1041>3.0.CO;2-8.
- [29] A.L. Whitworth, D. Mandler, P.R. Unwin, Theory of scanning electrochemical microscopy (SECM) as a probe of surface conductivity, *Phys. Chem. Chem. Phys.* 7 (2005) 356–365. doi:10.1039/B407397E.
- [30] J. Kwak, A.J. Bard, Scanning electrochemical microscopy. Theory of the feedback mode, *Anal. Chem.* 61 (1989) 1221–1227. doi:10.1021/ac00186a009.
- [31] Y. Shao, M. V. Mirkin, Probing Ion Transfer at the Liquid/Liquid Interface by Scanning Electrochemical Microscopy (SECM), *J. Phys. Chem. B.* 102 (1998) 9915–9921. doi:10.1021/jp9828282.
- [32] C. Lefrou, A unified new analytical-approximation for positive feedback currents with a microdisk SECM tip, *J. Electroanal. Chem.* 592 (2006) 103–112. doi:10.1016/j.je;echem.2006.05.003.
- [33] R. Cornut, C. Lefrou, A unified new analytical approximation for negative feedback currents with a microdisk SECM tip, *J. Electroanal. Chem.* 608 (2007) 59–66. doi:10.1016/j.jelechem.2007.05.007.
- [34] C. Iffelsberger, T. Raith, H. Patrick, P. Vatsyayan, F.-M. Matysik, Trends in der elektrochemischen Rastermikroskopie, *Chrom+food FORUM*. 4 (2017) 20–22.
- [35] S. Bergner, P. Vatsyayan, F. Matysik, Recent advances in high resolution scanning electrochemical microscopy of living cells-a review., *Anal. Chim. Acta.* 775 (2013) 1–13. doi:10.1016/j.aca.2012.12.042.
- [36] C. Combellas, M. Fermigier, A. Fuchs, F. Kanoufi, Scanning electrochemical microscopy. Hydrodynamics generated by the motion of a scanning tip and its consequences on the tip current, *Anal. Chem.* 77 (2005) 7966–7975. doi:10.1021/ac0513358.
- [37] R. Cornut, S. Poirier, J. Mauzeroll, Forced convection during feedback approach curve measurements in scanning electrochemical microscopy: Maximal displacement velocity with a microdisk, *Anal. Chem.* 84 (2012) 3531–3537. doi:10.1021/ac203047d.
- [38] S. Kuss, D. Trinh, L. Danis, J. Mauzeroll, High-Speed Scanning Electrochemical Microscopy Method for Substrate Kinetic Determination: Method and Theory, *Anal. Chem.* 87 (2015) 8096–8101. doi:10.1021/acs.analchem.5b01268.

- [39] S. Kuss, C. Kuss, D. Trinh, S.B. Schougaard, J. Mauzeroll, Forced convection during scanning electrochemical microscopy imaging over living cells: Effect of topographies and kinetics on the microelectrode current, *Electrochim. Acta.* 110 (2013) 42–48. doi:10.1016/j.electacta.2013.03.149.
- [40] T. Raith, S. Wert, C. Iffelsberger, F.M. Matysik, Development and characterization of an electrochemical flow cell for scanning electrochemical microscopy, *Monatshefte Für Chemie - Chem. Mon.* 149 (2018) 1671-1677. doi:10.1007/s00706-018-2201-3.

3. Experimental

In the following, a general overview of software, instrumentation, materials and chemicals utilized for the presented research is given in alphabetical order. Furthermore, general procedures are described. Any specialized equipment and procedures are characterized in the individual chapters within the results section.

3.1 Software, instrumentation, materials, chemicals

Software

COMSOL Multiphysics (CFD module and mixer module)	COMSOL Multiphysics GmbH, Berlin, Germany
Motion Manager 5	Dr. Fritz Faulhaber GmbH & Co. KG, Schönaich, Germany
Microsoft Office 2016	Microsoft, Redmond, Washington, USA
Origin 2019	OriginLab, Northampton, Massachusetts, USA
SECM software 920C	920C, CH Instruments, Austin, Texas, USA

Instrumentation

electrical BL-DC-motor (2250S012BX4 CSD 3830)	Dr. Fritz Faulhaber GmbH & Co., KG, Schönaich, Germany
HPLC pump (6400 884)	Knauer, Berlin, Germany
isolation transformer (230/230 V-50Hz 550 VA)	Voltcraft, Hirschau, Germany
Milli-Q Advantage A10 system	Merck Millipore, Darmstadt, Germany
platinum disk electrode (d = 2 mm)	CH Instruments, Austin, Texas, USA
reference electrode (Ag/AgCl/3M KCl)	CH Instruments, Austin, Texas, USA
scanning electrochemical microscope 920C	CH Instruments, Austin, Texas, USA
soldering equipment (WE CP-20)	Weller, Wetzlar, Germany
wide stand microscope x100	PEAK, Bornheim-Roisdorf, Germany

Materials

circular level (1034)	Glas- und Meßtechnik GmbH, Wächtersbach, Germany
copper cables	Leonische Drahtwerke AG, Nürnberg, Germany
soda lime glass capillaries ($d_{\text{outer}} = 1.8 \text{ mm}$, $d_{\text{inner}} = 1.1 \text{ mm}$)	Glaswerke Ilmenau, Ilmenau, Germany
lapping foils (30, 10, 3, 0.3 micron)	Sigma-Aldrich, Seelze, Germany
platinum wires ($d_1 = 25 \text{ }\mu\text{m}$, $d_2 = 12.5 \text{ }\mu\text{m}$)	Goodfellow, Cambridge, Great Britain
thin-film electrodes	MicruX, Asturias, Spain
two-component epoxide adhesive glue	Uhu, Bühl, Germany

Chemicals

11-mercaptoundecanoic acid	Sigma-Aldrich, St. Louis, USA
di-sodium hydrogen phosphate dodecahydrate	Merck KGaA, Darmstadt, Germany
ferrocenemethanol	ABCR, Karlsruhe, Germany
glucose oxidase type VII from <i>Aspergillus niger</i>	Sigma-Aldrich, St. Louis, USA
N-(3-dimethylaminopropyl)-N'-ethylcarbodiimide hydrochloride	Sigma-Aldrich, St. Louis, USA
N-hydroxysuccinimide	Sigma-Aldrich, St. Louis, USA
potassium nitrate	Merck KGaA, Darmstadt, Germany
sodium dihydrogen phosphate monohydrate	Merck KGaA, Darmstadt, Germany

3.2 Electrochemical mediators

Ferrocenemethanol was used as electrochemical redox mediator for a majority of the conducted experiments. During heating at $T = 80\text{ }^{\circ}\text{C}$, milli-Q water was deaerated via nitrogen bubbling for $t = 1\text{ h}$. At room temperature, 0.2 M potassium nitrate as supporting electrolyte and 1.5 mM ferrocenemethanol were dissolved, followed by sonication at $T = 45\text{ }^{\circ}\text{C}$ for 30 min. After 24 h storage at room temperature, the mediator solution was ready to use. Any visible precipitates were removed via filtration prior to measurements.

Furthermore, phosphate buffer and ferrocenemethanol in phosphate buffer were used as mediator solutions during individual projects. Their detailed composition is given in the corresponding chapters within the results section.

3.3 Fabrication of ultramicroelectrodes

Platinum UMEs with diameters of 12.5 μm and 25 μm were fabricated according to literature [1–5]. Briefly, a soda lime glass capillary with $d_{outer} = 1.8 \text{ mm}$ and $d_{inner} = 1.1 \text{ mm}$ was pulled while heating it thermally. After removing the insulation of a copper cable at both ends, platinum wires with $d_1 = 25 \text{ }\mu\text{m}$ or $d_2 = 12.5 \text{ }\mu\text{m}$ were soldered to one end of the cable. For isolation, the electrode was placed inside the pulled glass capillary with the end of the platinum wire being located roughly 50 μm behind the narrowed opening of the capillary. After melting the tip of the capillary thermally, polishing was performed manually utilizing different-sized lapping foils with 30, 10, 3 or 0.3 micron grain size to expose the active electrode area and define the RG value. For mechanical relief, the copper cable was fixed on the glass capillary at the other side of the electrode utilizing a two-component epoxide adhesive glue. These procedures were monitored via an optical wide stand microscope. The fabrication process is schematically summed up in Figure 3.1. The quality and size of the UMEs were checked prior to measurements via cyclic voltammetry and probe approach curves as described in section 2.2.2.

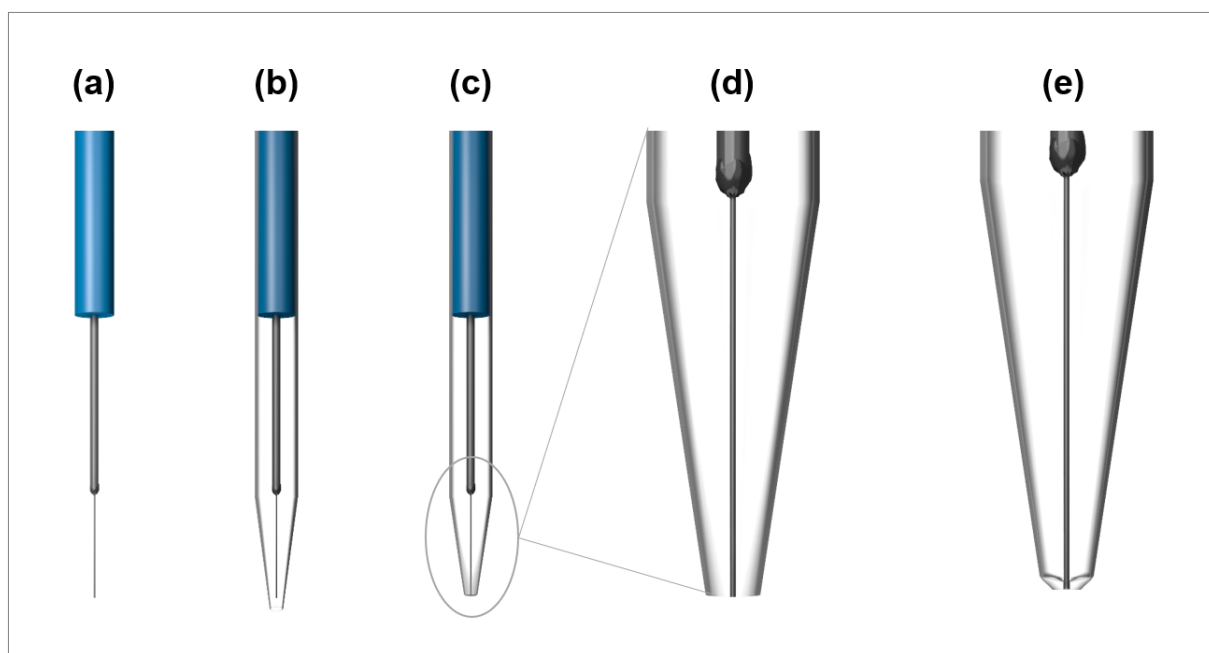


Figure 3.1: Schematic overview of the ultramicroelectrode fabrication process. After soldering a platinum wire to a copper cable (a) and placing it inside a pulled glass capillary (b), the tip of the capillary was closed by melting the glass (c, d). The active electrode area was exhibited via manual polishing (e).

3.4 Scanning electrochemical microscopy setup

A commercially available SECM 920C from CH Instruments was utilized for the majority of the conducted experiments. The system was placed inside a self-constructed Faraday cage on a vibration-cushioned workbench to prevent any electrical noises and mechanical vibrations. The electrochemical cell was mounted on a carrier platform positioned on three micrometer adjustment screws. By adjusting these screws, the cell was leveled utilizing a circular level prior to measurements. Fine adjustment was done via recording repetitive probe approach curves to ensure an orthogonal orientation between UME and substrate. After performing an initial probe approach, the UME was placed in a fixed plane 300 μm away from the surface. This procedure of recording an approach curve and retrieving the UME to reach the original plane was repeated at three triangular spots around the area of interest to determine the distance from the surface at these spots. The distance was adjusted using the micrometer screws and the protocol was repeated until a range of 3 μm height difference within the investigated area was obtained. For leveling and all other experiments, the UME was scanned using solely the stepper motors of the instrument. All imaging experiments were conducted in constant-height mode.

3.5 Electrochemical flow cells

Two electrochemical flow cells were developed to diversify the possibilities for the generation of forced convection within the SECM system next to the already established high-precision stirrer setup. To be able to use a flow cell for SECM, it had to fulfill multiple requirements such as accessibility of the cell interior for the UME, laminar flow through the cell and a circular flow of the mediator solution. The following section delivers an overview concerning the most important aspects for both the open slide cell design as well as the semi-closed cell design which met the requirements following different strategies. As cell material, polytetrafluoroethylene was chosen due to its inert characteristics. Both cell prototypes were fabricated in cooperation with the fine mechanical workshop of the Faculty of Chemistry and Pharmacy at the University of Regensburg.

The construction plan for the open slide cell design is depicted in Figure 3.2.

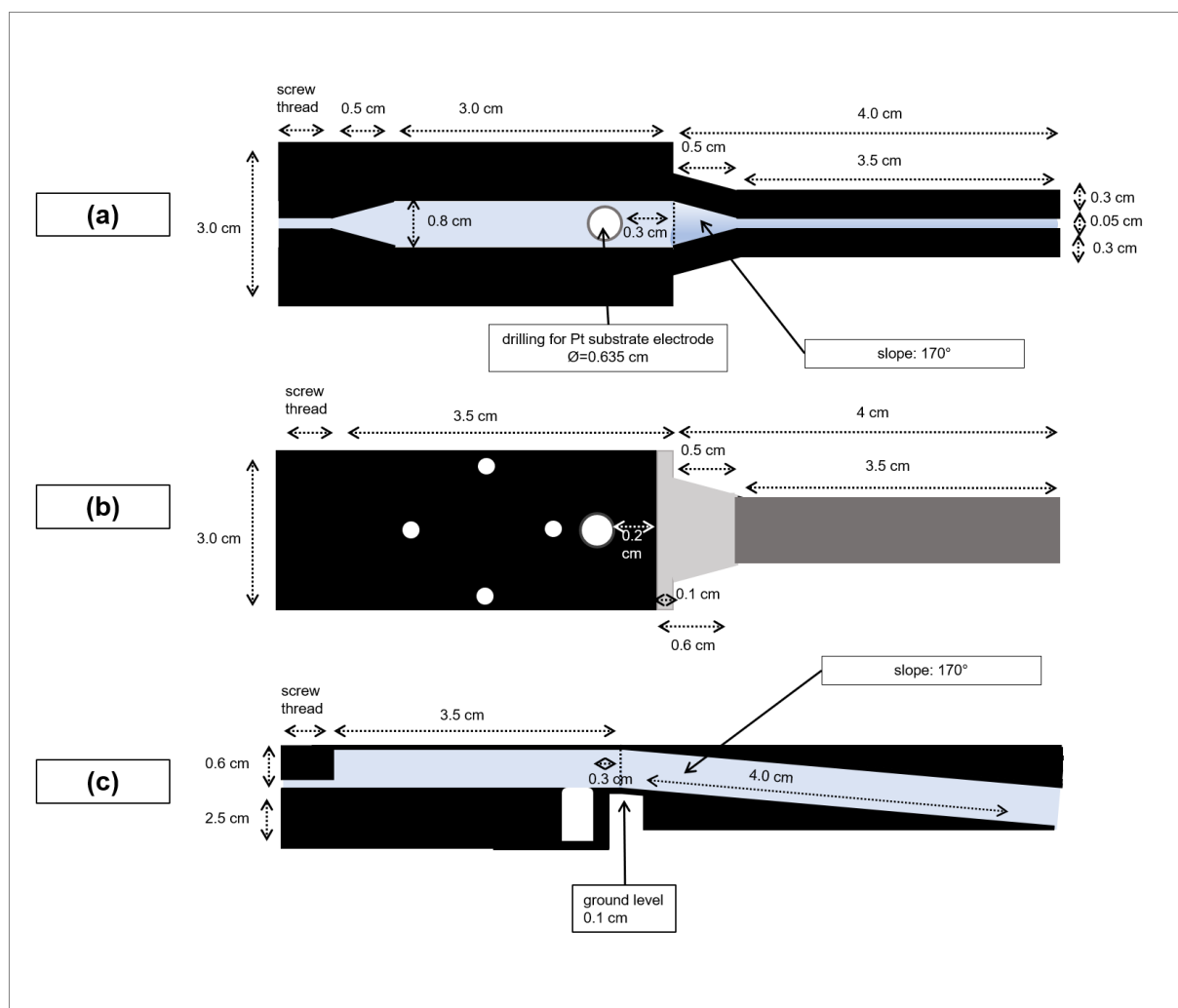


Figure 3.2: Construction plan for the open slide cell design in top view (a), bottom view (b) and side view (c).

The cell consisted of a main channel segment and a slide outlet for the outflow of solution. The slope of the slide had to be chosen very carefully in a way that the rate of outflow was sufficient to prevent any backflow of solution but small enough to prevent the cell from running dry. Moreover, the dimensions of the cutout and the slide had to be chosen in a way that the end of the slide could be placed in a beaker reservoir.

The semi-closed cell consisted of three parts with the first one being the main cell body exhibiting a channel section and a mediator reservoir as depicted in Figure 3.3.

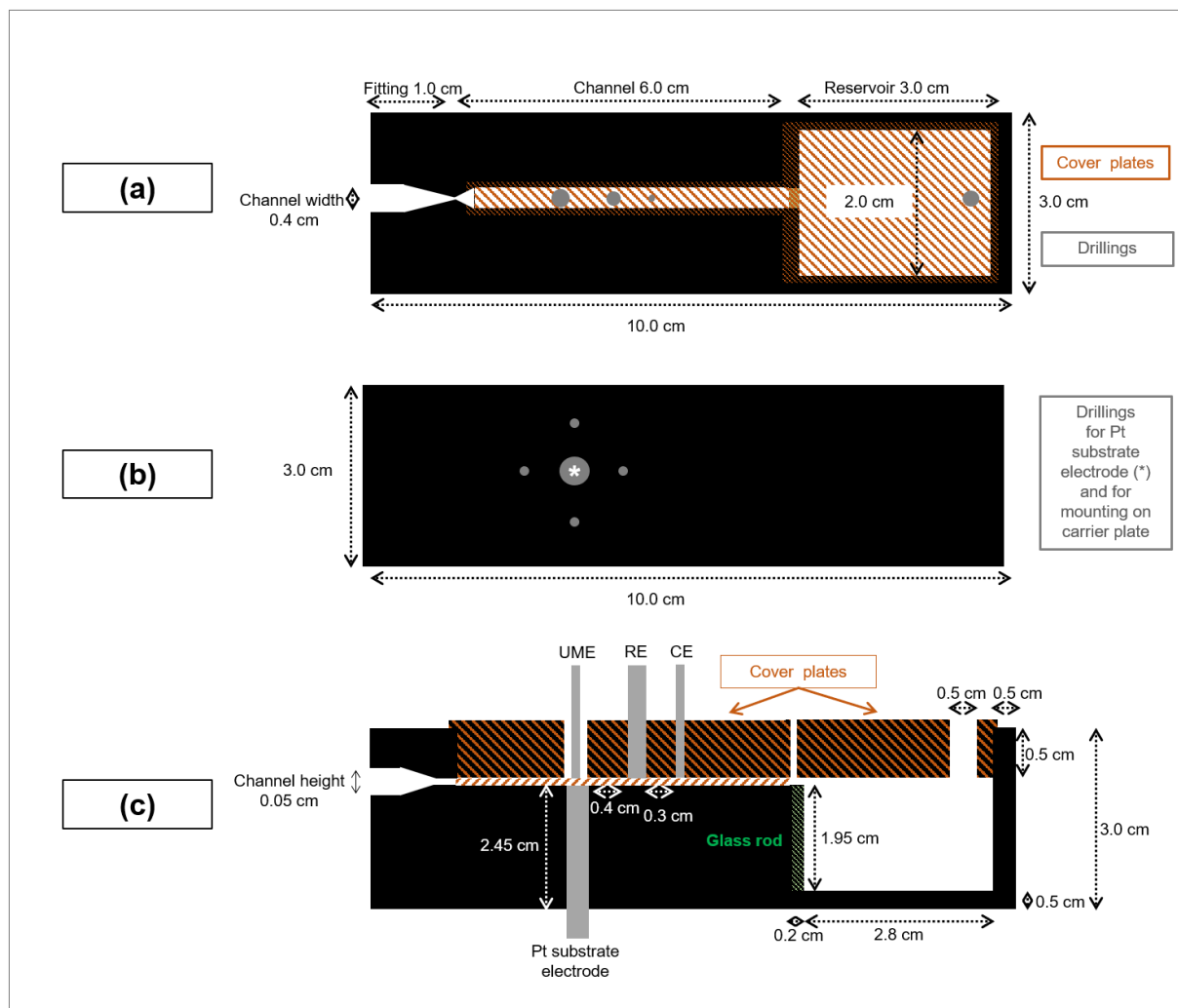


Figure 3.3: Construction plan for the main cell body of the semi-closed cell design in top view (a), bottom view (b) and side view (c).

Figure 3.4 presents the two cover plates necessary to fully ensemble the flow cell. The cover plate for the channel segment exhibited holes for positioning of the UME, RE and CE. The cover plate for the reservoir exhibited two holes, one for pumping out the mediator solution and one for pressure compensation purposes.

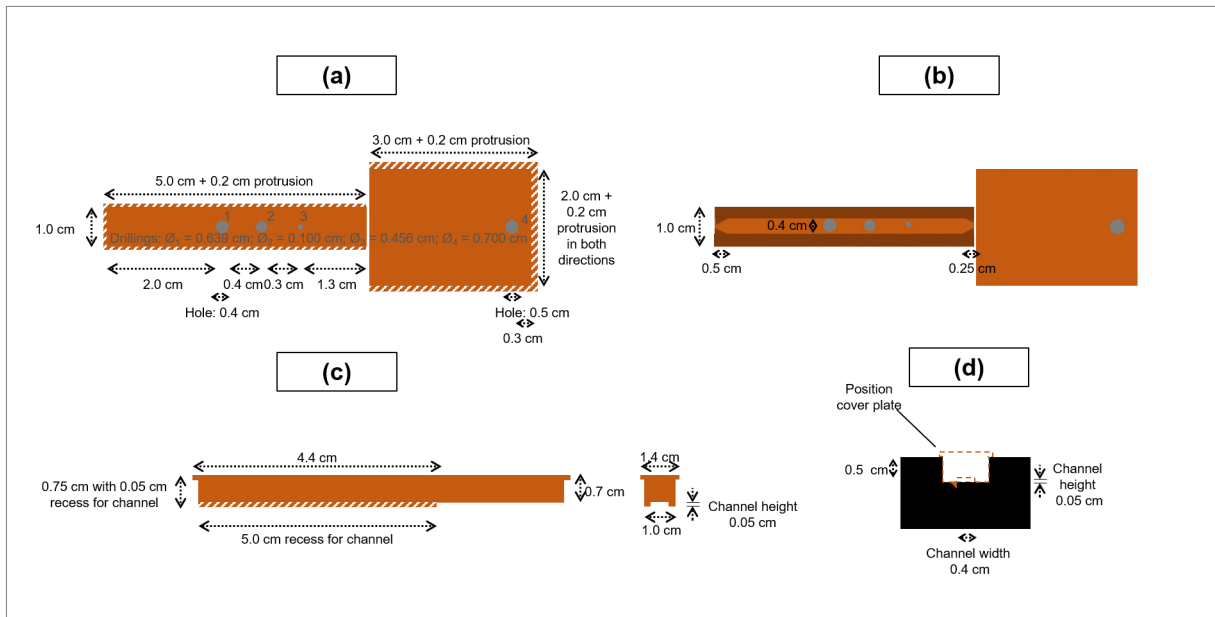


Figure 3.4: Construction plan for the two cover plates of the semi-closed cell design in top view (a), bottom view (b) and side view (c). The view along the channel is shown in (d).

Further details concerning both cell designs and their experimental characterization can be found in section 4.1.

References

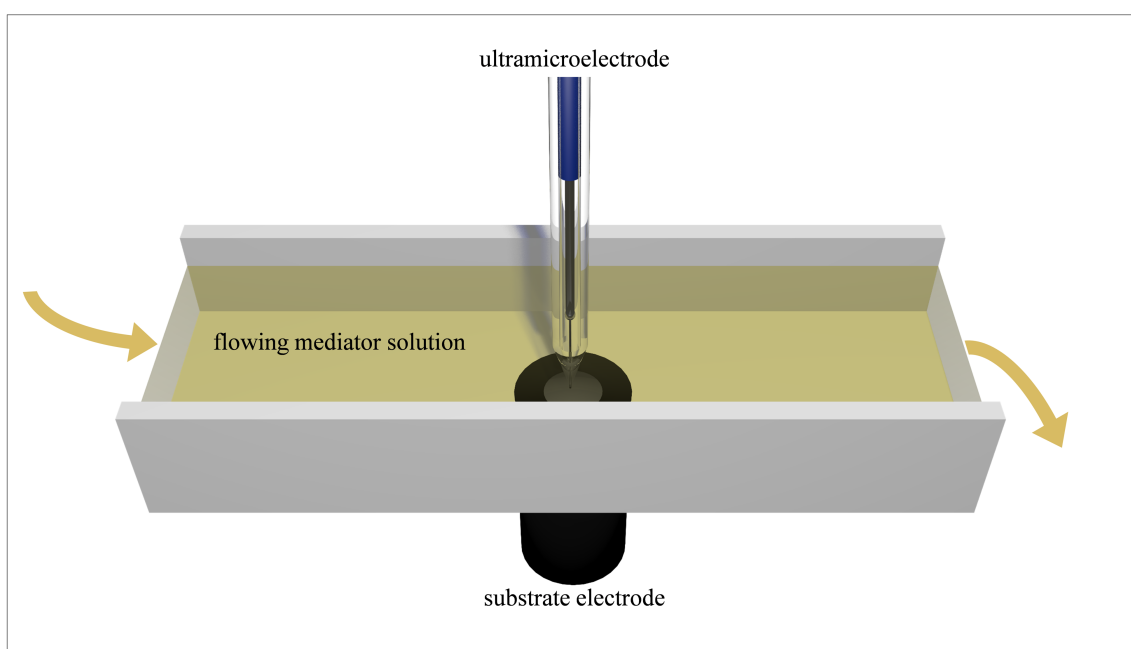
- [1] C. Lee, C.J. Miller, A.J. Bard, Scanning Electrochemical Microscopy: Preparation of Submicrometer Electrodes, *Anal. Chem.* 63 (1991) 78–83. doi:10.1021/ac00001a016.
- [2] C.G. Zoski, Ultramicroelectrodes: Design, fabrication, and characterization, *Electroanalysis*. 14 (2002) 1041–1051. doi:10.1002/1521-4109(200208)14:15/16<1041::AID-ELAN1041>3.0.CO;2-8.
- [3] S. Bergner, P. Palatzky, J. Wegener, F.M. Matysik, High-resolution imaging of nanostructured Si/SiO₂ substrates and cell monolayers using scanning electrochemical microscopy, *Electroanalysis*. 23 (2011) 196–200. doi:10.1002/elan.201000446.
- [4] P. Vatsyayan, C. Iffelsberger, C.C. Mayorga-Martinez, F.M. Matysik, Imaging of localized enzymatic peroxidase activity over unbiased individual gold nanowires by scanning electrochemical microscopy, *Anal. Methods*. 8 (2016) 6847–6855. doi:10.1039/c6ay01875k.
- [5] D. Polcari, P. Dauphin-Ducharme, J. Mauzeroll, Scanning Electrochemical Microscopy: A Comprehensive Review of Experimental Parameters from 1989 to 2015, *Chem. Rev.* 116 (2016) 13234–13278. doi:10.1021/acs.chemrev.6b00067.

4. Results and discussion

4.1 Development and characterization of electrochemical flow cells for hydrodynamic scanning electrochemical microscopy

Timo Raith, Stefan Wert, Christian Iffelsberger, Frank-Michael Matysik

Monatshefte für Chemie - Chemical Monthly 149 (2018) 1671–1677



Abstract

In the frame of this contribution, two electrochemical flow cells developed for scanning electrochemical microscopy (SECM) are presented. Forced convection was generated by a flow of the mediator solution through the flow cells. A description of the mandatory design aspects of the experimental flow cell setups is included.

Using a macroscopic working electrode as a substrate electrode, forced convection leads to the formation of a stable diffusion layer during amperometric experiments in contrast to a growing diffusion layer in quiescent solution. To characterize the effects of forced convection, the diffusion layer around a platinum substrate electrode integrated into the cells was

investigated utilizing chronoamperometric measurements and hydrodynamic SECM imaging in amperometric substrate generation-tip collection (SG/TC) mode. Both methods proved the stability and the time-independency of the diffusion layer. Mathematical simulations using COMSOL Multiphysics were computed in order to investigate the flow profile generated by the flowing mediator solution in the relevant region close to the substrate electrode.

In summary, two different electrochemical flow cells for SECM were developed and characterized. Both cell designs enabled steady state diffusion layer characteristics at a macroscopic substrate electrode offering interesting possibilities such as time-independent measurements in the context of the SG/TC mode.

4.1.1 Introduction

Scanning electrochemical microscopy (SECM) [1–3] is a versatile analytical method for imaging the electrochemical activity and topographic details of a surface [4–7]. It pertains to the field of scanning probe techniques and is therefore closely related to atomic force microscopy and electrochemical scanning tunneling microscopy. A common feature of these methods is that a small probe is scanned across the surface of interest in order to create a three-dimensional image that depends on properties and topography of the surface. In SECM, a miniaturized electrode – an ultramicroelectrode (UME) – is utilized as a probe.

When operating the SECM in the amperometric substrate generation-tip collection (SG/TC) mode, the species that is to be recorded at the UME (collector electrode) is initially generated at a second working electrode (generator electrode) placed below [8]. Problems arise if a macroscopic generator electrode is used due to the time-dependent growing diffusion layer of the generated species. This leads to a continuous change of the concentration profile detected at the UME, which is placed within the diffusion layer in a fixed distance from the generator substrate electrode.

A rather new approach regarding the performance of SECM experiments is to externally introduce forced convection to the system by stirring the electrolyte solution, as previously established by Matysik and coworkers [9]. Usually, in SECM convection is avoided and only a few experiments are described in literature where the convection is generated intrinsically via fast movement of the UME [10–16]. Iffelsberger et al. [9] observed that forced convection externally applied to the SECM cell led to an enhanced mass transfer, which resulted in increased currents and the formation of a stable diffusion layer with a defined thickness around a macroscopic electrode. Consequently, time-independent measurements in the context of the SG/TC mode were enabled, which offers interesting possibilities for future applications.

In the frame of this contribution, forced convection was generated by a flow of the mediator solution through electrochemical flow cells, developed especially for this purpose.

4.1.2 Results and discussion

Different cell designs and geometries were studied during the process of development in order to optimize the flow through the cells and to obtain a laminar flow with a constant liquid level. This was rather challenging in comparison to classical closed channel electrode configurations described by Compton and coworkers [17,18] as in SECM studies the accessibility of the cell interior is mandatory for the positioning of the UME.

Open slide cell design

To characterize the effects of the forced convection, the diffusion layer around an inserted platinum substrate electrode was investigated utilizing chronoamperometric measurements and hydrodynamic SECM imaging. Using the open slide cell design, the flow rate of the mediator solution for the generation of forced convection was set to $2.1 \text{ cm}^3 \text{ min}^{-1}$ in all experiments, as this was the optimum flow rate to ensure a constant liquid level.

Chronoamperometry

As can be seen in Figure 4.1.1, the current at the macroscopic electrode for the oxidation of ferrocenemethanol (FcMeOH) decreased in quiescent solution according to the Cottrell equation. This corresponded to the growing diffusion layer of the generated species. Hence, the concentration gradient of the electroactive species flattened with time, resulting in a decreased mass transfer towards the electrode.

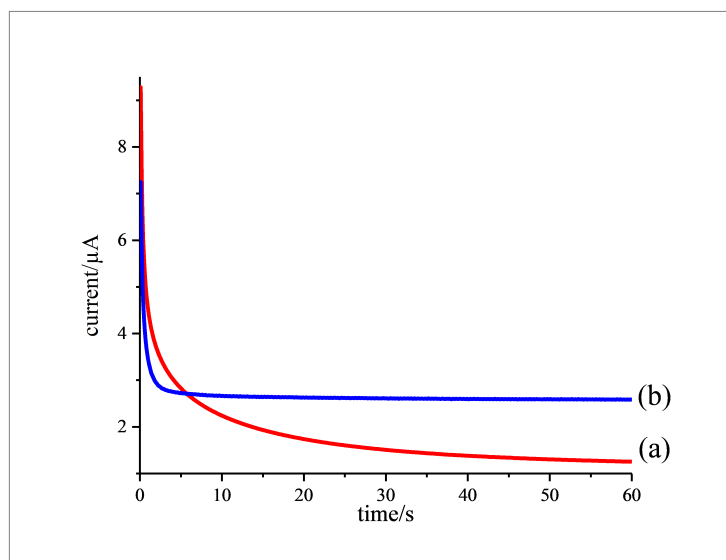


Figure 4.1.1: Chronoamperometric response of a 2 mm platinum disk substrate electrode for the oxidation of FcMeOH (1.5 mM with 0.2 M KNO_3) using the open cell design setup. $E_{\text{substrate}} = 0.45 \text{ V}$; (a) without forced convection; (b) with forced convection (flow rate: $2.1 \text{ cm}^3 \text{ min}^{-1}$).

In contrast, the application of forced convection led to a constant current response corresponding to the formation of a stable time-independent diffusion layer around the electrode. Furthermore, the current increased from $1.3 \mu\text{A}$ to $2.5 \mu\text{A}$ (mean values were calculated from the last 20 s of each measurement) due to an enhanced mass transfer inside the system. Thus, steady state diffusion layer characteristics at a macroscopic working electrode were generated by a flow of the mediator solution in the open slide cell design setup.

Hydrodynamic SECM imaging

To study the stability and uniformity of the diffusion layer, SECM images were recorded repetitively in SG/TC mode both in quiescent solution and with forced convection.

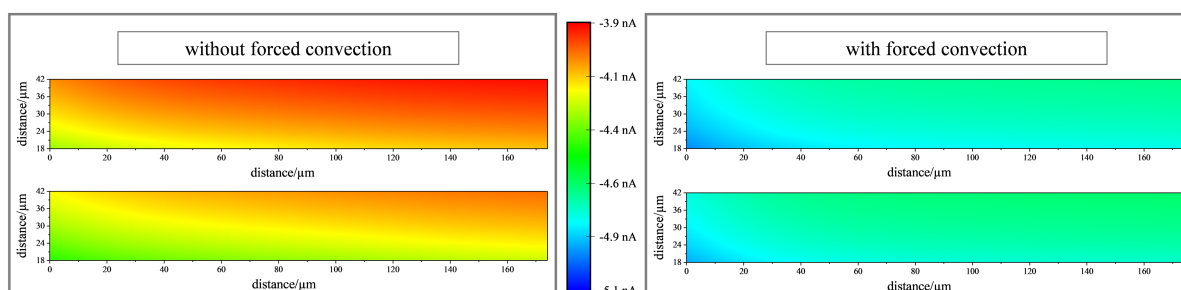


Figure 4.1.2.: Repetitive SECM images within the diffusion layer of a 2 mm platinum disk substrate electrode without and with forced convection in SG/TC mode using the open cell design setup. The UME (diameter: $25 \mu\text{m}$) was positioned $30 \mu\text{m}$ above the generator substrate electrode. $E_{\text{substrate}} = 0.45 \text{ V}$; $E_{\text{probe}} = 0 \text{ V}$; probe scan rate: $100 \mu\text{m s}^{-1}$; quiet time: 1 s; flow rate for convection: $2.1 \text{ cm}^3 \text{ min}^{-1}$. All measurements were performed in FcMeOH (1.5 mM with 0.2 M KNO_3).

As depicted in Figure 4.1.2, the images without forced convection differed from each other, corresponding to the growing diffusion layer and the changing concentration profile of the oxidized FcMeOH detected at the UME, which was placed within the diffusion layer in a fixed distance from the generator substrate electrode. For measurements with forced convection the reductive current at the UME increased due to the increased mass transfer within the system. Furthermore, almost identical images with a constant current throughout the recorded area were obtained corresponding to a stable diffusion layer. This proved the stability and uniformity of the steady state diffusion layer generated by a flow of the mediator solution in the open slide cell design setup.

Semi-closed cell design

As the open slide cell design was limited to the optimum flow rate of $2.1 \text{ cm}^3 \text{ min}^{-1}$, a second flow cell was developed on its basis in order to allow for the application of varying flow rates. Apart from characterizing the effects of the forced convection via chronoamperometric measurements and hydrodynamic SECM imaging, mathematical simulations using COMSOL Multiphysics were performed in order to investigate the flow profile in the relevant region close to the substrate electrode.

Flow profile analysis

Figure 4.1.3 displays the velocity profile computed via COMSOL Multiphysics for a flow rate of $9.0 \text{ cm}^3 \text{ min}^{-1}$, which represents the highest flow rate applied within this study.

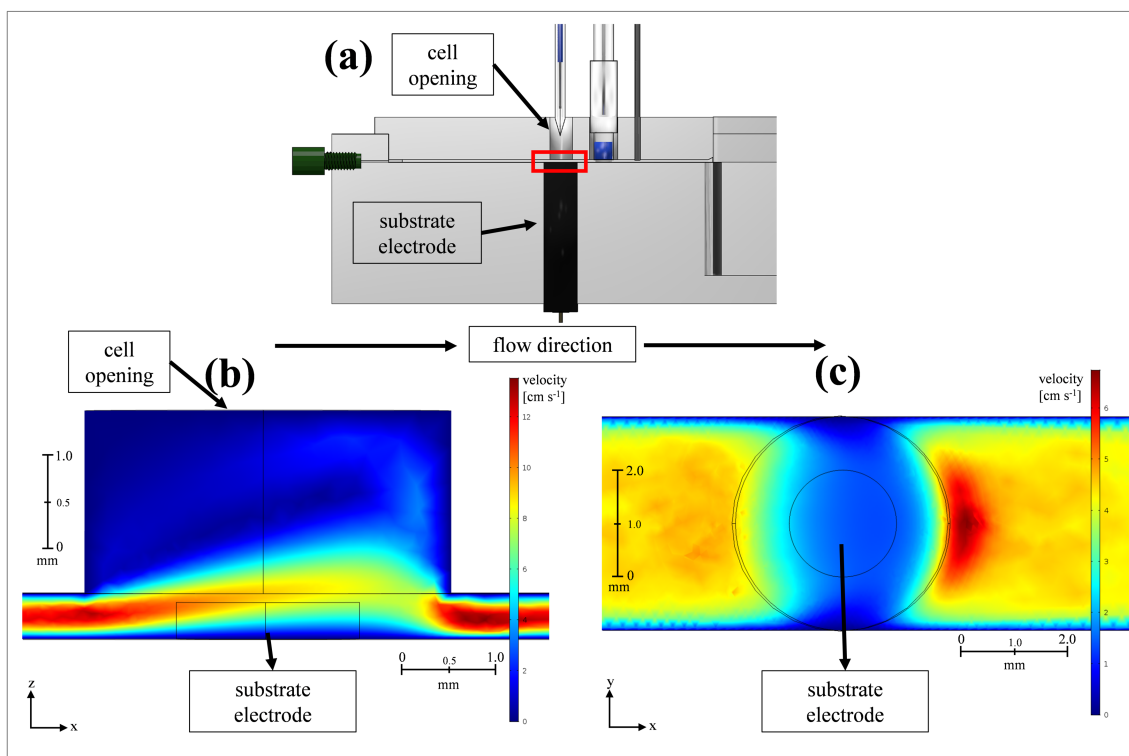


Figure 4.1.3: Mathematical simulations of the flow profile performed with COMSOL Multiphysics to characterize the convection generated by a flowing mediator solution in the relevant region close to the substrate electrode. The investigated area is marked red in scheme (a). False color plots of the velocity profile are shown in side view (b) and in top view 50 μm above the substrate (c). The flow rate of the mediator solution for the simulations was set to $9.0 \text{ cm}^3 \text{ min}^{-1}$.

As expected, the side view in Figure 4.1.3 (b) shows that the highest velocities were observed in the center of the closed channel segments on both sides of the cylindrical cavity, which represented the hole for positioning of the UME. The incoming liquid streamed upwards in the area of the cell opening covering the additional space available. A perturbed pattern in the flow profile was visible around 1 mm above the substrate electrode, which was integrated into the ground of the flow cell. Nevertheless, the velocity was quite uniform in a distance to the electrode where SECM experiments are usually performed ($< 100 \mu\text{m}$). The same observation was made from the top view presented in Figure 4.1.3 (c), which showed that at a height of $50 \mu\text{m}$ a constant velocity profile was predicted within the active area of the electrode. Consequently, the simulations indicated that a constant convective environment was to be expected in the relevant region above the substrate electrode.

Chronoamperometry

As depicted in Figure 4.1.4, chronoamperometric measurements were performed at flow rates of $1.0 \text{ cm}^3 \text{ min}^{-1}$, $3.0 \text{ cm}^3 \text{ min}^{-1}$, $5.0 \text{ cm}^3 \text{ min}^{-1}$, $7.0 \text{ cm}^3 \text{ min}^{-1}$ and $9.0 \text{ cm}^3 \text{ min}^{-1}$ to investigate the flow behavior within the semi-closed cell design setup.

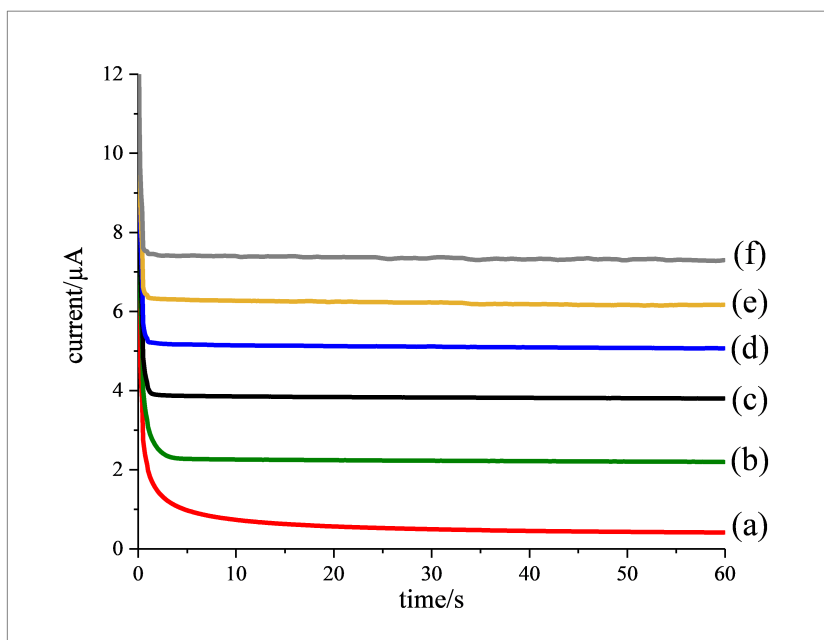


Figure 4.1.4: Chronoamperometric response of a 2 mm platinum disk substrate electrode for the oxidation of FcMeOH (1.5 mM with 0.2 M KNO_3) using the semi-closed cell design. $E_{\text{substrate}} = 0.45 \text{ V}$; (a) without forced convection; flow rates for convection: (b) $1.0 \text{ cm}^3 \text{ min}^{-1}$, (c) $3.0 \text{ cm}^3 \text{ min}^{-1}$, (d) $5.0 \text{ cm}^3 \text{ min}^{-1}$, (e) $7.0 \text{ cm}^3 \text{ min}^{-1}$, (f) $9.0 \text{ cm}^3 \text{ min}^{-1}$.

Likewise during measurements using the open slide cell design, the current at the macroscopic electrode for the oxidation of FcMeOH decreased in quiescent solution. The application of forced convection led to a constant current response due to the formation of a stable time-independent diffusion layer around the electrode. Furthermore, the current increased from $2.2 \text{ } \mu\text{A}$ to $7.4 \text{ } \mu\text{A}$ (mean values were calculated from the last 20 s of each measurement) with increasing the flow rate from $1.0 \text{ cm}^3 \text{ min}^{-1}$ to $9.0 \text{ cm}^3 \text{ min}^{-1}$ because of an enhanced mass transfer inside the system. This equaled an increase in the mass transport coefficient of FcMeOH from $5 \text{ } \mu\text{m s}^{-1}$ to $16 \text{ } \mu\text{m s}^{-1}$. Thus, steady state diffusion layer characteristics with varying limiting currents corresponding to the varying flow rates were generated by a flow of the mediator solution in the semi-closed cell design setup. As already described in literature [9], the varying limiting currents correlated with different thicknesses of the diffusion layer.

Hydrodynamic SECM imaging

In order to characterize the diffusion layer at the substrate electrode with respect to its uniformity and stability under different convective conditions, SECM images were recorded repetitively in SG/TC mode in quiescent solution and with applied flow rates of $1.0 \text{ cm}^3 \text{ min}^{-1}$, $5.0 \text{ cm}^3 \text{ min}^{-1}$ and $9.0 \text{ cm}^3 \text{ min}^{-1}$.

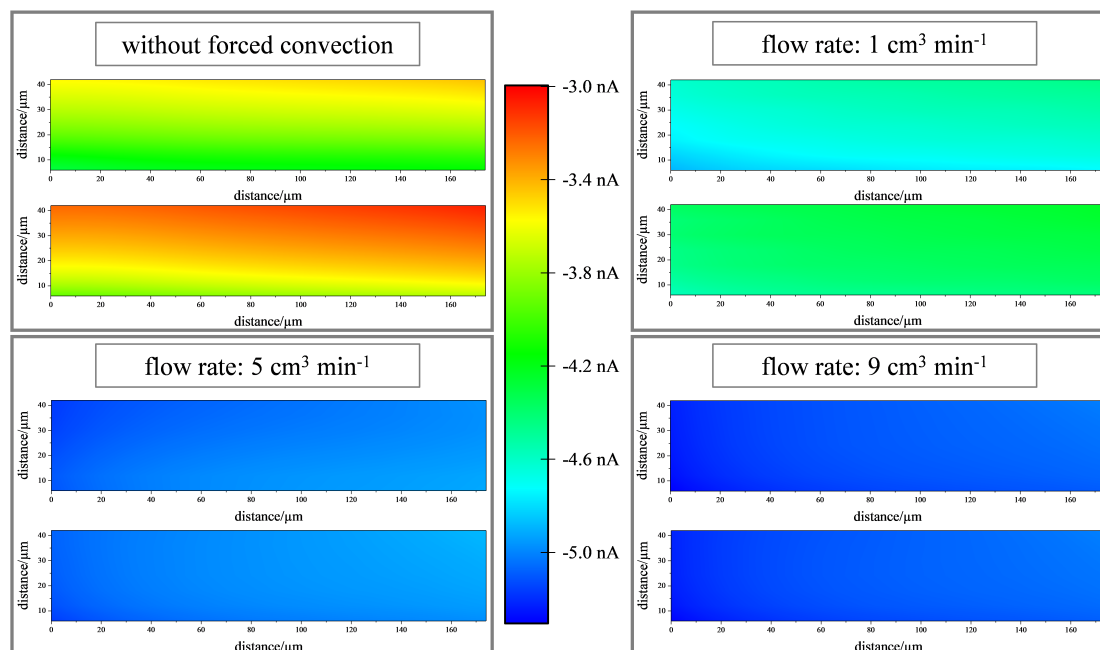


Figure 4.1.5: Repetitive SECM images within the diffusion layer of a 2 mm platinum disk substrate electrode without and with different magnitudes of forced convection in SG/TC mode using the semi-closed cell design. The UME (diameter: $25 \mu\text{m}$) was positioned $30 \mu\text{m}$ above the generator substrate electrode. $E_{\text{substrate}} = 0.45 \text{ V}$; $E_{\text{probe}} = 0 \text{ V}$; probe scan rate: $33 \mu\text{m s}^{-1}$; quiet time: 1 s; flow rates for convection: $1.0 \text{ cm}^3 \text{ min}^{-1}$, $5.0 \text{ cm}^3 \text{ min}^{-1}$, $9.0 \text{ cm}^3 \text{ min}^{-1}$. All measurements were performed in FcMeOH (1.5 mM with 0.2 M KNO_3).

As illustrated in Figure 4.1.5, the images without forced convection differed from each other, corresponding to the growing diffusion layer. Initially a current of -3.8 nA was measured with the SECM probe which decreased to -3.0 nA by end of the measurement. When a flow rate of $1.0 \text{ cm}^3 \text{ min}^{-1}$ was applied to the system, the current increased and remained nearly constant within the measurement, but still differed slightly between the measurements. A further increase in flow rate led to almost identical images with a constant and increased current throughout the recorded area corresponding to a stable diffusion layer.

This proved the stability and uniformity of the steady state diffusion layer generated by a flow of the mediator solution at different flow rates. Moreover, the reductive probe current in SG/TC experiments increased with increasing flow rate due to the increased mass transfer to and from the macroscopic generator electrode.

4.1.3 Conclusion

Two different electrochemical flow cells for SECM were developed and characterized regarding the effects of a flowing mediator solution. While the open slide cell design was limited to one specific flow rate, it was possible to refine the setup and create a semi-closed cell design, which enabled the application of varying flow rates ranging from $1.0 \text{ cm}^3 \text{ min}^{-1}$ to $9.0 \text{ cm}^3 \text{ min}^{-1}$.

It was shown that the forced convection generated with both flow cell designs enabled steady state diffusion layer characteristics with increased currents due to an increased mass transfer at a macroscopic substrate electrode. Applying the highest flow rate of $9.0 \text{ cm}^3 \text{ min}^{-1}$, a mass transport coefficient of $16 \mu\text{m s}^{-1}$ was calculated for FcMeOH. Hence, more intensive convection was generated in comparison to the previously published stirrer setup where a coefficient of $13 \mu\text{m s}^{-1}$ was obtained [9].

By varying the flow rate in the setup of the semi-closed cell design it was also possible to adjust the thickness of the diffusion layer according to the desired purpose as it is dependent on the magnitude of the convection. COMSOL simulations were computed to investigate the uniformity of the flow profile in the relevant region close to the substrate electrode for different flow rates.

Both flow cell designs facilitated the recording of reproducible SECM images in SG/TC mode, which is difficult to obtain in quiescent solution. Consequently, the generation of a constant convective environment was established, which promises interesting possibilities for future applications such as time-independent measurements in the context of the SG/TC mode.

4.1.4 Experimental

Chemicals

For all experiments ferrocenemethanol (99%, ABCR, Karlsruhe, Germany) with a concentration of 1.5 mM was used as mediator. An aqueous solution was prepared with Milli-Q water (Milli-Q Advantage A10 system, Merck Millipore, Darmstadt, Germany). As supporting electrolyte, potassium nitrate (KNO_3 , analytical grade, Merck KGaA, Darmstadt, Germany) with a concentration of 0.2 M was added.

Experimental setup

The electrochemical flow cells consisting of polytetrafluorethylene (PTFE) were fabricated at the fine mechanical workshop of the Faculty of Chemistry and Pharmacy at the University of Regensburg.

Open slide cell design

Figure 4.1.6 displays the first manufactured electrochemical flow cell for SECM and gives an overview of the most important aspects of the open slide cell design. The accessibility of the cell interior was facilitated by leaving the cell open on top, while a constant liquid level was ensured by the slide at the end of the cell.

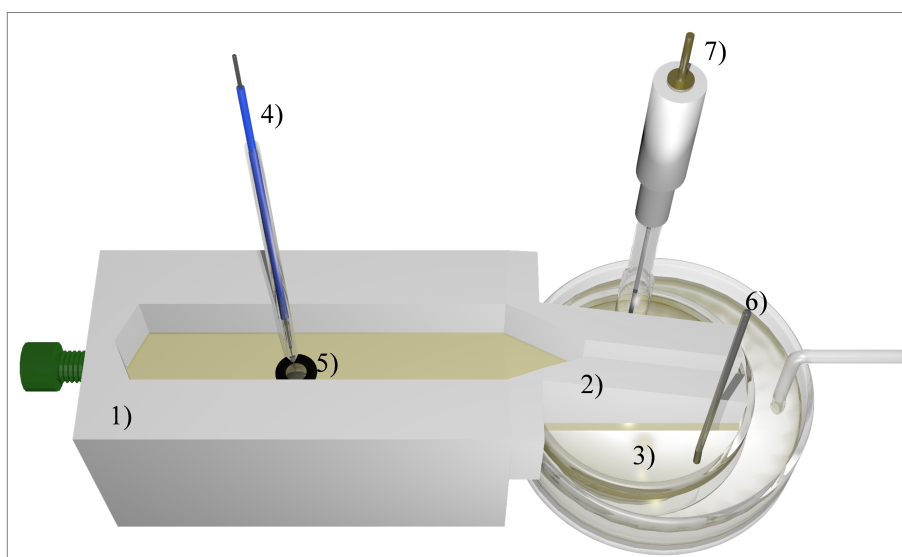


Figure 4.1.6: Schematic representation of the open slide cell design with a bend between the cell (1) and the slide (2). The slide was immersed into a reservoir (3) enhancing the outward flow and thus ensuring a constant liquid level. An UME (4) with a diameter of 25 μm was used as SECM probe. A platinum substrate electrode (5) with a diameter of 2 mm was integrated into the cell. A platinum wire (6) acted as counter electrode, while an Ag/AgCl/sat. KCl electrode was used as reference electrode (7).

The cell exhibited a length of 3.5 cm and a width of 0.8 cm, while the slide was 4 cm long and was narrowed to a width of 0.05 cm after 0.5 cm. The slide was tilted by an angle of 10° to enhance the outward flow of the liquid at the end of the cell. Starting from a beaker, the mediator solution was pumped into the electrochemical cell with an HPLC pump (model HPLC 6400 884, Knauer, Berlin, Germany), which was placed outside the SECM instrument. A constant flow was achieved as soon as the liquid had contact to a reservoir filled with the same solution. The liquid level inside the reservoir remained constant due to a continuous flow-off into a second reservoir placed below. From this second reservoir, the liquid was pumped back

into the beaker using a peristaltic pump (model IPS 16, Ismatec, Zurich, Switzerland) in order to enable circulation of the mediator solution. Consequently, generating a constant liquid level with a cell open on top was enabled by the slide at the end of the cell and its continuous contact to the solution in the reservoir.

One limitation of the open cell design was the outward flow from the cell depending on the dimensions of the slide. This fact restricted its applicability to the optimum flow rate of $2.1 \text{ cm}^3 \text{ min}^{-1}$. Hence, setup and design were optimized, and a second cell was developed in order to facilitate the variation between a range of flow rates.

Semi-closed cell design

Figure 4.1.7 illustrates the second manufactured electrochemical flow cell for SECM and gives an overview of the most important aspects of the semi-closed cell design. In comparison to the open cell design, the cell was closed from all sides except for a small cavity, which enabled positioning of the UME.

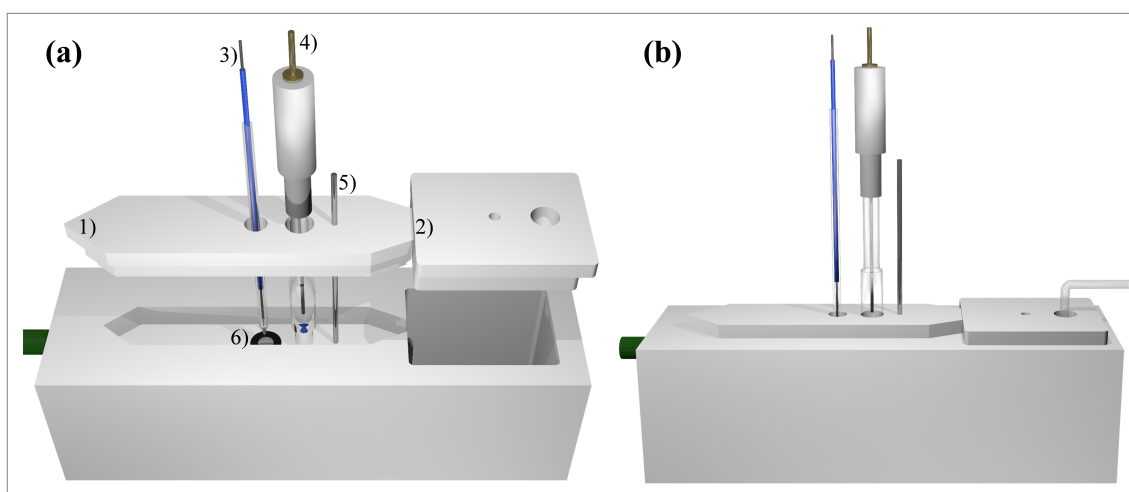


Figure 4.1.7: (a) Schematic representation of the semi-closed cell design consisting of the main cell body and cover plates for the cell (1) and the reservoir (2). Cover plate 1 exhibited holes for the positioning of a $25 \mu\text{m}$ UME (3), an Ag/AgCl/sat. KCl reference electrode (4) and a counter electrode (5). A platinum substrate electrode (6) with a diameter of 2 mm was integrated into the cell. Cover plate 2 exhibited holes for pumping out the mediator solution and for pressure compensation. The assembled experimental setup is shown in part (b).

The whole setup consisted of three PTFE parts. The main cell body exhibited a channel section (width: 0.4 cm, length: 5.7 cm, height: 0.05 cm) and a recess serving as reservoir for the outflowing mediator solution. The second component was a cover plate for the cell including three holes for the electrodes. The hole for the UME was located above a platinum substrate electrode integrated into the cell, which enabled scanning of the UME across its surface. No

leakage of liquid was caused by the cavity if sufficient outflow was ensured at the end of the channel section. The holes for the reference electrode and the counter electrode fitted the dimensions of the corresponding electrodes and were located downstream of the UME to prevent disturbances of the flow. The setup was completed by another plate, which covered the reservoir and featured two holes, one for pumping out the solution and one for pressure compensation purposes. The semi-closed cell design allowed for the application of flow rates ranging from $1.0 \text{ cm}^3 \text{ min}^{-1}$ to $9.0 \text{ cm}^3 \text{ min}^{-1}$.

Experimental procedures

SECM experiments were performed with a commercially available SECM 920C from CH Instruments (Austin, Texas). A platinum substrate electrode ($d = 2 \text{ mm}$, CH Instruments, Austin, Texas) integrated into the flow cells was polished with $0.3 \mu\text{m}$ alumina on polishing cloth (TexMed, Buehler, Lake Bluff) prior to each measurement session. A platinum wire with a diameter of 0.5 mm and a length of 2 cm was used as counter electrode and an Ag/AgCl/sat. KCl electrode as reference electrode. All potentials mentioned refer to this reference system. An UME with a diameter of $25 \mu\text{m}$ and a RG value of 10 fabricated according to Bard and co-workers [19] with certain modifications as previously described [9] was utilized for all measurements. The UME was checked prior to each measurement session in terms of quality and size.

Chronoamperometry

The chronoamperometric response of the macroscopic platinum substrate electrode was recorded for the oxidation of FcMeOH in order to investigate the diffusion layer characteristics at the macroscopic substrate electrode generated by a flow of the mediator solution through the respective cell. The potential of the substrate electrode $E_{\text{substrate}}$ was set to 0.45 V . Using the open cell design, a flow rate of $2.1 \text{ cm}^3 \text{ min}^{-1}$ was applied, while $1.0 \text{ cm}^3 \text{ min}^{-1}$, $3.0 \text{ cm}^3 \text{ min}^{-1}$, $5.0 \text{ cm}^3 \text{ min}^{-1}$, $7.0 \text{ cm}^3 \text{ min}^{-1}$ and $9.0 \text{ cm}^3 \text{ min}^{-1}$ were used in combination with the semi-closed cell design.

Hydrodynamic SECM imaging

To further characterize the effects of the forced convection, the stability and uniformity of the diffusion layer was studied via hydrodynamic SECM imaging in SG/TC mode. For this purpose, the UME was positioned within the diffusion layer of the generator substrate electrode

(distance to electrode: 30 μm) and an area of 180 μm times 40 μm was imaged repetitively without and with forced convection, respectively. $E_{\text{substrate}}$ was set to 0.45 V for the oxidization of FcMeOH, while a potential of 0 V was chosen for the reduction of the generated species at the UME (E_{probe}). Using the open cell design, a flow rate of 2.1 $\text{cm}^3 \text{min}^{-1}$ was applied, while 1.0 $\text{cm}^3 \text{min}^{-1}$, 5.0 $\text{cm}^3 \text{min}^{-1}$ and 9.0 $\text{cm}^3 \text{min}^{-1}$ were used in combination with the semi-closed cell design.

Flow profile analysis via COMSOL Multiphysics

Mathematical simulations of the flow profile using COMSOL Multiphysics (CFD Module) were performed for the semi-closed cell in order to investigate the flow profile generated by the flowing mediator solution at different flow rates. Constant flow velocities were required in the area of the substrate electrode, resulting in a uniform diffusion layer. The channel dimensions of the model for the simulations were 6.0 cm in length, 0.4 cm in width and 0.05 cm in height with a cylindrical cavity above the substrate electrode representing the hole for positioning of the UME. The model was treated as a body of water while the side walls were defined as PTFE with no slip as boundary condition. The front wall and the end wall of the channel were defined as inlet and outlet. The cylindrical cavity was also defined as an outlet, but without liquid passing through. In this way, a constant liquid level above the substrate was simulated corresponding to the situation during an experiment. The presence of the SECM probe was excluded from the simulations. Flow rates of 1.0 $\text{cm}^3 \text{min}^{-1}$, 5.0 $\text{cm}^3 \text{min}^{-1}$ and 9.0 $\text{cm}^3 \text{min}^{-1}$ were computed covering the range of flow rates applied during SECM experiments.

References

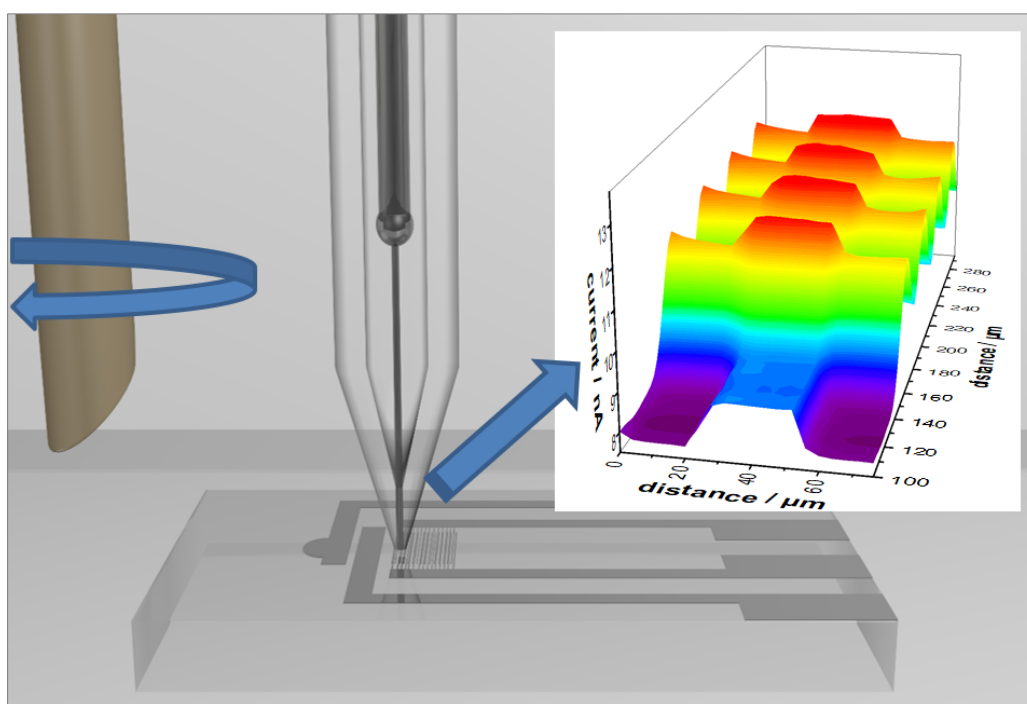
- [1] Kwak J, Bard AJ (1989) Scanning electrochemical microscopy. Apparatus and two-dimensional scans of conductive and insulating substrates. *Anal Chem* 61:1794–1799. <https://doi.org/10.1021/ja3106434>.
- [2] A.J. Bard, F.R.F. Fan, J. Kwak, O. Lev, Scanning electrochemical microscopy. Introduction and principles, *Anal. Chem.* 61 (1989) 132–138. doi:10.1021/ac00177a011.
- [3] H.Y. Liu, F.R.F. Fan, C.W. Lin, A.J. Bard, Scanning electrochemical and tunneling ultramicroelectrode microscope for high-resolution examination of electrode surfaces in solution, *J. Am. Chem. Soc.* 108 (1986) 3838–3839. doi:10.1021/ja00273a054.
- [4] Bergner S, Vatsyayan P, Matysik F (2013) Recent advances in high resolution scanning electrochemical microscopy of living cells--a review. *Anal Chim Acta* 775:1–13. <https://doi.org/10.1016/j.aca.2012.12.042>.
- [5] Polcari D, Dauphin-Ducharme P, Mauzeroll J (2016) Scanning Electrochemical Microscopy: A Comprehensive Review of Experimental Parameters from 1989 to 2015. *Chem Rev* 116:13234–13278. <https://doi.org/10.1021/acs.chemrev.6b00067>.
- [6] Bard AJ, Mirkin M V. (2012) Scanning Electrochemical Microscopy Second Edition.
- [7] Wiesendanger R (1994) Scanning Probe Microscopy and Spectroscopy: Methods and Applications. Cambridge University Press.
- [8] Wittstock G, Burchardt M, Pust SE, et al (2007) Elektrochemische Rastermikroskopie zur direkten Abbildung von Reaktionsgeschwindigkeiten. *Angew Chemie* 119:1604–1640. <https://doi.org/10.1002/ange.200602750>.
- [9] Iffelsberger C, Vatsyayan P, Matysik F (2017) Scanning Electrochemical Microscopy with Forced Convection Introduced by High-Precision Stirring. *Anal Chem* 89:1658–1664. <https://doi.org/10.1021/acs.analchem.6b03764>.
- [10] Combellas C, Fermigier M, Fuchs A, Kanoufi F (2005) Scanning electrochemical microscopy. Hydrodynamics generated by the motion of a scanning tip and its consequences on the tip current. *Anal Chem* 77:7966–7975. <https://doi.org/10.1021/ac0513358>.
- [11] Kottke PA, Fedorov AG (2005) Advective and transient effects in combined AFM/SECM operation. *J Electroanal Chem* 583:221–231. <https://doi.org/10.1016/j.jelechem.2005.06.017>.

- [12] Nkuku C a, LeSuer RJ (2007) Electrochemistry in deep eutectic solvents. *J Phys Chem B* 111:13271–13277. <https://doi.org/10.1021/jp075794j>.
- [13] Cornut R, Poirier S, Mauzeroll J (2012) Forced convection during feedback approach curve measurements in scanning electrochemical microscopy: Maximal displacement velocity with a microdisk. *Anal Chem* 84:3531–3537. <https://doi.org/10.1021/ac203047d>.
- [14] Kuss S, Kuss C, Trinh D, et al (2013) Forced convection during scanning electrochemical microscopy imaging over living cells: Effect of topographies and kinetics on the microelectrode current. *Electrochim Acta* 110:42–48. <https://doi.org/10.1016/j.electacta.2013.03.149>.
- [15] Kuss S, Trinh D, Danis L, Mauzeroll J (2015) High-Speed Scanning Electrochemical Microscopy Method for Substrate Kinetic Determination: Method and Theory. *Anal Chem* 87:8096–8101. <https://doi.org/10.1021/acs.analchem.5b01268>.
- [16] Edwards MA, Whitworth AL, Unwin PR (2011) Quantitative analysis and application of tip position modulation-scanning electrochemical microscopy. *Anal Chem* 83:1977–1984. <https://doi.org/10.1021/ac102680v>.
- [17] Cooper JA, Compton RG (1998) Channel Electrodes - A Review. *Electroanalysis* 10:141–155. [https://doi.org/10.1002/\(SICI\)1521-4109\(199803\)10:3<141::AID-ELAN141>3.0.CO;2-F](https://doi.org/10.1002/(SICI)1521-4109(199803)10:3<141::AID-ELAN141>3.0.CO;2-F).
- [18] Fisher AC, Compton RG (1991) Chronoamperometry at channel electrodes: A general computational approach. *J Phys Chem* 95:7538–7542. <https://doi.org/10.1021/j100172a075>.
- [19] Lee C, Miller CJ, Bard AJ (1991) Scanning Electrochemical Microscopy: Preparation of Submicrometer Electrodes. *Anal Chem* 63:78–83. <https://doi.org/10.1021/ac00001a016>.

4.2 Impacts of forced convection generated via high precision stirring on scanning electrochemical microscopy experiments in feedback mode

Timo Raith, Christian Iffelsberger, Preety Vatsyayan, Frank-Michael Matysik

Electroanalysis 31 (2019) 273-281



Abstract

In this study, the effects of forced convection on scanning electrochemical microscopy (SECM) experiments in feedback mode using ferrocenemethanol as redox mediator are presented. Forced convection, which enhances the mass transfer inside the system, was generated via an electrical high precision stirrer integrated into the SECM setup. A thin-film interdigitated array electrode serving as model substrate was investigated with probe scan curves in z-direction and SECM imaging in constant-height mode utilizing ultramicroelectrodes (UME) with diameters (d_{probe}) of 25 μm and 12.5 μm . It was found that forced convection increased the overall current during SECM imaging without distorting distinctive features of the imaged structure when working with a 25 μm UME at substrate-to-tip distances of 14 μm and 11 μm . Furthermore, the electrochemical contrast was improved under hydrodynamic conditions for a substrate-to-tip distance of 11 μm and scan rates of 5 $\mu\text{m s}^{-1}$, 10 $\mu\text{m s}^{-1}$, 20 $\mu\text{m s}^{-1}$ and

$40 \mu\text{m s}^{-1}$. When further decreasing the gap between the UME and the substrate to $9 \mu\text{m}$, almost no effects of the forced convection were observed. Consequently, for a $25 \mu\text{m}$ UME, forced convection led to higher currents and improved performance during SECM experiments in feedback mode at substrate-to-tip distances of $14 \mu\text{m}$ and $11 \mu\text{m}$, whereas no effects were observed for a $12.5 \mu\text{m}$ UME at a distance of $8 \mu\text{m}$.

4.2.1 Introduction

Since its introduction by Allen J. Bard and coworkers [1, 2] in 1989, scanning electrochemical microscopy (SECM) has evolved into a versatile analytical method for mapping the electrochemical activity and topography of a surface [3]. The non-invasive method belonging to the field of scanning probe techniques facilitates high spatial resolution and can be used to investigate both conducting and nonconducting material [4]. In SECM a miniaturized electrode, which is termed ultramicroelectrode (UME), is utilized as a probe. When the instrument is operated in amperometric mode, an electroactive species is either oxidized or reduced at the UME which is scanned across the examined surface area. The electrochemical conversion results in a faradaic current which can be associated with distinctive features of the substrate.

In electrochemical applications, apart from the electron transfer reaction, the mass transfer towards and away from the electrode has to be considered as one of the most important aspects. Mass transfer can be accomplished by diffusion, migration and convection [5]. Diffusion due to the formation of a concentration gradient is a direct result of the electrochemical reaction, while the influence of migration is mostly suppressed by addition of an inert supporting electrolyte. For the third component both forced and natural convection have to be taken into account [6]. In SECM it is usually mandatory to avoid the generation of forced convection as the valid data interpretation is based on purely diffusive currents. Only a small number of SECM experiments with forced convection are described in literature: Combellas et al. [7] demonstrated that the increase in mass transfer that evolves from the horizontal movement of the UME above an insulating substrate already perturbs its current response when being moved faster than $10 \mu\text{m s}^{-1}$. Kottke et al. [8] described that the hydrodynamic effects arising from the horizontal probe movement can be neglected for a combined AFM/SECM frame electrode geometry when the Peclet number is less than 0.1. Cornut et al. [9] delivered an expression to determine the maximal approach velocity for steady state measurements dependent on the geometry of the UME and the properties of the medium. Nkuku et al. [10] showed that the current during negative feedback approach curves in deep eutectic solvents increased above the steady-state value with increasing velocity. Kuss et al. [11] observed a quasi-linear dependence of the normalized current recorded during constant-

height imaging on the velocity of the UME and further discussed the evaluation of high-speed SECM studies for the examination of cell cultures [12, 13]. Edwards et al. [14] investigated the vertical oscillation in the so-called tip position modulation SECM mode. In all of the given examples forced convection is generated intrinsically via movement of the UME when the probe scan rate exceeds a certain value. Accordingly, forced convection in SECM can be avoided by measuring with moderate scan rates and by excluding external forces such as stirring.

Nevertheless, the contribution of natural convection to the mass transfer due to density gradients (buoyancy-driven convection [6]) or temperature gradients (thermal convection [15]) is hard to omit [6]. Though for a long time buoyancy-driven convection was considered negligible for microelectrodes and for low redox mediator concentrations [16], it was recently shown that it is important to consider its impact at concentrations lower than 10 mM [6]. Thermal convection on the other hand can be avoided by controlling the temperature of the entire system. Only a few experiments with exact temperature control are described in literature for example by Schuhmann [17], Komatsu [18], Amemiya [19] and coworkers, respectively. Hence, in SECM without temperature control thermal convection which arises due to temperature differences between the electrolyte solution and the surrounding area or due to locally different thermal conductivity of the substrate has to be considered as shown by Compton and coworkers [20, 21]. Therefore, the application of external forced convection in SECM can be a feasible approach to minimize the effects of natural convection. As recently shown by the Matysik group [22, 23], it is possible to introduce external forced convection to the SECM system by integrating an electrical high-precision stirrer unit into the setup or by a flow of the mediator solution. A constant convective environment with steady-state diffusion layer characteristics at a macroscopic working electrode was generated. Accordingly, time-independent SECM measurements in substrate generation/tip collection mode (SG/TC) were enabled showing attractive analytical characteristics.

In the study presented here, the effects of forced convection introduced by high-precision stirring on SECM experiments in feedback mode were characterized regarding different electrode sizes, different substrate-to-tip distances and different probe scan rates.

4.2.2 Experimental

Chemicals

Ferrocenemethanol (FcMeOH; 99%, ABCR, Karlsruhe, Germany) with a concentration of 1.5 mM was used as electrochemical mediator for all experiments. An aqueous solution was prepared using Milli-Q water (Milli-Q Advantage A10 system, Merck Millipore, Darmstadt, Germany). 0.2 M potassium nitrate (KNO_3 , analytical grade, Merck KGaA, Darmstadt, Germany) was added as supporting electrolyte.

Experimental setup

SECM experiments were performed with a commercially available SECM 920C from CH Instruments (Austin, Texas). A laboratory-constructed electrochemical cell made out of polytetrafluoroethylene was placed inside a Faraday cage on a damper plate to protect the system from electrical noise and vibrations. An electrical high precision stirrer (2250S012BX4 CSD 3830, BL-DC-Motor with integrated motion controller, Dr. Fritz Faulhaber GmbH & Co. KG, Schönaich, Germany) in combination with a laboratory-constructed rotating cylinder (PEEK; diameter $d = 3$ mm with a beveled edge (45°)) was integrated into the SECM setup as previously described [22]. Different intensities of convection were generated by the application of varying stirrer rotation frequencies.

A thin-film interdigitated array microelectrode (ED-IDA1-Pt, MicruX, Asturias, Spain) with platinum as electrode material was used as substrate. The chip exhibited two microelectrode arrays with 15 pairs of fingers each. As it was not required to contact the thin-film electrode, the protective photoresist layer was dissolved with concentrated sulfuric acid to facilitate easier accessibility of the UMEs especially to the outer part of the interdigitated structure. The MicruX chip was fixed on a glass microscope slide with an UV adhesive to ensure reproducible positioning.

Prior to each measuring session, the electrochemical cell was cleaned with piranha solution and the slide was fixed on the bottom of the cell with a few droplets of polydimethylsiloxane (ELASTOSIL® RT 601, Wacker Chemie AG, München). A platinum wire with a diameter of 0.5 mm and a length of 2 cm acted as counter electrode and pseudo reference electrode. All potentials mentioned refer to this pseudo reference system. A 3D-printed mask ensured the well defined horizontal position of the stirrer (8 mm away from the center of the substrate) while a mark on the rotating cylinder ensured its exact vertical position (1 mm above the glass slide). A schematic representation of the experimental setup can be seen in Figure 4.2.1.

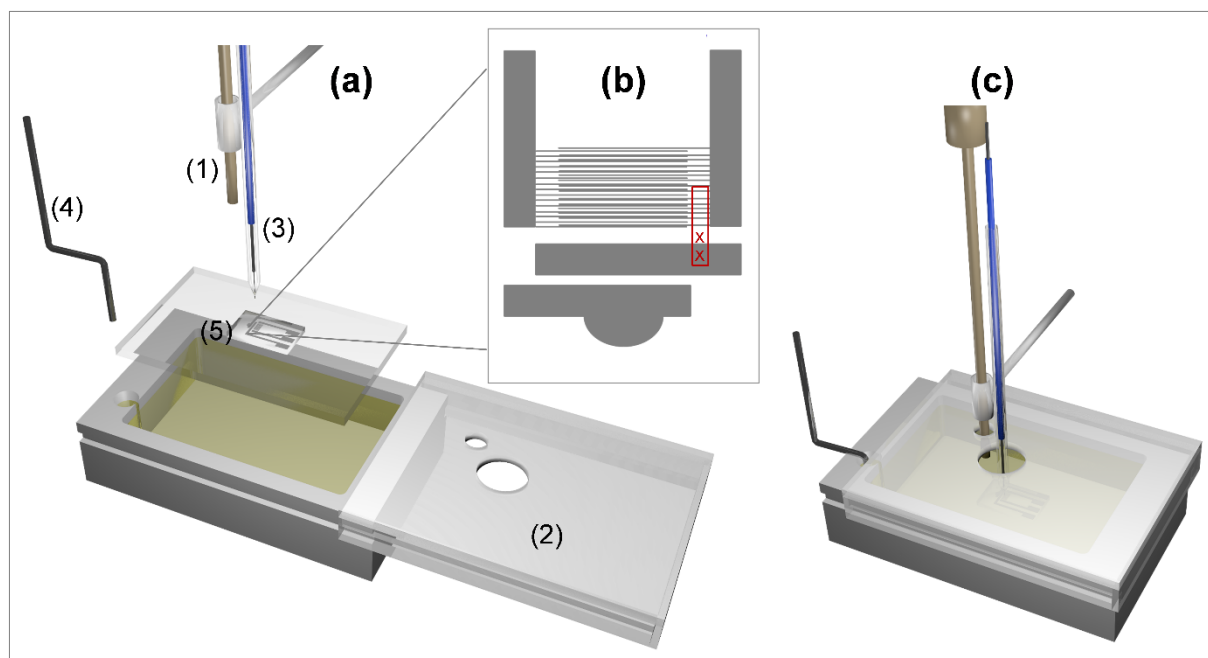


Figure 4.2.1: Schematic representation of the individual components of the experimental setup (a). The high precision stirrer (1) was integrated into the electrochemical cell with a 3D-printed mask (2) fixing its position. An UME (3) was used as working electrode, while a platinum wire (4) acted as counter electrode and pseudo reference electrode. The enlarged area (b) shows the thin-film interdigitated array microelectrode (5) which was mounted into the electrochemical cell. The area for SECM imaging and the locations for probe scan curves are marked in red. The assembled experimental setup is shown in (c).

Experimental procedures

UMEs with diameters (d_{probe}) of 25 μm and 12.5 μm were prepared according to literature [24, 25] with certain modifications as previously described [22, 26]. The quality and size of the UMEs were checked prior to each measuring session. All experiments were carried out in 6 ml of 1.5 mM FcMeOH solution with 0.2 M KNO_3 as supporting electrolyte. A constant potential of $E_{probe} = +0.3$ V was applied to the UME in all measurements for the oxidation of FcMeOH. Prior to measurements, the surface of the thin-film electrode was cleaned with 1 M sulfuric acid and the electrochemical cell was leveled within a range of 10 μm height difference in the investigated area of 2.25 cm^2 . The corresponding locations for the measurements are marked in the schematic drawing of the experimental setup in Figure 4.2.1 (b).

Velocity profile analysis

Mathematical simulations of the flow profile using COMSOL Multiphysics (CFD Module and Mixer Module) were performed to ensure that the 0.75 mm thick interdigitated array electrode used as substrate did not disturb the laminar convection generated by the high precision stirrer

and that the velocity profile of the convection was uniform in the area of the substrate. The dimensions of the model for the simulations were 38 mm in length, 24 mm in width and 6 mm in height. The dimensions of the substrate were 10 mm in length, 6 mm in width and 0.75 mm in height. Hence, all dimensions as well as the position of the substrate inside the electrochemical cell were matching the actual experimental setup. The model was treated as a body of water with no slip being defined as boundary condition for both the sides as well as the bottom and slip being defined for the top. The presence of the SECM probe was excluded from the simulations.

Probe scan curves with forced convection applied to the system

Probe scan curves in z-direction (PSC – defined as probe scan with fixed scan distance, increment distance and increment time) over conducting and insulating material were recorded both in quiescent solution and with forced convection introduced by applying varying stirrer rotation frequencies. Prior to the scan curves the UME was approached to the normalized current value $I_T/I_{T,\infty} \times 100$ of 200% positive feedback without stirring. The probe scan curves were recorded with a constant approach velocity of $0.5 \mu\text{m s}^{-1}$ over a distance of $200 \mu\text{m}$. Between measurements the probe was retrieved $200 \mu\text{m}$ using the SECM stepper motors. Each approach over conducting and insulating material was performed without convection and with stirrer rotation frequencies of 8.3 s^{-1} , 12.5 s^{-1} and 16.7 s^{-1} , respectively. UMEs with diameters of $25 \mu\text{m}$ and $12.5 \mu\text{m}$ and RG values of approximately 2 were utilized for this set of experiments.

SECM imaging in feedback mode with forced convection applied to the system

SECM images of the outer part of the interdigitated structure were recorded both in quiescent solution and with forced convection introduced by applying varying stirrer rotation frequencies. In this manner, the effects of the convection on imaging in feedback mode were investigated. The stirrer, which was set to a certain rotation frequency, was switched on during the measurement and switched off after a number of line scans. Within a single image, either a constant stirrer rotation frequency was applied or different rotation frequencies were applied subsequently. The UME was scanned across the interdigitated structure in constant-height mode with probe scan rates ranging from $5 \mu\text{m s}^{-1}$ to $200 \mu\text{m s}^{-1}$. It was moved into the convection which means in a direction opposite to the flow of the fluid generated by stirring the solution [22]. Stirrer rotation frequencies of 12.5 s^{-1} and 25 s^{-1} were applied at each scan rate, respectively. This combination of experiments was carried out for three different substrate-to-tip distances. Therefore, prior to each set of images the UME was approached to the

normalized current value $I_T/I_{T,\infty} \times 100$ of 140%, 160% or 180% positive feedback. An UME with a diameter of 25 μm and RG of approximately 2 was utilized for characterizing the effects of the convection. Furthermore, the impact of the stirring on a smaller electrode with a diameter of 12.5 μm and RG of approximately 2 was investigated at a distance of $I_T/I_{T,\infty} \times 100 = 140\%$.

4.2.3 Results and discussion

Flow profile analysis

Figure 4.2.2 displays the velocity profile computed via COMSOL Multiphysics for a stirrer rotation frequency of 25 s^{-1} which represents the highest rotation frequency applied within this study.

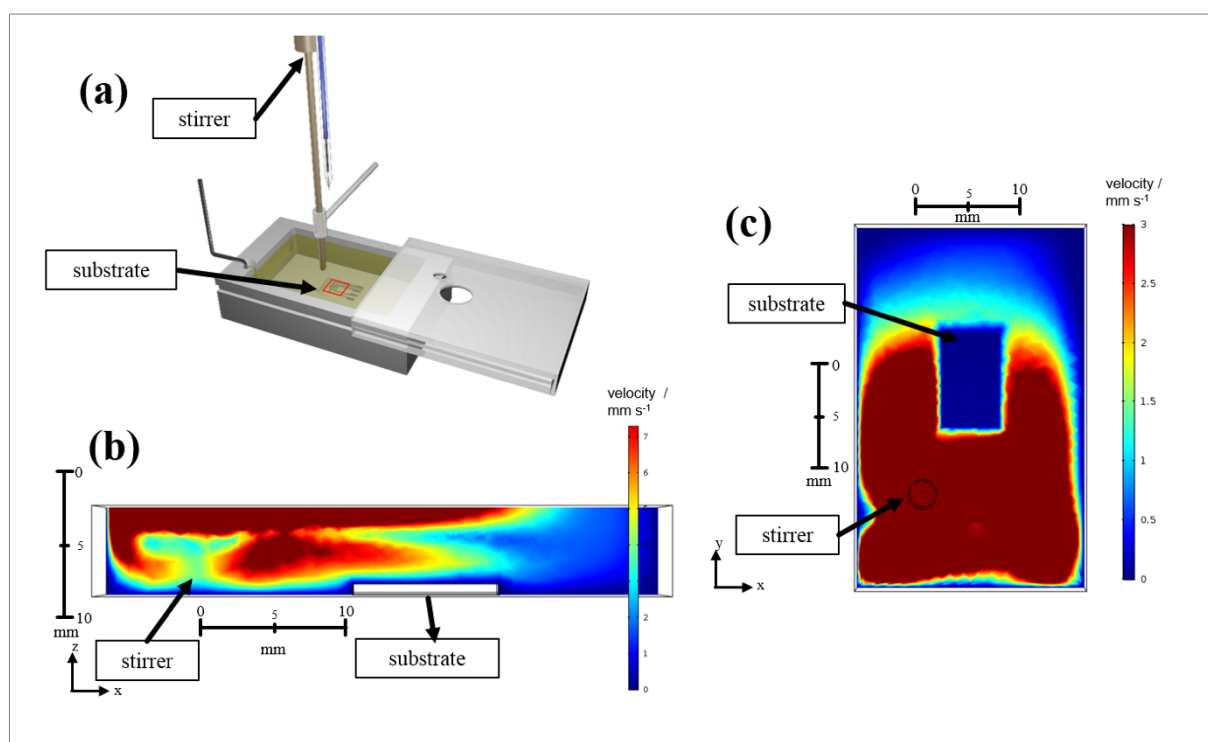


Figure 4.2.2: Mathematical simulations of the velocity profile performed with COMSOL Multiphysics 5.3 to characterize the convection generated via high-precision stirring in the relevant region close to the substrate (marked red (a)). False color plots of the velocity profile are shown in side view (b) and in top view 10 μm above the substrate (c). The stirrer rotation frequency for the simulations was set to 25 s^{-1} .

The side view in Figure 4.2.2 (b) shows that the highest velocity was to be expected close to the stirrer unit, whereas lower velocities were observable at the opposite side of the electrochemical cell. A drastic change in the velocity profile was visible within circa 5 mm above the substrate which was mounted at the bottom of the cell. Nevertheless, a uniform velocity pattern was calculated within a small distance to the substrate where SECM experiments are

usually performed ($< 50 \mu\text{m}$). The same observation can be made from the top view presented in Figure 4.2.2 (c) which showed that, at a height of $10 \mu\text{m}$, in agreement with literature [22] a quite small but constant velocity was predicted within the relevant region above the substrate. Consequently, the simulations indicated that the 0.75 mm thick interdigitated array electrode utilized as substrate did not disturb the laminar convection generated by the high precision stirrer and that a constant convective environment was to be expected in the relevant region above the substrate.

Probe scan curves with forced convection applied to the system

Probe scan curves in z-direction were recorded both in quiescent solution and with forced convection applied to the system to characterize the effects of the forced convection. The current was normalized to the current measured in quiescent bulk solution and the distance was normalized to the radius of the UMEs. The PSCs obtained for different stirrer rotation frequencies are shown in Figure 4.2.3.

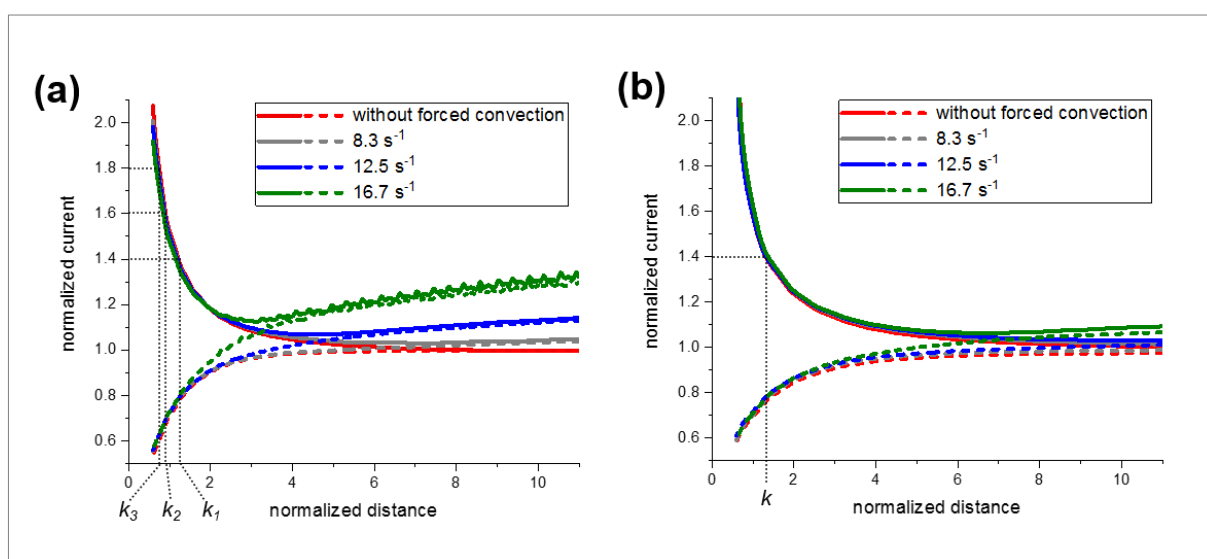


Figure 4.2.3: Probe scan curves in z-direction for positive and negative feedback over the substrate in quiescent solution and with forced convection. Positive feedback PSCs are displayed with continuous lines, while dashed lines represent the negative feedback PSCs. The current was normalized to the current measured in quiescent bulk solution and the distance was normalized to the radius of the UMEs. The substrate-to-tip distances for the following imaging experiments are indicated with $k_1 \approx 14 \mu\text{m}$, $k_2 \approx 11 \mu\text{m}$ and $k_3 \approx 9 \mu\text{m}$ for the UME with a diameter of $25 \mu\text{m}$ (a) and with $k \approx 8 \mu\text{m}$ for the UME with diameter of $12.5 \mu\text{m}$ (b). $RG \approx 2$; mediator: 1.5 mM FcMeOH with 0.2 M KNO_3 ; $E_{\text{probe}} = +0.3 \text{ V}$; probe velocity: $0.5 \mu\text{m s}^{-1}$; stirrer rotation frequencies: 8.3 s^{-1} , 12.5 s^{-1} , 16.7 s^{-1} .

In the bulk solution at a normalized distance of 11 it can be seen that the current increased with increasing stirrer rotation frequency and thus with increasing convection due to an enhanced mass transfer inside the system. The observed increase was more pronounced for

a 25 μm UME and only marginal for a 12.5 μm UME. As expected, the recorded currents of the positive and negative feedback PSCs were nearly identical for the corresponding stirrer rotation frequencies as long as the UME was located outside the feedback range. Along with the results of the COMSOL simulations, this fact proved the uniformity of the velocity profile in the area of the substrate as there was a distance of 100 μm between the locations of the positive and negative PSCs. When approaching the surface, the currents for the PSCs recorded with stirring decreased as the magnitude of the convection decreased towards the surface [27]. Within the working distance of the 25 μm UME, at a normalized distance of ≈ 1.5 , only minor differences were visible in the currents for the different convective conditions. For positive feedback approaches the current slightly decreased with increasing convection, while it slightly increased for negative feedback approaches. This means that the positive feedback loop was diminished by stirring, whereas the negative feedback current increased due to increased mass transfer. When recording the current with a 12.5 μm UME, no effects of the stirring were visible at these small distances. Consequently, with forced convection applied to the system no or only minor differences for positive or negative feedback currents were to be expected at the working distances for the following imaging experiments. These working distances corresponding to $I_T/I_{T,\infty} \times 100 = 140\%$, 160% and 180% feedback approaches are indicated with $k_1 \approx 14 \mu\text{m}$, $k_2 \approx 11 \mu\text{m}$ and $k_3 \approx 9 \mu\text{m}$ for the 25 μm UME in Figure 4.2.3 (a) and with $k \approx 8 \mu\text{m}$ for the 12.5 μm UME in Figure 4.2.3 (b).

Last-mentioned, a fluctuating current was observed in the bulk solution for the 25 μm UME and a stirrer rotation frequency of 16.7 s^{-1} which vanished in close vicinity to the surface. Accordingly, the laminar convection turned into turbulent convection for higher stirrer rotation frequencies. Nonetheless, the convection became laminar again for smaller substrate-to-tip distances as the effects of the convection decreased towards the surface. The laminar convection in close vicinity to the substrate was also ensured for the highest stirrer rotation frequency used (25 s^{-1}).

SECM imaging in feedback mode with forced convection applied to the system

For all following figures SECM images at distances of $I_T/I_{T,\infty} \times 100 = 140\%$, 160% and 180% positive feedback approach were measured for each probe scan rate and each stirrer rotation frequency. Line scans were extracted from the images for data evaluation of the recorded sets of images. The extracted line scans for the corresponding probe scan rates and distances can be found in the supporting information. From these line scans, the electrochemical contrast was obtained by calculating the difference between the current over conducting and insulating material [17, 28]. Thereby, a high value represents a high electrochemical contrast, whereas a small contrast is expressed by a small value. One representative set of line scans and one

representative SECM image per figure are displayed to visualize the effects of the forced convection on the imaging process itself.

Impact of forced convection on an UME with a diameter of 25 μm

$I_T/I_{T,\infty} \times 100 = 140\%$ (substrate-to-tip distance $k_1 \approx 14 \mu\text{m}$): Figure 4.2.4 presents the described set of experiments for a substrate-to-tip distance of $k_1 \approx 14 \mu\text{m}$.

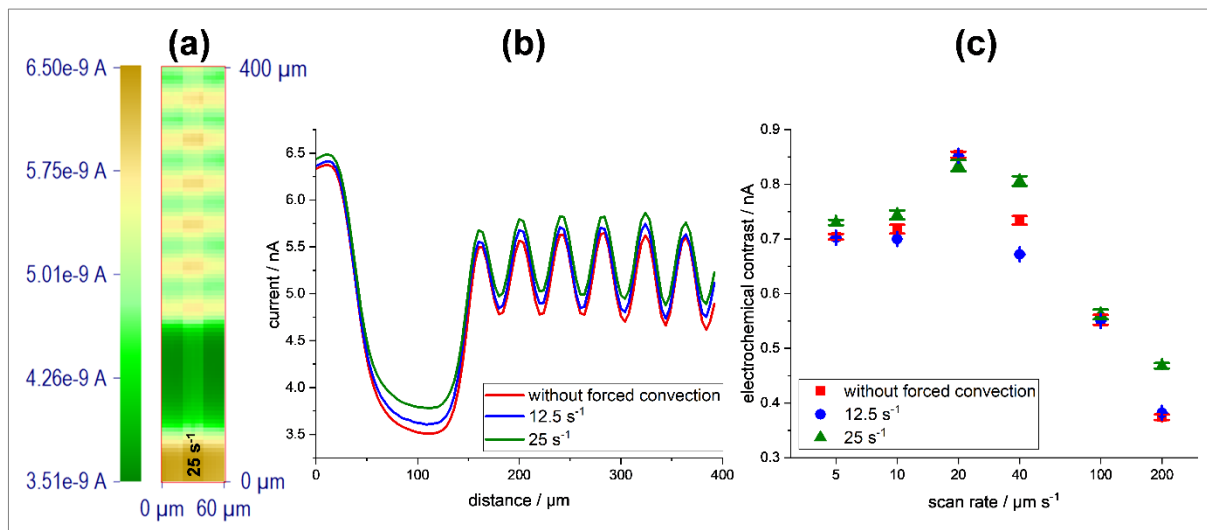


Figure 4.2.4: The UME was approached to the normalized current value $I_T/I_{T,\infty} \times 100$ of 140% ($k_1 \approx 14 \mu\text{m}$). (a) Representative SECM image in feedback mode (probe scan rate: $20 \mu\text{m s}^{-1}$) in quiescent solution and with forced convection introduced by applying a stirrer rotation frequency of 25 s^{-1} in the middle part of the measurement. (b) Representative line scans (probe scan rate: $20 \mu\text{m s}^{-1}$). (c) Electrochemical contrast for different probe scan rates (logarithmic x-axis). Errors determined by calculating the standard deviations for three line scans. Mediator: 1.5 mM FcMeOH with 0.2 M KNO_3 ; $d_{\text{probe}} = 25 \mu\text{m}$, $RG \approx 2$; $E_{\text{probe}} = +0.3 \text{ V}$; probe scan rates: $5 \mu\text{m s}^{-1}$, $10 \mu\text{m s}^{-1}$, $20 \mu\text{m s}^{-1}$, $40 \mu\text{m s}^{-1}$, $100 \mu\text{m s}^{-1}$, $200 \mu\text{m s}^{-1}$; stirrer rotation frequency: 12.5 s^{-1} , 25 s^{-1} .

In part (a) of Figure 4.2.4, one representative SECM image recorded with a probe scan rate of $20 \mu\text{m s}^{-1}$ at a substrate-to-tip distance of $k_1 \approx 14 \mu\text{m}$ is shown. Forced convection was applied by switching on the electrical high precision stirrer with a rotation frequency of 25 s^{-1} in the middle part of the measurement. Though at such small substrate-to-tip distances only minor effects of the forced convection or even decreased currents for positive feedback were expected based on the PSCs displayed in Figure 4.2.3, convection led to an increased overall current during imaging. Consequently, the effects of forced convection depended on the movement direction of the UME. Furthermore, when activating the stirring no equilibration time was necessary. The impacts on the current measured at the tip of the UME were visible without any delay. The same observation was made when deactivating the stirring.

The corresponding representative set of line scans visible in part (b) of Figure 4.2.4 allows for a more detailed look into the effects of the convection. No negative impacts of the stirring like turbulences in the measured current or distortions in the distinctive structure of the imaged structure were observed. This is consistent with the previously published results concerning SECM images in SG/TC mode with forced convection applied to the system [22]. Accordingly, though the PSCs did not show laminar convection in the bulk phase for stirrer rotation frequencies higher than 16.7 s^{-1} , SECM imaging with a constant current in close vicinity to the substrate was still possible when high stirrer rotation frequencies were applied. Moreover, as already visible in the SECM image, the entire line scan was shifted to higher currents for increasing stirrer rotation frequencies in comparison to the scan without forced convection applied to the system. In Figure 4.2.4 (c) it can be seen that for the investigated probe scan rates the forced convection had almost no effects on the electrochemical contrast of the SECM images in feedback mode. This implies that mostly the currents for positive and for negative feedback were increased by the same ratio when stirring was applied.

In summary, for a substrate-to-tip distance of $k_1 \approx 14 \text{ }\mu\text{m}$, considering solely electrochemical contrast, no clear trend was visible for the impact of the forced convection. Its effects were distributed throughout the different scan rates and the different stirrer rotation frequencies. But the analysis of the line scans and images showed that the forced convection amplified the signal of the measurements by increasing the overall current without negative impacts such as turbulences in the current or distortions in the recorded structure.

$I_T/I_{T,\infty} \times 100 = 160\%$ (substrate-to-tip distance $k_2 \approx 11 \mu\text{m}$): Figure 4.2.5 presents the described set of experiments for a substrate-to-tip distance of $k_2 \approx 11 \mu\text{m}$.

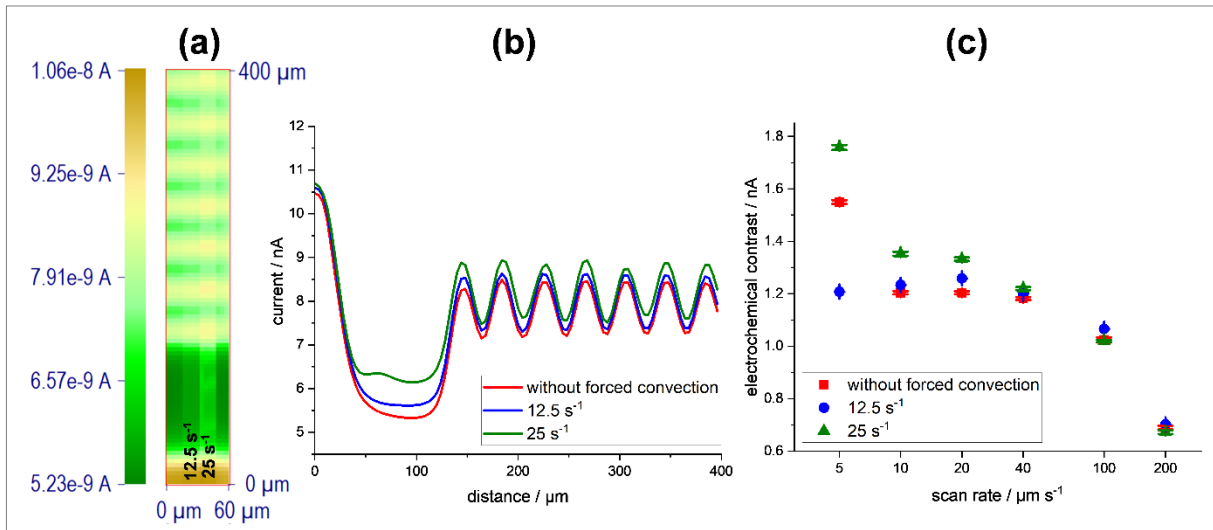


Figure 4.2.5: The UME was approached to the normalized current value $I_T/I_{T,\infty} \times 100$ of 160% ($k_2 \approx 11 \mu\text{m}$). (a) Representative SECM image in feedback mode (probe scan rate: $20 \mu\text{m s}^{-1}$) in quiescent solution and with forced convection introduced by applying stirrer rotation frequencies of 12.5 s^{-1} and 25 s^{-1} . (b) Representative line scans (probe scan rate: $20 \mu\text{m s}^{-1}$). (c) Electrochemical contrast for different probe scan rates (logarithmic x-axis). Errors determined by calculating the standard deviations for three line scans. Mediator: 1.5 mM FcMeOH with 0.2 M KNO_3 ; $d_{\text{probe}} = 25 \mu\text{m}$, $RG \approx 2$; $E_{\text{probe}} = +0.3 \text{ V}$; probe scan rates: $5 \mu\text{m s}^{-1}$, $10 \mu\text{m s}^{-1}$, $20 \mu\text{m s}^{-1}$, $40 \mu\text{m s}^{-1}$, $100 \mu\text{m s}^{-1}$, $200 \mu\text{m s}^{-1}$; stirrer rotation frequencies: 12.5 s^{-1} , 25 s^{-1} .

Similar effects as for a substrate-to-tip distance $k_1 \approx 14 \mu\text{m}$ could be observed in the representative SECM image in Figure 4.2.5 (a) when forced convection was applied. As it was monitored before that the current at the UME immediately responded to changes in the convective conditions, in this case both stirrer rotation frequencies were measured within one image. Forced convection led to an increased overall current during the image, which was more distinctive when the stirrer rotation frequency was increased from 12.5 s^{-1} to 25 s^{-1} . The corresponding set of line scans visible in Figure 4.2.5 (b) shows that no turbulences or distortions were caused by the stirring. Analogous to a distance of $k_1 \approx 14 \mu\text{m}$, the whole line scan was shifted to higher currents for increasing stirrer rotation frequencies in comparison to the scan without forced convection. Part (c) of Figure 4.2.5 displays that for a substrate-to-tip distance of $k_2 \approx 11 \mu\text{m}$ the application of forced convection led to an improvement of the electrochemical contrast when the probe was scanned with slower scan rates: For scan rates of $10 \mu\text{m s}^{-1}$, $20 \mu\text{m s}^{-1}$ and $40 \mu\text{m s}^{-1}$ the contrast improved with increasing stirrer rotation frequency, while for $5 \mu\text{m s}^{-1}$ it decreased for 12.5 s^{-1} before it increased for 25 s^{-1} . The line scans revealed that the improvement of the contrast was due to a more pronounced increase of the positive feedback current in comparison to the negative feedback current when forced convection was applied. This led to a larger difference in current and thus to an increased

electrochemical contrast for these probe scan rates. For the faster probe scan rates of $100 \mu\text{m s}^{-1}$ and $200 \mu\text{m s}^{-1}$, the contrast remained unaltered, meaning that positive and negative feedback current were increased by the same ratio. Consequently, for a substrate-to-tip distance of $k_2 \approx 11 \mu\text{m}$ forced convection, which led to increased overall currents during the SECM images, could also improve the electrochemical contrast for certain probe scan rates.

$I_T/I_{T,\infty} \times 100 = 180\%$ (substrate-to-tip distance $k_3 \approx 9 \mu\text{m}$): Figure 4.2.6 presents the described set of experiments for a substrate-to-tip distance of $k_3 \approx 9 \mu\text{m}$.

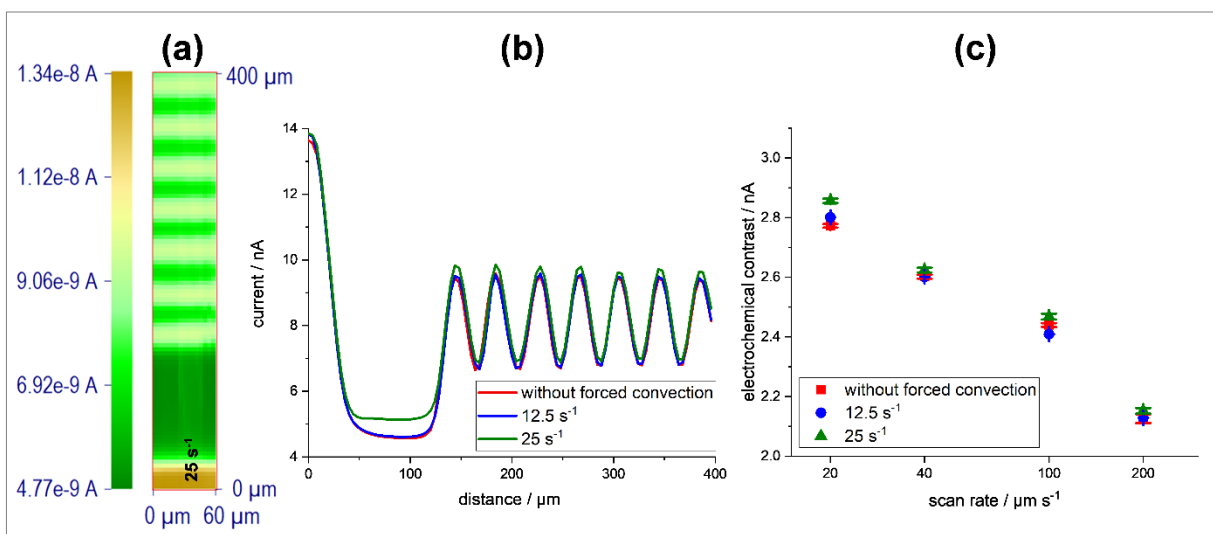


Figure 4.2.6. The UME was approached to the normalized current value $I_T/I_{T,\infty} \times 100$ of 180% ($k_3 \approx 9 \mu\text{m}$). (a) Representative SECM image in feedback mode (probe scan rate: $20 \mu\text{m s}^{-1}$) in quiescent solution and with forced convection introduced by applying a stirrer rotation frequency of 25 s^{-1} in the middle part of the measurement. (b) Representative line scans (probe scan rate: $20 \mu\text{m s}^{-1}$). (c) Electrochemical contrast for different probe scan rates (logarithmic x-axis). Errors determined by calculating the standard deviations for three line scans. Mediator: 1.5 mM FcMeOH with 0.2 M KNO_3 ; $d_{\text{probe}} = 25 \mu\text{m}$, $RG \approx 2$; $E_{\text{probe}} = +0.3 \text{ V}$; probe scan rates: $20 \mu\text{m s}^{-1}$, $40 \mu\text{m s}^{-1}$, $100 \mu\text{m s}^{-1}$, $200 \mu\text{m s}^{-1}$; stirrer rotation frequencies: 12.5 s^{-1} , 25 s^{-1} .

For a substrate-to-tip distance of $k_3 \approx 9 \mu\text{m}$, the SECM image in Figure 4.2.6 shows almost no difference in the area where the stirrer was active with a rotation frequency of 25 s^{-1} . In accordance with the set of line scans in Figure 4.2.6 (b), the increase in current for increasing stirrer rotation frequencies in the area of the interdigitated structure was only marginal. Accordingly, the electrochemical contrast in Figure 4.2.6 (c) with forced convection differed only slightly from measurements in quiescent solution. This means, as already visible in the scan curves presented in Figure 4.2.3 with a further decrease of the gap between the UME and the substrate, almost no effects of the forced convection were visible anymore.

Impact of forced convection on an UME with a diameter of $12.5\ \mu\text{m}$: $I_T/I_{T,\infty} \times 100 = 140\%$ (substrate-to-tip distance $k \approx 8\ \mu\text{m}$)

Figure 4.2.7 presents the described set of experiments for a substrate-to-tip distance of $k \approx 8\ \mu\text{m}$.

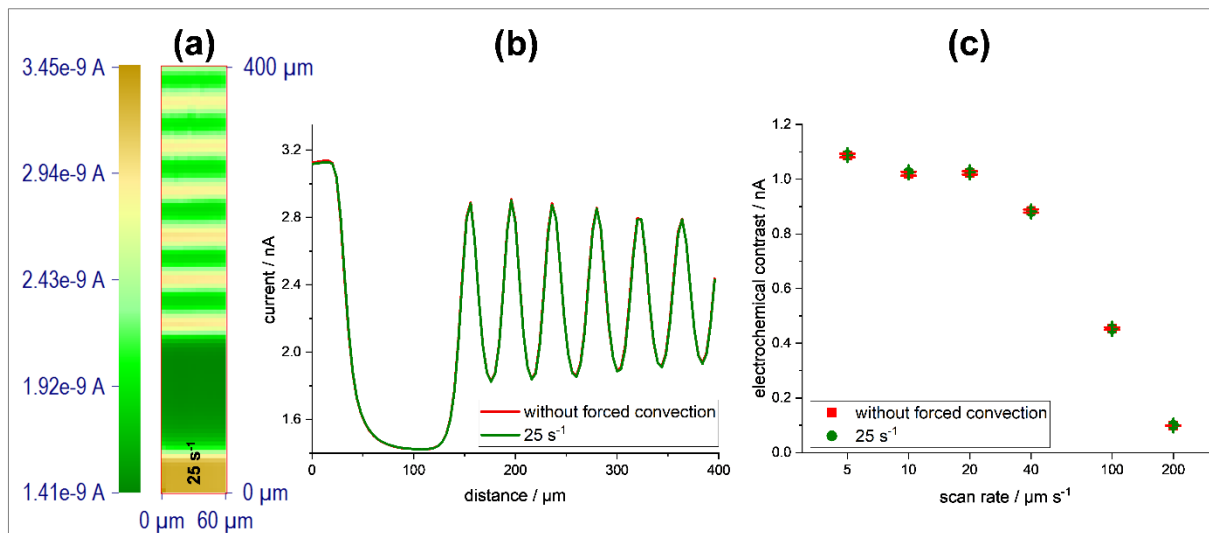


Figure 4.2.7: The UME was approached to the normalized current value $I_T/I_{T,\infty} \times 100$ of 140% ($k \approx 8\ \mu\text{m}$). (a) Representative SECM image in feedback mode (probe scan rate: $20\ \mu\text{m s}^{-1}$) in quiescent solution and with forced convection introduced by applying a stirrer rotation frequency of $25\ \text{s}^{-1}$ in the middle part of the measurement is. (b) Representative line scans (probe scan rate: $20\ \mu\text{m s}^{-1}$). (c) Electrochemical contrast for different probe scan rates (logarithmic x-axis). Errors determined by calculating the standard deviations for three line scans. Mediator: $1.5\ \text{mM FcMeOH}$ with $0.2\ \text{M KNO}_3$; $d_{\text{probe}} = 12.5\ \mu\text{m}$, $RG \approx 2$; $E_{\text{probe}} = +0.3\ \text{V}$; probe scan rates: $5\ \mu\text{m s}^{-1}$, $10\ \mu\text{m s}^{-1}$, $20\ \mu\text{m s}^{-1}$, $40\ \mu\text{m s}^{-1}$, $100\ \mu\text{m s}^{-1}$, $200\ \mu\text{m s}^{-1}$; stirrer rotation frequency: $25\ \text{s}^{-1}$.

Figure 4.2.7 displays that for an UME with a diameter of $12.5\ \mu\text{m}$ no effects of the forced convection were observed. The SECM image in Figure 4.2.7 (a), the corresponding set of line scans in part (b) of Figure 4.2.7 and the electrochemical contrast in Figure 4.2.7 (c) remained the same without and with forced convection applied to the system. Consequently, as already observed in the scan curves depicted in Figure 4.2.3, an electrode with smaller active area exhibited a convection-independent feedback response for the applied stirrer rotation frequencies at small substrate-to-tip distances.

4.2.4 Conclusion

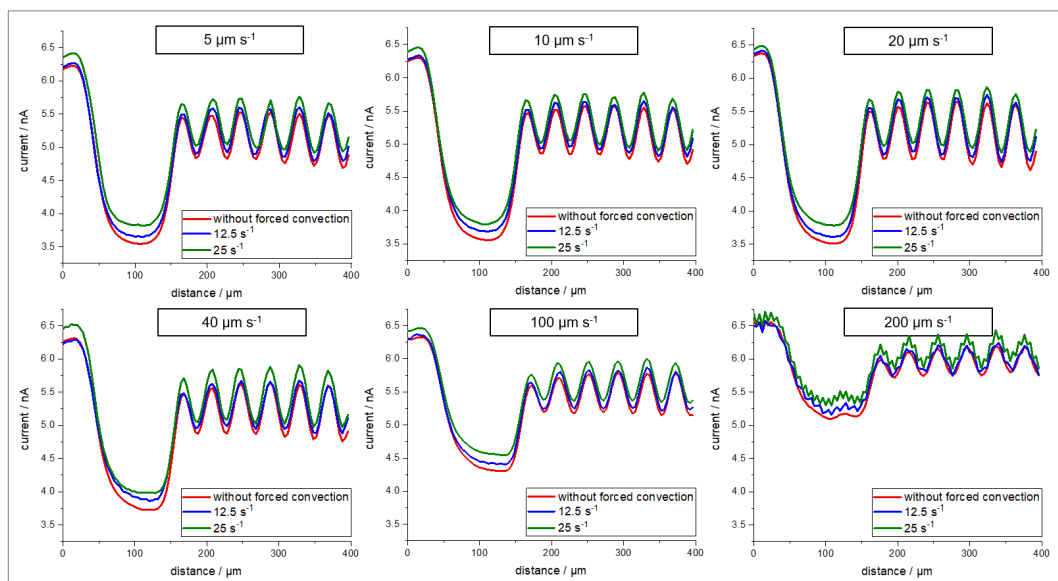
In this study it was shown that the feedback mode can be applied in SECM experiments with forced convection. COMSOL simulations were computed to investigate the uniformity of the velocity profile in the relevant region close to the substrate. The characterization of the

convection in vertical direction via probe scan curves suggested that at small substrate-to-tip distances, where SECM images are preferably to be recorded, no ($d_{probe} = 12.5 \mu\text{m}$) or only marginal ($d_{probe} = 25 \mu\text{m}$) differences in the probe current were visible for different stirrer rotation frequencies in comparison to measurements without forced convection. Nonetheless, well pronounced effects were still monitored while recording SECM images with convection using a $25 \mu\text{m}$ UME. Stirrer rotation frequencies up to 25 s^{-1} were applicable although the probe scan curves indicated that turbulences occurred at rotation frequencies that high. Therefore, laminar convection inside the entire electrochemical cell was no necessity for SECM imaging with forced convection.

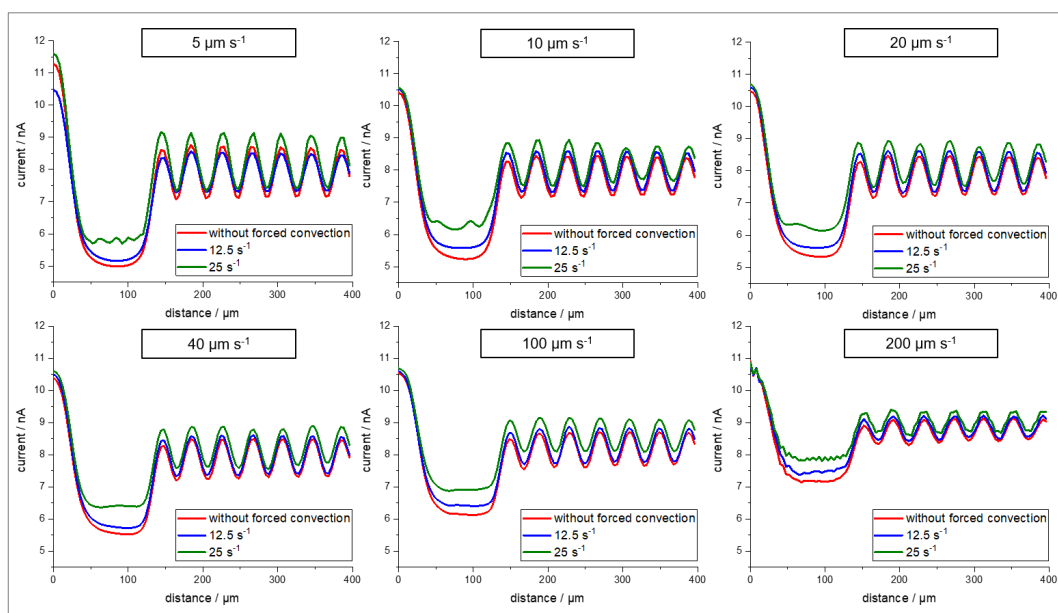
Negative impacts of stirring such as turbulences in the measured current or distortions in the distinctive structure of the imaged interdigitated structure were not observed. For the investigated distances of $k_1 \approx 14 \mu\text{m}$ and $k_2 \approx 11 \mu\text{m}$, the current at the tip of the UME increased during imaging with forced convection in comparison to measurements in quiescent solution. Thus, the performance of the SECM experiments was improved as the application of forced convection amplified the signal of the measurements in feedback mode. Interestingly, it was observed that with forced convection the electrochemical contrast calculated from the SECM images improved for probe scan rates of $5 \mu\text{m s}^{-1}$, $10 \mu\text{m s}^{-1}$, $20 \mu\text{m s}^{-1}$ and $40 \mu\text{m s}^{-1}$ at a substrate-to-tip distance of $k_2 \approx 11 \mu\text{m}$, while it remained mostly unaffected for $k_1 \approx 14 \mu\text{m}$. The effects of convection were visible immediately after turning on the stirrer which means that no equilibration time was necessary and the rotation frequency could be varied arbitrarily during measurements. For a substrate-to-tip distance of $k_3 \approx 9 \mu\text{m}$ almost no effects of the forced convection were observed. Furthermore, the current at a probe with a diameter of $12.5 \mu\text{m}$ showed no response to the forced convection while imaging at a distance of $k \approx 8 \mu\text{m}$. Consequently, applying forced convection at small substrate-to-tip distances offers interesting possibilities. For example, a substance which is added to the measuring solution during imaging can be distributed in the electrochemical cell via stirring without altering the current at the UME. Thus, a change of pH value can be induced by adding an acid or a base and its effects on surfaces can be investigated in real time.

Although working in feedback mode with forced convection was principally possible, its application to the SECM electrolyte delivers more obvious advantages when experiments are operated in amperometric [22] or voltammetric [29] substrate generation/tip collection mode. Nevertheless, by showing that no distortions of the imaged structure were observed, feedback mode with forced convection can be applied as a complementary mode to hydrodynamic SG/TC mode without altering the experimental conditions.

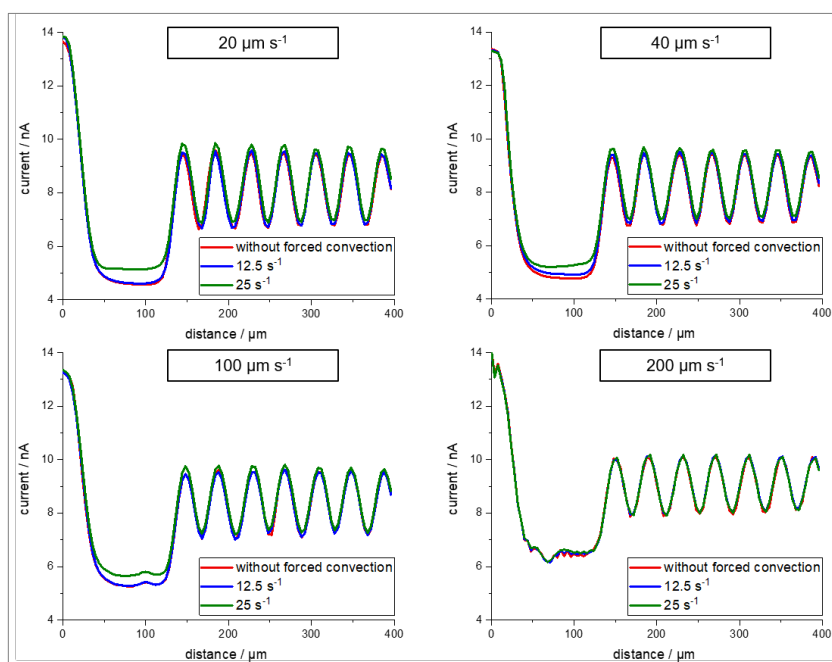
4.2.5 Supporting information



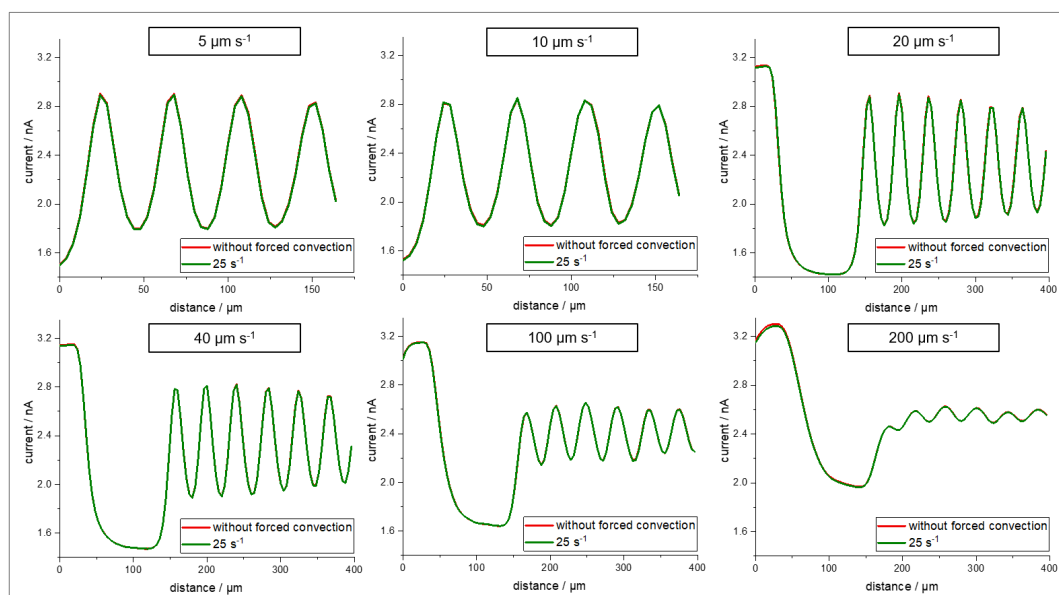
Supporting Figure 4.2.A: The UME was approached to the normalized current value $I_T/I_{T,\infty} \times 100$ of 140% ($k_1 \approx 14 \mu\text{m}$). The line scans were used for the calculation of the electrochemical contrast presented in Figure 4.2.4. The line scans were obtained from SECM images measured for each probe scan rate and each stirrer rotation frequency shown, respectively. Mediator: 1.5 mM FcMeOH with 0.2 M KNO_3 ; $d_{\text{probe}} = 25 \mu\text{m}$, $RG \approx 2$; $E_{\text{probe}} = +0.3 \text{ V}$; probe scan rates: $5 \mu\text{m s}^{-1}$, $10 \mu\text{m s}^{-1}$, $20 \mu\text{m s}^{-1}$, $40 \mu\text{m s}^{-1}$, $100 \mu\text{m s}^{-1}$, $200 \mu\text{m s}^{-1}$; stirrer rotation frequencies: 12.5 s^{-1} , 25 s^{-1} .



Supporting Figure 4.2.B: The UME was approached to the normalized current value $I_T/I_{T,\infty} \times 100$ of 160% ($k_2 \approx 11 \mu\text{m}$). The line scans were used for the calculation of the electrochemical contrast presented in Figure 4.2.5. The line scans were obtained from SECM images measured for each probe scan rate and each stirrer rotation frequency shown, respectively. Mediator: 1.5 mM FcMeOH with 0.2 M KNO_3 ; $d_{\text{probe}} = 25 \mu\text{m}$, $RG \approx 2$; $E_{\text{probe}} = +0.3 \text{ V}$; probe scan rates: $5 \mu\text{m s}^{-1}$, $10 \mu\text{m s}^{-1}$, $20 \mu\text{m s}^{-1}$, $40 \mu\text{m s}^{-1}$, $100 \mu\text{m s}^{-1}$, $200 \mu\text{m s}^{-1}$; stirrer rotation frequencies: 12.5 s^{-1} , 25 s^{-1} .



Supporting Figure 4.2.C: The UME was approached to the normalized current value $I_T/I_{T,\infty} \times 100$ of 180% ($k_3 \approx 9 \mu\text{m}$). The line scans were used for the calculation of the electrochemical contrast presented in Figure 4.2.6. The line scans were obtained from SECM images measured for each probe scan rate and each stirrer rotation frequency shown, respectively. Mediator: 1.5 mM FcMeOH with 0.2 M KNO_3 ; $d_{\text{probe}} = 25 \mu\text{m}$, $RG \approx 2$; $E_{\text{probe}} = +0.3 \text{ V}$; probe scan rates: $20 \mu\text{m s}^{-1}$, $40 \mu\text{m s}^{-1}$, $100 \mu\text{m s}^{-1}$, $200 \mu\text{m s}^{-1}$; stirrer rotation frequencies: 12.5 s^{-1} , 25 s^{-1} .



Supporting Figure 4.2.D: The UME was approached to the normalized current value $I_T/I_{T,\infty} \times 100$ of 140% ($k \approx 8 \mu\text{m}$). The line scans were used for the calculation of the electrochemical contrast presented in Figure 4.2.7. The line scans are obtained from SECM images measured for each probe scan rate and each stirrer rotation frequency shown, respectively. Mediator: 1.5 mM FcMeOHs with 0.2 M KNO_3 ; $d_{\text{probe}} = 12.5 \mu\text{m}$, $RG \approx 2$; $E_{\text{probe}} = +0.3 \text{ V}$; probe scan rates: $5 \mu\text{m s}^{-1}$, $10 \mu\text{m s}^{-1}$, $20 \mu\text{m s}^{-1}$, $40 \mu\text{m s}^{-1}$, $100 \mu\text{m s}^{-1}$, $200 \mu\text{m s}^{-1}$; stirrer rotation frequencies: 25 s^{-1} .

References

- [1] J. Kwak, A.J. Bard, Scanning electrochemical microscopy. Apparatus and two-dimensional scans of conductive and insulating substrates, *Anal. Chem.* 61 (1989) 1794–1799. doi:10.1021/ja3106434.
- [2] A.J. Bard, F.F. Fan, J. Kwak, O. Lev, *Scanning Electrochemical Microscopy. Introduction and Principles*, 138 (1989) 132–138.
- [3] A.J. Bard, M. V. Mirkin, *Scanning Electrochemical Microscopy Second Edition*, 2012.
- [4] S. Bergner, P. Vatsyayan, F. Matysik, Recent advances in high resolution scanning electrochemical microscopy of living cells-a review., *Anal. Chim. Acta.* 775 (2013) 1–13. doi:10.1016/j.aca.2012.12.042.
- [5] A. Bard, L. Faulkner, *Electrochemical methods: fundamentals and applications*, John Wiley&Sons, INC., 2001.
- [6] K. Ngamchuea, S. Eloul, K. Tschulik, R.G. Compton, Advancing from Rules of Thumb: Quantifying the Effects of Small Density Changes in Mass Transport to Electrodes. Understanding Natural Convection, *Anal. Chem.* 87 (2015) 7226–7234. doi:10.1021/acs.analchem.5b01293.
- [7] C. Combellas, M. Fermigier, A. Fuchs, F. Kanoufi, Scanning electrochemical microscopy. Hydrodynamics generated by the motion of a scanning tip and its consequences on the tip current, *Anal. Chem.* 77 (2005) 7966–7975. doi:10.1021/ac0513358.
- [8] P.A. Kottke, A.G. Fedorov, Advective and transient effects in combined AFM/SECM operation, *J. Electroanal. Chem.* 583 (2005) 221–231. doi:10.1016/j.jelechem.2005.06.017.
- [9] R. Cornut, S. Poirier, J. Mauzeroll, Forced convection during feedback approach curve measurements in scanning electrochemical microscopy: Maximal displacement velocity with a microdisk, *Anal. Chem.* 84 (2012) 3531–3537. doi:10.1021/ac203047d.
- [10] C. a Nkuku, R.J. LeSuer, Electrochemistry in deep eutectic solvents., *J. Phys. Chem. B.* 111 (2007) 13271–13277. doi:10.1021/jp075794j.
- [11] S. Kuss, C. Kuss, D. Trinh, S.B. Schougaard, J. Mauzeroll, Forced convection during scanning electrochemical microscopy imaging over living cells: Effect of topographies and kinetics on the microelectrode current, *Electrochim. Acta.* 110 (2013) 42–48. doi:10.1016/j.electacta.2013.03.149.

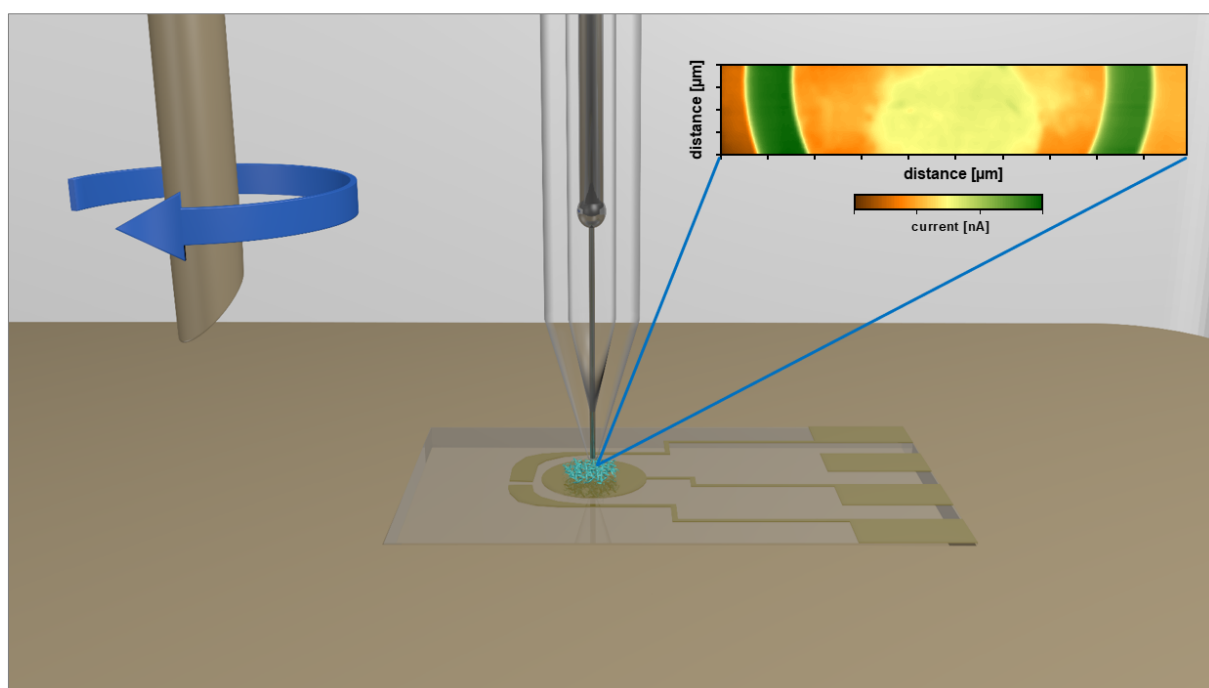
- [12] S. Kuss, D. Trinh, J. Mauzeroll, High-Speed Scanning Electrochemical Microscopy Method for Substrate Kinetic Determination: Application to Live Cell Imaging in Human Cancer, *Anal. Chem.* 87 (2015) 8102–8106. doi:10.1021/acs.analchem.5b01269.
- [13] S. Kuss, D. Trinh, L. Danis, J. Mauzeroll, High-Speed Scanning Electrochemical Microscopy Method for Substrate Kinetic Determination: Method and Theory, *Anal. Chem.* 87 (2015) 8096–8101. doi:10.1021/acs.analchem.5b01268.
- [14] M.A. Edwards, A.L. Whitworth, P.R. Unwin, Quantitative analysis and application of tip position modulation-scanning electrochemical microscopy, *Anal. Chem.* 83 (2011) 1977–1984. doi:10.1021/ac102680v.
- [15] J.K. Novev, S. Eloul, R.G. Compton, Influence of Reaction-Induced Thermal Convection on the Electrical Currents Measured in Chronoamperometry and Cyclic Voltammetry, *J. Phys. Chem. C.* 120 (2016) 13549–13562. doi:10.1021/acs.jpcc.6b03413.
- [16] X. Gao, J. Lee, H.S. White, Natural Convection at Microelectrodes, *Anal. Chem.* 67 (1995) 1541–1545. doi:10.1021/ac00105a011.
- [17] D. Schäfer, A. Puschhof, W. Schuhmann, Scanning electrochemical microscopy at variable temperatures, *Phys. Chem. Chem. Phys.* 15 (2013) 5215. doi:10.1039/c3cp43520b.
- [18] Y. Hirano, Y. Nishimiya, K. Kowata, F. Mizutani, S. Tsuda, Y. Komatsu, Construction of Time-Lapse Scanning Electrochemical Microscopy with Temperature Control and Its Application To Evaluate the Living Cells, *Anal. Chem.* 80 (2008) 9349–9354. doi:10.1021/ac8018334.
- [19] J. Kim, M. Shen, N. Nioradze, S. Amemiya, Stabilizing nanometer scale tip-to-substrate gaps in scanning electrochemical microscopy using an isothermal chamber for thermal drift suppression, *Anal. Chem.* 84 (2012) 3489–3492. doi:10.1021/ac300564g.
- [20] J.K. Novev, R.G. Compton, Convective heat transfer in a measurement cell for scanning electrochemical microscopy, *Phys. Chem. Chem. Phys.* 18 (2016) 29836–29846. doi:10.1039/C6CP06121D.
- [21] J.K. Novev, R.G. Compton, Thermal convection in electrochemical cells. Boundaries with heterogeneous thermal conductivity and implications for scanning electrochemical microscopy, *Phys. Chem. Chem. Phys.* 19 (2017) 12759–12775. doi:10.1039/C7CP01797A.

- [22] C. Iffelsberger, P. Vatsyayan, F. Matysik, Scanning Electrochemical Microscopy with Forced Convection Introduced by High-Precision Stirring, *Anal. Chem.* 89 (2017) 1658–1664. doi:10.1021/acs.analchem.6b03764.
- [23] T. Raith, S. Wert, C. Iffelsberger, F.-M. Matysik, Development and characterization of electrochemical flow cells for hydrodynamic scanning electrochemical microscopy, *Monatshefte Für Chemie - Chem. Mon.* 149 (2018) 1671–1677. doi:10.1007/s00706-018-2201-3.
- [24] C. Lee, C.J. Miller, A.J. Bard, Scanning Electrochemical microscopy: Preparation of Submicrometer Electrodes, *Anal. Chem.* 63 (1991) 78–83.
- [25] C.G. Zoski, Ultramicroelectrodes: Design, fabrication, and characterization, *Electroanalysis*. 14 (2002) 1041–1051. doi:10.1002/1521-4109(200208)14:15/16<1041::AID-ELAN1041>3.0.CO;2-8.
- [26] S. Bergner, P. Palatzky, J. Wegener, F.-M. Matysik, High-Resolution Imaging of Nanostructured Si/SiO₂ Substrates and Cell Monolayers Using Scanning Electrochemical Microscopy, *Electroanalysis*. 23 (2011) 196–200. doi:10.1002/elan.201000446.
- [27] C.M.A. Brett, A.M.O. Brett, *Electrochemistry: principles, methods and applications*, Oxford Science Publications, 1994.
- [28] S.E. Pust, M. Salomo, E. Oesterschulze, G. Wittstock, Influence of electrode size and geometry on electrochemical experiments with combined SECM-SFM probes, *Nanotechnology*. 21 (2010) 105709. doi:10.1088/0957-4484/21/10/105709.
- [29] C. Iffelsberger, T. Raith, P. Vatsyayan, V. Vyskočil, F.-M. Matysik, Detection and imaging of reactive oxygen species associated with the electrochemical oxygen evolution by hydrodynamic scanning electrochemical microscopy, *Electrochim. Acta*. 281 (2018) 494–501. doi:10.1016/j.electacta.2018.05.115.

4.3 Enhanced resolution of generator-collector studies of enzymatic structures by means of hydrodynamic scanning electrochemical microscopy

Timo Raith, Anna Kröninger, Matthias J. Mickert, Hans H. Gorris and Frank-Michael Matysik

Talanta DOI: 10.1016/j.talanta.2020.120844



Abstract

In this report, the effects of forced convection on scanning electrochemical microscopy (SECM) studies of enzymes in the context of the generator-collector mode (G/C mode) were investigated. Forced convection was generated via an electrical high precision stirrer integrated into the electrochemical cell. Circular spots of glucose oxidase were immobilized on a gold support serving as model substrate. The diffusion layer of enzymatically generated H_2O_2 was characterized recording probe scan curves (PSCs) in z-direction. Furthermore, the enzyme-modified surfaces were investigated via constant-height SECM imaging in feedback mode and in G/C mode. For methodical comparison all sets of experiments were performed in quiescent solution (conventional approach) and with forced convection, respectively. In contrast to a growing diffusion layer without forced convection by applying forced convection,

a constant diffusion layer of produced H_2O_2 was observed. Hence, via hydrodynamic SECM time-independent SECM images within a reasonable time scale of SECM measurements in G/C mode were enabled and their resolution was enhanced.

4.3.1 Introduction

Scanning electrochemical microscopy (SECM) is a versatile analytical method [1–3] not only for the characterization of inorganic surfaces, but also for biological samples including DNA [4–7], cells [8–15] and enzymes [16–27]. Concerning enzymes, in contrast to other scanning probe techniques, SECM can provide information about their catalytic activity. Furthermore, SECM can be operated in aqueous buffered solutions under similar conditions as the native environment of the biomolecules [28].

In literature, enzyme activity was studied both in feedback mode and in generator-collector mode (G/C mode) [22,29]. In feedback mode, one reactant of the enzyme reaction is produced electrochemically at the ultramicroelectrode (UME) resulting in the enzyme reaction only taking place at the current position of the UME. In G/C mode, all reactants are present in the bulk solution and the enzyme reaction takes place independent of the UME location and simultaneously at all enzymatically active spots on the investigated surface. In this mode, an electrochemically active product of the enzyme reaction is detected at the UME delivering the measurement signal. In case of glucose oxidase, glucose is added to an air-saturated solution to start the enzyme reaction. Alongside glucono lactone, H_2O_2 is produced during the reaction which can be oxidized at the UME. Thus, H_2O_2 can be utilized as mediator species probing the enzymatic activity.

Comparing both modes, G/C mode has its advantage in a lower background signal, but its resolution is worse than feedback mode due to diffusive broadening and an increasing background signal if the enzyme spot is larger than $50\ \mu\text{m}$ [17,21,22,30]. In this regard, it was shown that in an amperometric glucose microsensor array, the product of the enzyme reaction can be detected at an electrode situated $150\ \mu\text{m}$ away from the enzyme-modified electrode [23]. In another report it was observed that different enzyme spots with $100\ \mu\text{m}$ spacing merge to a single broad signal when they are recorded in G/C mode [17]. Problems concerning the time-dependent change of the signal during SECM imaging of enzymes were addressed via addition of the enzyme catalase to the working solution which decomposes H_2O_2 [21] or via the combination of the SECM with a continuous nanoflow [31].

Hence, comparable to the amperometric substrate generation-tip collection (SG/TC) mode with macroscopic substrate electrodes, time-dependency of the signal and diffusive broadening are

important aspects when working with enzymes in G/C mode of the SECM. Concerning amperometric SG/TC, it was presented that the generation of forced convection via an electrical high precision stirrer or an electrochemical flow cell can be a feasible approach to address these aspects [32–35]. Within this project, the high precision stirrer setup was used to investigate the effects of forced convection on SECM studies of enzymes in the context of the G/C mode with the enzyme reaction of glucose oxidase producing H₂O₂ as mediator species.

4.3.2 Experimental

Chemicals

0.1 M phosphate buffer (PB) with a pH of 7 was utilized for the preparation of all aqueous solutions within this study. The buffer was prepared dissolving sodium dihydrogen phosphate monohydrate (Merck KGaA, Darmstadt, Germany) and di-sodium hydrogen phosphate dodecahydrate (Merck KGaA, Darmstadt, Germany) in Milli-Q water (Milli-Q Advantage A10 system, Merck Millipore, Darmstadt, Germany). 1.5 mM ferrocenemethanol (FcMeOH; 99%, ABCR, Karlsruhe, Germany) in PB was used for SECM studies in feedback mode, whereas pure PB or air-saturated glucose (25 mM or 50 mM; Merck KGaA, Darmstadt, Germany) solution in PB were used for SECM studies in G/C mode. Glucose oxidase (Type VII, from *Aspergillus niger*, Sigma-Aldrich, St. Louis, USA) was chosen as target enzyme. Ethanol (>99,8%, Sigma-Aldrich, St. Louis, USA), 11-mercaptoundecanoic acid (Sigma-Aldrich, St. Louis, USA), N-(3-dimethylaminopropyl)-N'-ethylcarbodiimide hydrochloride (EDC, Sigma-Aldrich, St. Louis, USA) and N-hydroxysuccinimide (NHS, Sigma-Aldrich, St. Louis, USA) were used for the enzyme immobilization protocol.

Experimental setup

A commercially available SECM 920C from CH Instruments (Austin, Texas, USA) was used for all SECM experiments. An electrical high precision stirrer (2250S012BX4 CSD 3830, BL-DC-Motor with integrated motion controller, Dr. Fritz Faulhaber GmbH & Co. KG, Schönaich, Germany) was integrated into the SECM setup as described in literature [32,35]. The experimental setup is depicted schematically in Figure 4.3.1.

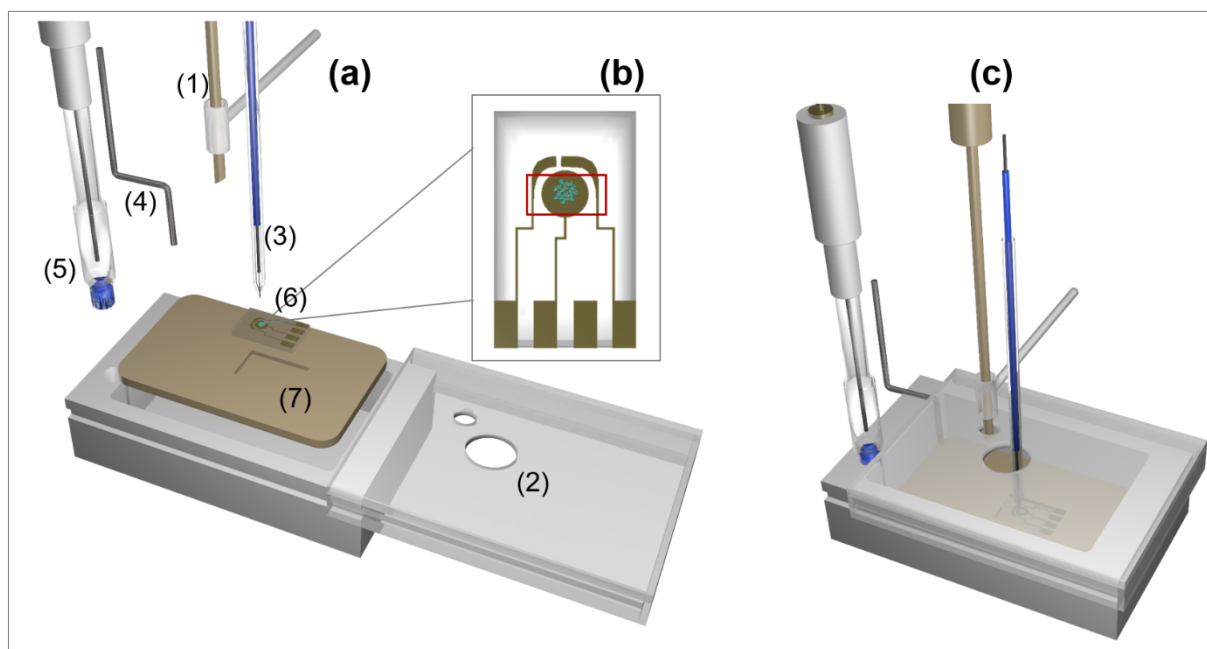


Figure 4.3.1: Schematic representation of the individual components of the experimental setup (a). The high precision stirrer (1) was integrated into the electrochemical cell with a 3D-printed mask (2) fixing its position. An UME (3) was used as working electrode. A platinum wire (4) was employed as counter electrode in combination with an Ag/AgCl/3 M KCl reference electrode (5). The enlarged area (b) shows the solid support for enzyme immobilization (6) which was mounted into the electrochemical cell in a special substrate holder (7). The area for the immobilization and SECM experiments is marked in red. The assembled experimental setup is shown in (c).

Thin-film gold single electrodes (ED-SE1-Au, MicruX, Asturias, Spain) were chosen as a solid support to prepare model substrates. As they were only used as immobilization platforms it was not necessary to contact them. Hence, the protective photoresist layer was removed in concentrated H_2SO_4 . A special sample holder made out of polyether ether ketone was fabricated to mount the substrates within the electrochemical cell in a region where previous results proved a constant convective environment [32,35]. This constant convective environment is mandatory for the formation of constant diffusion layers during electrochemical reactions. The electrochemical cell was covered with a 3D printed mask to ensure reproducible positioning of the high-precision stirrer. Details of the setup such as the size and the exact positioning of the stirrer were identical to our previously published studies [32, 35]. A platinum wire was employed as counter electrode in combination with an Ag/AgCl/3 M KCl reference electrode.

Experimental procedures

Enzyme immobilization

Glucose oxidase was immobilized within the red-marked area of the gold support visible in Figure 4.3.1 (b). The surface was cleaned with concentrated H₂SO₄ prior to the immobilization procedure. As described in literature, glucose oxidase binds non-specifically to glass, although following a self-assembled monolayer strategy for the immobilization [17]. Therefore, the gold support was covered with a tape (CT-F-1603, Chem-Tec, Mülheim-Kärlich, Germany) exhibiting circular holes with diameters of 500 μm or 200 μm to immobilize the enzymes only in a specific area of the substrate. Well-defined cut-outs within the tape were produced utilizing a laser scribe (Universal Laser System VLS2.30) in combination with a HPDFO lens (High Power Density Focusing Optics lens; power 20%; speed 50%; PPI 1000).

For the formation of a self-assembled monolayer, the substrates were immersed in 1 mM 11-mercaptoundecanoic acid in ethanol for 24 h at room temperature. After rinsing with ethanol and water, the surface was activated for 10 minutes adding a 25 μL drop of 200 mM EDC and 50 mM NHS in water. Prior to the addition of a 25 μL drop of 4 mg/mL glucose oxidase in PB, the substrates were cleaned with water and PB. After immobilization for 90 minutes at room temperature, a final washing step with PB was performed. The enzyme-modified substrates were stored in PB at 7 °C.

The tape was removed prior to measurements leaving the bare support with an enzyme spot of 500 μm or 200 μm in the center of the gold area behind. Following this procedure, a structure with four enzyme spots and 150 μm gaps of unmodified surface between them was fabricated. The immobilization was checked via SECM imaging in quiescent solution applying both the feedback mode utilizing FcMeOH as redox mediator as well as the G/C mode in PB before and after the addition of glucose.

SECM experiments

A platinum UME with a diameter of 25 μm and a RG value of 5 was fabricated according to literature [16,36–38]. The RG value of an UME is defined as the ratio between the radius of the isolating glass and the radius of the active electrode area. Quality and size of the electrode were checked optically and electrochemically via cyclic voltammetry and probe approach curves in 1.5 mM FcMeOH solution with 0.2 M KNO₃ as supporting electrolyte. All experiments were performed in a three-electrode setup with an Ag/AgCl/3 M KCl reference electrode. All potentials mentioned within the manuscript refer to this reference system. Prior to

measurements, the electrochemical cell was leveled within a range of 5 μm height difference in the investigated area.

Vertical characterization of the H_2O_2 diffusion layer via probe scan curves: The effects of forced convection were characterized vertically by recording the diffusion layer of H_2O_2 produced during the enzyme reaction via probe scan curves (PSCs – defined as probe scan with fixed scan distance, increment distance, and increment time) in z-direction over a 500 μm enzyme spot. The UME was first approached to a normalized current value $I_T/I_{T\infty} \times 100$ of 140% positive feedback in quiescent solution utilizing FcMeOH as mediator ($E_{\text{probe}} = + 0.5 \text{ V}$) and then retracted 200 μm . After rinsing the electrochemical cell to remove all FcMeOH, it was filled with 25 mM glucose solution in PB. Three successive PSCs were recorded in quiescent solution and with forced convection, respectively. After each measurement, the probe was retracted 200 μm using the SECM stepper motors. The scan curves were recorded with a constant probe velocity of 1 $\mu\text{m s}^{-1}$ over a distance of 200 μm . A potential of $E_{\text{probe}} = + 0.7 \text{ V}$ was applied to the UME for the detection of H_2O_2 via an oxidation reaction. The detection potential was obtained during preliminary studies where interferences of other species were excluded. The stirrer rotation frequency for the scan curves with forced convection was $f_{\text{rot}} = 16.67 \text{ s}^{-1}$. Between the sets of experiments without and with forced convection, the cell was rinsed with PB to remove H_2O_2 from the previous experiments.

SECM imaging in generator-collector mode with forced convection applied to the system: The effects of forced convection on SECM imaging of the enzyme activity in G/C mode was investigated. Prior to measurement sessions, the UME was approached to a normalized current value $I_T/I_{T\infty} \times 100$ of 140% positive feedback. The enzyme spot was located via feedback mode imaging in quiescent solution with FcMeOH acting as mediator ($E_{\text{probe}} = + 0.5 \text{ V}$). After rinsing the electrochemical cell and filling it with 25 mM or 50 mM glucose solution in PB, two successive SECM images were recorded in quiescent solution and with forced convection, respectively. Between the sets of experiments without and with forced convection the cell was rinsed with PB to remove H_2O_2 from the previous experiments. Following this procedure, both a 500 μm and a 200 μm enzyme spot were investigated via successive SECM imaging. Furthermore, a structure of four enzyme spots with 150 μm gaps of unmodified surface between them was imaged without and with forced convection, respectively. All images were recorded with a scan rate of 100 $\mu\text{m s}^{-1}$ applying a detection potential for H_2O_2 of $E_{\text{probe}} = + 0.7 \text{ V}$ to the UME. The stirrer rotation frequency for all SECM images with forced convection was $f_{\text{rot}} = 16.67 \text{ s}^{-1}$.

4.3.3 Results and discussion

Enzyme immobilization

As presented in Figure 4.3.2, before investigating the effects of forced convection, the enzyme immobilization was checked in a control experiment via SECM imaging in feedback mode with FcMeOH as mediator (Figure 4.3.2 (a)) and with imaging in G/C mode in PB before (Figure 4.3.2 (b)) and after (Figure 4.3.2 (c)) the addition of glucose.

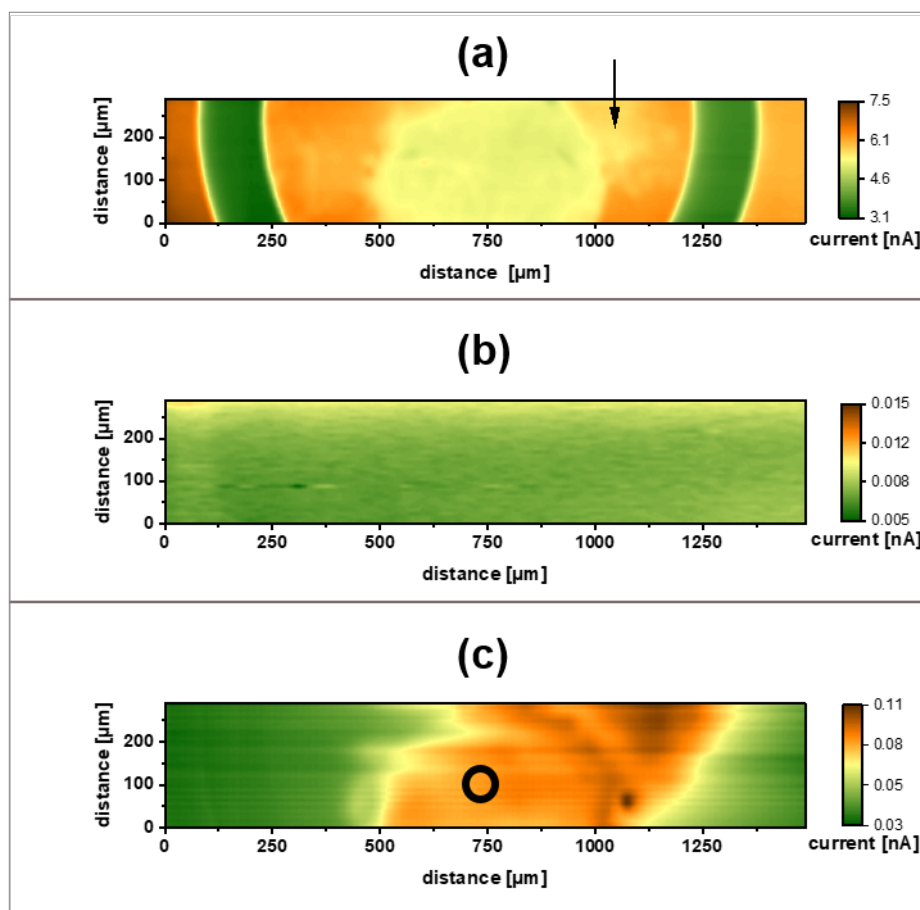


Figure 4.3.2: SECM images of a 500 μm glucose oxidase spot in quiescent solution. Substrate-to-tip distance: 10 μm ; probe scan rate: 100 $\mu\text{m s}^{-1}$; probe diameter: 25 μm ; RG value: 5; (a) feedback mode: electrolyte: 1.5 mM ferrocenemethanol in 0.1 M PB pH 7; $E_{\text{probe}} = +0.5$ V; (b) generator-collector mode: electrolyte: 0.1 M PB pH 7; $E_{\text{probe}} = +0.7$ V; (c) generator-collector mode: electrolyte: 25 mM glucose in 0.1 M PB pH 7; $E_{\text{probe}} = +0.7$ V. The arrow in part (a) indicates that the enzyme spread partially underneath the tape during the immobilization. The location for the recorded probe scan curves is marked in black.

An enzyme spot with a diameter of 500 μm matching the dimensions of the cut-out in the tape was observed in the feedback mode image in Figure 4.3.2 (a) with a decreased positive feedback current due to the enzyme acting as a diffusion barrier [23,39] and thus hindering the electrochemical reaction of the tip-generated FcMeOH cation at the gold surface. Furthermore, as indicated by the arrow, small areas of decreased positive feedback current were visible

around the circular enzyme spot meaning that the enzyme also spread partially underneath the tape during the immobilization. As can be seen in Figure 4.3.2 (b), changing the electrolyte from FcMeOH to PB and switching the detection potential to $E_{\text{probe}} = + 0.7 \text{ V}$ delivered only a very small background current due to the absence of mediator species in G/C mode. The PB was replaced with glucose solution to investigate the activity of the enzymes. A signal increase in the area of the immobilized enzymes was visible in Figure 4.3.2 (c) at a detection potential of $E_{\text{probe}} = + 0.7 \text{ V}$ resulting from the H_2O_2 which was produced during the enzyme reaction. In comparison to the feedback mode image, the enzyme spot was slightly distorted in x-direction corresponding to the movement direction of the UME which disturbed the diffusion layer of the H_2O_2 during scanning [40-44].

Vertical characterization of the H_2O_2 diffusion layer via probe scan curves

As presented in Figure 4.3.3, three subsequent probe scan curves in z-direction were recorded without and with forced convection applied to the system to study the effects of the convection on the diffusion layer of the H_2O_2 produced during the enzyme reaction in presence of glucose.

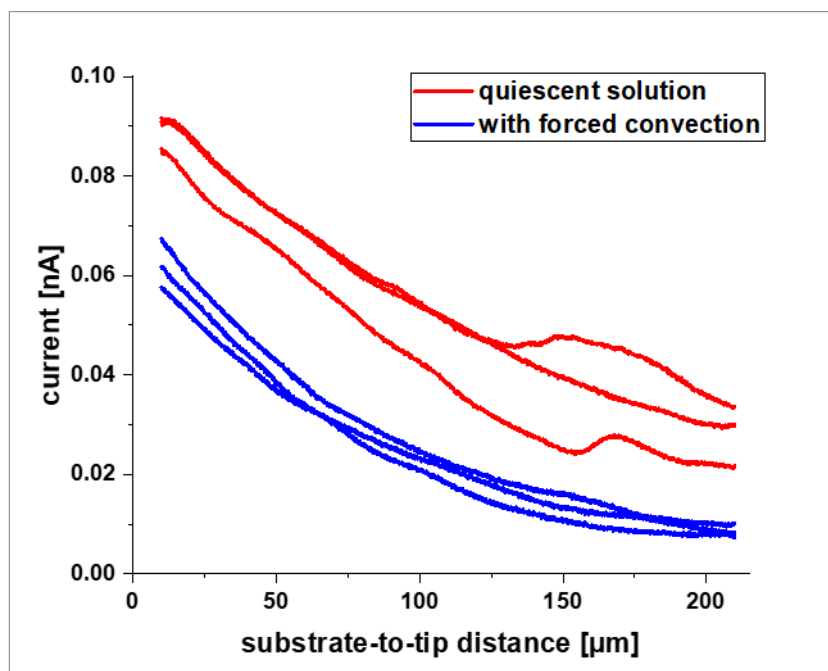


Figure 4.3.3: Subsequent probe scan curves in z-direction over a $500 \mu\text{m}$ glucose oxidase spot in quiescent solution and with forced convection applied to the system. Electrolyte: 25 mM glucose in 0.1 M PB pH 7; probe scan rate: $1.0 \mu\text{m s}^{-1}$; probe diameter: $25 \mu\text{m}$; RG value: 5; $E_{\text{probe}} = + 0.7 \text{ V}$; stirrer rotation frequency: 16.67 s^{-1} .

When approaching the surface, a more drastic change in signal between the scan curves without forced convection was observed in comparison to the ones with forced convection. These results corresponded to the growing diffusion layer without forced convection and a

stable diffusion layer that was generated when forced convection was applied to the system. Overall, a smaller current was observed due to the dilution of the produced H_2O_2 via forced convection leading to a thinner diffusion layer [32,33]. Moreover, no extremum was visible in all scan curves proving that enough glucose was present in the electrochemical cell to saturate the enzyme kinetics with respect to the substrate and prevent blocking effects of the UME [22].

SECM imaging in generator-collector mode with forced convection applied to the system

The time-dependent enzyme activity of substrates with different-sized enzyme spots was mapped recording SECM images in G/C mode in quiescent solution and with forced convection, respectively. Both a 500 μm and a 200 μm enzyme spot were investigated. Furthermore, to evaluate the resolution capabilities of hydrodynamic G/C measurements, a structure of four enzyme spots with 150 μm gaps of unmodified surface between them was imaged in quiescent solution and with forced convection.

Enzyme spot with a diameter of 500 μm

Figure 4.3.4 presents the described set of experiments for an enzyme spot with a diameter of 500 μm .

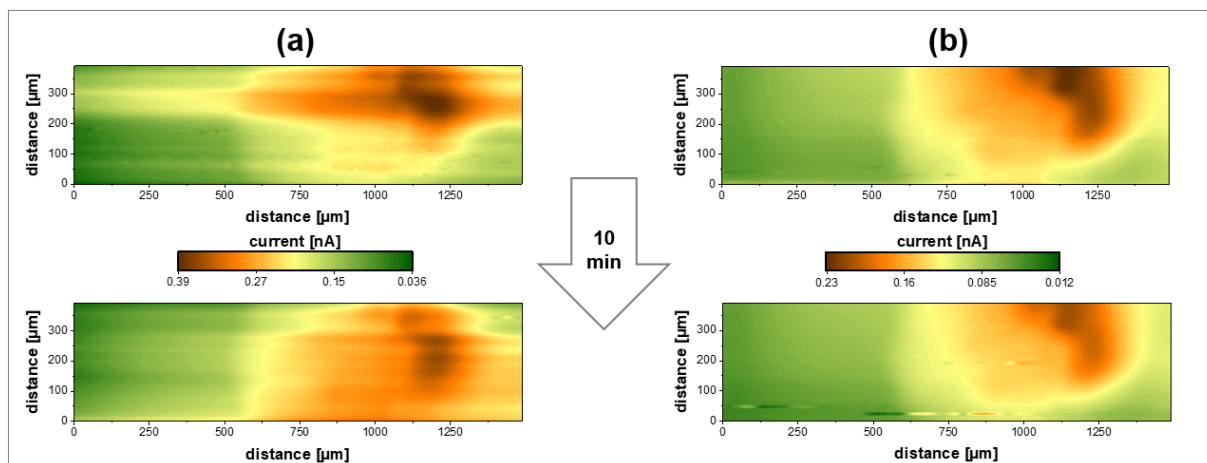


Figure 4.3.4: Subsequent SECM images of a 500 μm glucose oxidase spot in generator-collector mode in quiescent solution (a) and with forced convection applied to the system (b) directly after glucose addition (top) and ten minutes later (bottom). Substrate-to-tip distance: 10 μm ; electrolyte: 50 mM glucose in 0.1 M PB pH 7; probe scan rate: 100 $\mu\text{m s}^{-1}$; probe diameter: 25 μm ; RG value: 5; $E_{\text{probe}} = +0.7 \text{ V}$; stirrer rotation frequency: 16.67 s^{-1} .

The images of a 500 μm glucose oxidase spot without forced convection in Figure 4.3.4 (a) differed from each other corresponding the shape of the measured signal. This observation

was attributed to the diffusion layer of H_2O_2 produced during the enzyme reaction which changed with ongoing time of the experiment. Furthermore, the diffusion layer could also be disturbed by the scan movement of the UME. As visible in Figure 4.3.4 (b), the shape of the spot remained almost identical corresponding to a constant diffusion layer of H_2O_2 which was formed with forced convection applied to the system. Moreover, a smaller signal was observed for the enzyme activity due to a thinner diffusion layer with forced convection. This resulted in a smaller concentration of H_2O_2 during SECM imaging in constant height.

Enzyme spot with a diameter of 200 μm

Figure 4.3.5 presents the described set of experiments for an enzyme spot with a diameter of 200 μm .

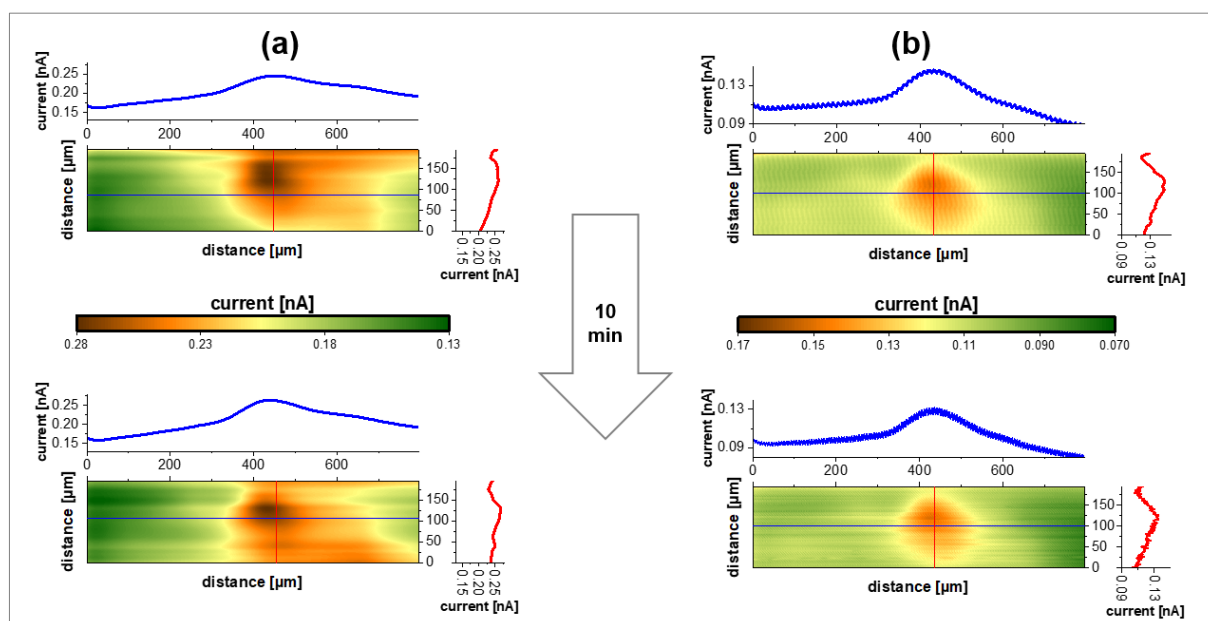


Figure 4.3.5: Subsequent SECM images of a 200 μm glucose oxidase spot in generator-collector mode in quiescent solution (a) and with forced convection applied to the system (b) directly after glucose addition (top) and ten minutes later (bottom). The top and right cross-sectional line scans in the individual graphs correspond to the blue and red lines, respectively. Substrate-to-tip distance: 10 μm ; electrolyte: 50 mM glucose in 0.1 M PB pH 7; probe scan rate: 100 $\mu\text{m s}^{-1}$; probe diameter: 25 μm ; RG value: 5; $E_{\text{probe}} = +0.7 \text{ V}$; stirrer rotation frequency: 16.67 s^{-1} .

When decreasing the size of the enzyme spot to 200 μm , the effects of forced convection on the diffusion layer of H_2O_2 were even more distinctive. The enzyme spot was blurred without forced convection due to diffusive broadening of H_2O_2 as can be seen in Figure 4.3.5 (a). In comparison, both a sharp transition between enzyme activity and background signal and time-independency of measurements were visible in Figure 4.3.5 (b) with forced convection applied to the system. The same observations were made from the extracted line scans in x- and y-

direction, which are marked blue and red within the SECM image, respectively. Without forced convection, the line scans in x-direction showed a slow decrease of the measured current to the background signal when UME was scanned across the enzyme spot. This was corresponding to both the diffusive broadening of H_2O_2 as well as the disturbance of its diffusion layer originating from the scan movement of the UME. With forced convection, however, the shape of the enzyme spot was clearly visible within the extracted line scans.

Structured enzyme surface

As depicted in Figure 4.3.6, a structure of four enzyme spots with $150\ \mu\text{m}$ gaps of unmodified surface between them was imaged to evaluate the resolution capabilities of hydrodynamic G/C measurements.

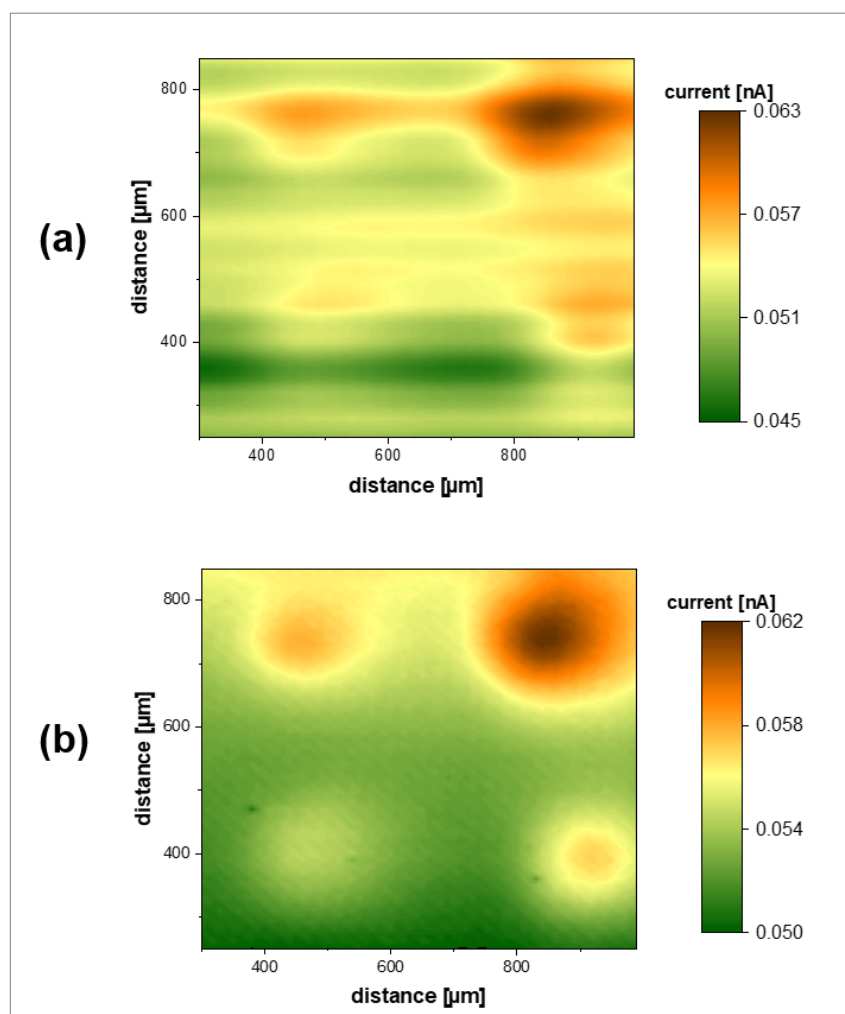


Figure 4.3.6: SECM images of an enzyme structure with four glucose oxidase spots divided by $150\ \mu\text{m}$ gaps of unmodified surface in generator-collector mode in quiescent solution (a) and with forced convection applied to the system (b). Substrate-to-tip distance: $10\ \mu\text{m}$; electrolyte: $50\ \text{mM}$ glucose in $0.1\ \text{M}$ PB pH 7; probe scan rate: $100\ \mu\text{m}\ \text{s}^{-1}$; probe diameter: $25\ \mu\text{m}$; RG value: 5; $E_{\text{probe}} = +0.7\ \text{V}$; stirrer rotation frequency: $16.67\ \text{s}^{-1}$.

As can be seen in Figure 4.3.6 (a), when the enzyme activity was recorded without forced convection, no clear transition between the enzyme spots was visible, although they were divided by 150 μm gaps of unmodified surface. Hence, as shown in literature [17], an enzyme structure could by mistake be interpreted as a single enzyme spot due to diffusive broadening of the produced species. When forced convection was applied to the system, the transition between the four spots and the gaps became visible again due to constant diffusion layers established via convection. Consequently, forced convection led to stable diffusion layers of H_2O_2 enabling time independent measurements within a reasonable time scale of SECM experiments in the context of the G/C mode and improved the resolution by preventing diffusive broadening.

4.3.4 Conclusion

It was shown that the approach of applying forced convection to generate constant diffusion layers around macroscopic substrate electrodes in the context of the SECM SG/TC mode [32–35] can be applied to biological systems. Enzyme spots with diameters of 500 μm and 200 μm were immobilized on gold and investigated via SECM utilizing H_2O_2 produced during the enzyme reaction in presence of glucose as mediator species. Probe scan curves in z-direction showed a constant diffusion layer of H_2O_2 when forced convection was applied to the system in contrast to a time-dependent changing diffusion layer without forced convection. Furthermore, images recorded under conditions of forced convection displayed a time-independent sharp transition between the enzyme spot and the background current, whereas the signals were blurred and time-dependent without convection. Thus, mapping of the enzyme activity via constant-height imaging in G/C mode proved the formation of a constant diffusion layer with forced convection applied to the system. A structure of four enzyme spots which was not visible in G/C mode without forced convection, was successfully imaged with forced convection applied to the system.

Hence, via forced convection an enhanced resolution of enzymatic structures was established enabling time-independent SECM measurements of enzyme activity in the context of the G/C mode within a reasonable time scale of SECM experiments. The addition of other enzymes like catalase could be avoided [21]. Consequently, forced convection can be a feasible approach to address problems occurring during SECM studies of biological systems.

References

- [1] A.J. Bard, F.-R.F. Fan, D.T. Pierce, P.R. Unwin, D.O. Wipf, F. Zhou, Chemical Imaging of Surfaces with the Scanning Electrochemical Microscope, *Science* (80). 254 (1991) 68–74. doi:10.1126/science.254.5028.68.
- [2] C.G. Zoski, Review—Advances in Scanning Electrochemical Microscopy (SECM), *J. Electrochem. Soc.* 163 (2016) H3088–H3100. doi:10.1149/2.0141604jes.
- [3] D. Polcari, P. Dauphin-Ducharme, J. Mauzeroll, Scanning Electrochemical Microscopy: A Comprehensive Review of Experimental Parameters from 1989 to 2015, *Chem. Rev.* 116 (2016) 13234–13278. doi:10.1021/acs.chemrev.6b00067.
- [4] W.S. Roberts, F. Davis, S.P.J. Higson, Scanning electrochemical microscopy of genomic DNA microarrays - Study of adsorption and subsequent interactions, *Analyst*. 134 (2009) 1302–1308. doi:10.1039/b822282g.
- [5] F. Turcu, A. Schulte, G. Hartwich, W. Schuhmann, Label-free electrochemical recognition of DNA hybridization by means of modulation of the feedback current in SECM, *Angew. Chemie - Int. Ed.* 43 (2004) 3482–3485. doi:10.1002/anie.200454228.
- [6] K. Nakano, K. Nakamura, K. Iwamoto, N. Soh, T. Imato, Positive-feedback-mode scanning electrochemical microscopy imaging of redox-active DNA-poly(1,4-benzoquinone) conjugate film deposited on carbon fiber electrode for micrometer-sized hybridization biosensor applications, *J. Electroanal. Chem.* 628 (2009) 113–118. doi:10.1016/j.jelechem.2009.01.014.
- [7] Z. Zhang, J. Zhou, A. Tang, Z. Wu, G. Shen, R. Yu, Scanning electrochemical microscopy assay of DNA based on hairpin probe and enzymatic amplification biosensor, *Biosens. Bioelectron.* 25 (2010) 1953–1957. doi:10.1016/j.bios.2010.01.013.
- [8] A. Schulte, W. Schuhmann, Single-cell microelectrochemistry, *Angew. Chemie - Int. Ed.* 46 (2007) 8760–8777. doi:10.1002/anie.200604851.
- [9] S. Bergner, P. Vatsyayan, F. Matysik, Recent advances in high resolution scanning electrochemical microscopy of living cells-a review., *Anal. Chim. Acta.* 775 (2013) 1–13. doi:10.1016/j.aca.2012.12.042.
- [10] A.J. Bard, X. Li, W. Zhan, Chemically imaging living cells by scanning electrochemical microscopy, *Biosens. Bioelectron.* 22 (2006) 461–472. doi:10.1016/j.bios.2006.04.028.
- [11] W.S. Roberts, D.J. Lonsdale, J. Griffiths, S.P.J. Higson, Advances in the application of scanning electrochemical microscopy to bioanalytical systems, *Biosens. Bioelectron.* 23 (2007) 301–318. doi:10.1016/j.bios.2007.06.020.

- [12] T. Yasukawa, T. Kaya, T. Matsue, Characterization and imaging of single cells with scanning electrochemical microscopy, *Electroanalysis*. 12 (2000) 653–659. doi:10.1002/1521-4109(200005)12:9<653::AID-ELAN653>3.0.CO;2-S.
- [13] J. Lin, D. Weixler, S. Daboss, G.M. Seibold, C. Andronescu, W. Schuhmann, C. Kranz, Time-resolved ATP measurements during vesicle respiration, *Talanta*. 205 (2019) 120083. doi:10.1016/j.talanta.2019.06.083.
- [14] L. Zhu, N. Gao, X. Zhang, W. Jin, Accurately measuring respiratory activity of single living cells by scanning electrochemical microscopy, *Talanta*. 77 (2008) 804–808. doi:10.1016/j.talanta.2008.07.050.
- [15] R. Obregon, Y. Horiguchi, T. Arai, S. Abe, Y. Zhou, Ryosuketakahashi, A. Hisada, K. Ino, H. Shiku, T. Matsue, A Pt layer/Pt disk electrode configuration to evaluate respiration and alkaline phosphatase activities of mouse embryoid bodies, *Talanta*. 94 (2012) 30–35. doi:10.1016/j.talanta.2012.01.059.
- [16] P. Vatsyayan, C. Iffelsberger, C. Mayorga, F.M. Matysik, Imaging of localized enzymatic peroxidase activity over individual unbiased gold nanowires by scanning electrochemical microscopy, *Anal. Methods*. (2016) 6847–6855. doi:10.1039/C6AY01875K.
- [17] T. Wilhelm, G. Wittstock, R. Szargan, Scanning electrochemical microscopy of enzymes immobilized on structured glass-gold substrates, *Fresenius. J. Anal. Chem.* 365 (1999) 163–167. doi:10.1007/s002160051465.
- [18] D. Schäfer, M. Maciejewska, W. Schuhmann, SECM visualization of spatial variability of enzyme-polymer spots. 1. Discretisation and interference elimination using artificial neural networks, *Biosens. Bioelectron.* 22 (2007) 1887–1895. doi:10.1016/j.bios.2006.07.039.
- [19] R. Cornut, P. Hapiot, C. Lefrou, Enzyme-mediator kinetics studies with SECM: Numerical results and procedures to determine kinetics constants, *J. Electroanal. Chem.* 633 (2009) 221–227. doi:10.1016/j.jelechem.2009.06.002.
- [20] D.T. Pierce, A.J. Bard, Scanning electrochemical microscopy. 23. Reaction localization of artificially patterned and tissue-bound enzymes., *Anal. Chem.* 65 (1993) 3598–3604. doi:10.1021/ac00072a012.
- [21] G. Wittstock, W. Schuhmann, Formation and Imaging of Microscopic Enzymatically Active Spots on an Alkanethiolate-Covered Gold Electrode by Scanning Electrochemical Microscopy, *Anal. Chem.* 69 (1997) 5059–5066. doi:10.1021/ac970504o.

- [22] G. Wittstock, Modification and characterization of artificially patterned enzymatically active surfaces by scanning electrochemical microscopy, *Fresenius. J. Anal. Chem.* 370 (2002) 303–315. doi:10.1007/s002160100795.
- [23] D.J. Strike, A. Hengstenberg, M. Quinto, C. Kurzawa, M. Koudelka-Hep, W. Schuhmann, Localized visualization of chemical cross-talk in microsensor arrays by using scanning electrochemical microscopy, *Mikrochim. Acta.* 131 (1999) 47–55. doi:10.1007/s006040050008.
- [24] L. Mureşan, M. Nistor, S. Gáspár, I.C. Popescu, E. Csöregi, Monitoring of glucose and glutamate using enzyme microstructures and scanning electrochemical microscopy, *Bioelectrochemistry.* 76 (2009) 81–86. doi:10.1016/j.bioelechem.2009.05.004.
- [25] G. Wittstock, T. Wilhelm, S. Bahrs, P. Steinrücke, SECM feedback imaging of enzymatic activity on agglomerated microbeads, *Electroanalysis.* 13 (2001) 669–675. doi:10.1002/1521-4109(200105)13:8/9<669::AID-ELAN669>3.0.CO;2-S.
- [26] J. Zhou, C. Campbell, A. Heller, A.J. Bard, Scanning electrochemical microscopy. 44. Imaging of horseradish peroxidase immobilized on insulating substrates, *Anal. Chem.* 74 (2002) 4007–4010. doi:10.1021/ac015721a.
- [27] C. Kranz, A. Kueng, A. Lugstein, E. Bertagnolli, B. Mizaikoff, Mapping of enzyme activity by detection of enzymatic products during AFM imaging with integrated SECM-AFM probes, *Ultramicroscopy.* 100 (2004) 127–134. doi:10.1016/j.ultramic.2003.10.004.
- [28] D.T. Pierce, P.R. Unwin, A.J. Bard, Scanning electrochemical microscopy. 17. Studies of enzyme-mediator kinetics for membrane- and surface-immobilized glucose oxidase, *Anal. Chem.* 64 (1992) 1795–1804. doi:10.1021/ac00041a011.
- [29] R.E. Gyurcsányi, G. Jággerszki, G. Kiss, K. Tóth, Chemical imaging of biological systems with the scanning electrochemical microscope, *Bioelectrochemistry.* 63 (2004) 207–215. doi:10.1016/j.bioelechem.2003.12.011.
- [30] I. Morkvenaite-Vilkonciene, A. Ramanaviciene, A. Ramanavicius, Redox competition and generation-collection modes based scanning electrochemical microscopy for the evaluation of immobilised glucose oxidase-catalysed reactions, *RSC Adv.* 4 (2014) 50064–50069. doi:10.1039/C4RA08697J.
- [31] T. Kai, S. Chen, E. Monterroso, F. Zhou, Continuous nanoflow-scanning electrochemical microscopy: Voltammetric characterization and application for accurate and reproducible imaging of enzyme-labeled protein microarrays, *Anal. Chem.* 87 (2015) 4523–4529. doi:10.1021/acs.analchem.5b00625.

- [32] C. Iffelsberger, P. Vatsyayan, F. Matysik, Scanning Electrochemical Microscopy with Forced Convection Introduced by High-Precision Stirring, *Anal. Chem.* 89 (2017) 1658–1664. doi:10.1021/acs.analchem.6b03764.
- [33] C. Iffelsberger, T. Raith, P. Vatsyayan, V. Vyskočil, F.-M. Matysik, Detection and imaging of reactive oxygen species associated with the electrochemical oxygen evolution by hydrodynamic scanning electrochemical microscopy, *Electrochim. Acta.* 281 (2018) 494–501. doi:10.1016/j.electacta.2018.05.115.
- [34] T. Raith, S. Wert, C. Iffelsberger, F.-M. Matysik, Development and characterization of electrochemical flow cells for hydrodynamic scanning electrochemical microscopy, *Monatshefte Für Chemie - Chem. Mon.* 149 (2018) 1671–1677. doi:10.1007/s00706-018-2201-3.
- [35] T. Raith, C. Iffelsberger, P. Vatsyayan, F.M. Matysik, Impacts of Forced Convection Generated via High Precision Stirring on Scanning Electrochemical Microscopy Experiments in Feedback Mode, *Electroanalysis.* 31 (2019) 273–281. doi:10.1002/elan.201800562.
- [36] C. Lee, C.J. Miller, A.J. Bard, Scanning Electrochemical Microscopy: Preparation of Submicrometer Electrodes, *Anal. Chem.* 63 (1991) 78–83. doi:10.1021/ac00001a016.
- [37] C.G. Zoski, Ultramicroelectrodes: Design, fabrication, and characterization, *Electroanalysis.* 14 (2002) 1041–1051. doi:10.1002/1521-4109(200208)14:15/16<1041::AID-ELAN1041>3.0.CO;2-8.
- [38] S. Bergner, P. Palatzky, J. Wegener, F.M. Matysik, High-resolution imaging of nanostructured Si/SiO₂ substrates and cell monolayers using scanning electrochemical microscopy, *Electroanalysis.* 23 (2011) 196–200. doi:10.1002/elan.201000446.
- [39] T. Wilhelm, G. Wittstock, Generation of periodic enzyme patterns by soft lithography and activity imaging by scanning electrochemical microscopy, *Langmuir.* 18 (2002) 9485–9493. doi:10.1021/la026107c.
- [40] J.S. Zhao, Z.Y. Yang, Y.H. Zhang, Z.Y. Yang, Immobilization of glucose oxidase on cellulose/cellulose acetate membrane and its detection by scanning electrochemical microscope (SECM), *Chinese Chem. Lett.* 15 (2004) 1361–1364. <http://www.ccsublishing.org.cn/article/id/b8603658-b0fb-41c0-abd0-c809b282e349?pageType=en>.

- [41] S. Kuss, C. Kuss, D. Trinh, S.B. Schougaard, J. Mauzeroll, Forced convection during scanning electrochemical microscopy imaging over living cells: Effect of topographies and kinetics on the microelectrode current, *Electrochim. Acta.* 110 (2013) 42–48. doi:10.1016/j.electacta.2013.03.149.
- [42] S. Kuss, D. Trinh, L. Danis, J. Mauzeroll, High-Speed Scanning Electrochemical Microscopy Method for Substrate Kinetic Determination: Method and Theory, *Anal. Chem.* 87 (2015) 8096–8101. doi:10.1021/acs.analchem.5b01268.
- [43] S. Kuss, D. Trinh, J. Mauzeroll, High-Speed Scanning Electrochemical Microscopy Method for Substrate Kinetic Determination: Application to Live Cell Imaging in Human Cancer, *Anal. Chem.* 87 (2015) 8102–8106. doi:10.1021/acs.analchem.5b01269.

5. Summary

Within this thesis, the new research field of scanning electrochemical microscopy in combination with forced convection, that was started by the Matysik group in 2017, was extended to various directions. Within the first main project, compared to an electrical high precision stirrer, that was originally used to generate forced convection, two electrochemical flow cells were developed to diversify the methodical approaches for the generation of forced convection. The effects of forced convection originating from a flowing mediator solution on SECM experiments were investigated utilizing chronoamperometric measurements and SECM imaging in hydrodynamic SG/TC mode. Moreover, the velocity profile within the semi-closed cell design was characterized calculating Comsol simulations. Constant convection was successfully established within both flow cells resulting in stable diffusion layers around macroscopic substrate electrodes. Hence, next to the electrical high precision stirrer setup, a second methodical approach was established enabling time-independent and reproducible measurements in the context of the amperometric SG/TC mode.

In the majority of cases, complementary to the SG/TC mode, the conventional feedback mode is applied to gain additional information about the surface of interest. For better comparison, these two modes have to be applied with experimental parameters as similar as possible meaning that if the newly established hydrodynamic SG/TC mode is applied, ideally also feedback mode images have to be recorded with forced convection applied to the system. Thus, the effects of forced convection originating from the electrical high precision stirrer on the amperometric feedback mode were examined within the second main project. Within this broadly arranged fundamental study, the crucial SECM parameters being UME dimensions, substrate-to-tip distance and probe scan rate were characterized regarding their interdependence with forced convection. Most importantly, it was found that forced convection has no negative impacts on imaging in feedback mode meaning that the hydrodynamic feedback mode can be applied for complementary imaging. Interestingly, the performance of the SECM measurements was even enhanced with forced convection for a certain combination of experimental parameters.

Within the third main project, the applicability of forced convection on biological systems was investigated. Different-sized enzyme spots and a structured enzyme surface were investigated utilizing PSCs and SECM imaging. Analogous to the amperometric SG/TC, stable diffusion layers of H_2O_2 produced during the enzyme reaction of glucose oxidase were established. An enzyme structure not visible without forced convection due to time-dependent changing diffusion layers was successfully resolved with forced convection applied to the system. Consequently, in contrast to rather complex techniques from literature, here, with forced

convection, a feasible approach was presented preventing a loss of resolution due to diffusive broadening and enabling time-independent SECM measurements of enzyme activity in the context of the G/C mode.

Within a side project, forced convection was applied to generate constant diffusion layers around a macroscopic BDD electrode. Hence, whereas other techniques only deliver information about the whole electrode surface, utilizing hydrodynamic SECM the electrode was characterized locally concerning reactive oxygen species formed during the electrochemical oxygen evolution. Imaging in hydrodynamic SG/TC revealed that different reactive oxygen species were generated at different areas of the BDD electrode. Within another side project, resolving contrast between two conducting materials, which is not possible in conventional feedback mode, was established utilizing the hydrogen evolution reaction to generate the mediator species. In a third side project, a new electrochemical flow cell configuration was established to improve measurements in the presence of air bubbles.

In summary, the field of forced convection in SECM was successfully expanded concerning new methodical developments, fundamental research and applications of the concept.

6. Zusammenfassung in deutscher Sprache

Im Rahmen dieser Arbeit wurde das im Jahr 2017 von der Matysik-Forschungsgruppe gestartete neue Feld der elektrochemischen Rasterelektronenmikroskopie in Kombination mit forcierter Konvektion um verschiedene Bereiche erweitert.

Im Vergleich zu einem elektrischen Hochpräzisionsrührer, der ursprünglich zur Erzeugung von forcierter Konvektion eingesetzt worden war, wurden innerhalb des ersten Hauptprojekts zwei elektrochemische Fließzellen entwickelt, um die methodischen Ansätze zur Erzeugung von forcierter Konvektion zu diversifizieren. Die Auswirkungen der aus einer fließenden Mediatorlösung resultierenden Konvektion auf SECM-Experimente wurden mit Hilfe von chronoamperometrischen Messungen und SECM-Bildaufnahmen im hydrodynamischen SG/TC-Modus untersucht. Weiterhin wurde das Geschwindigkeitsprofil innerhalb der halbgeschlossenen Zelle mit Hilfe von Comsol-Simulationen charakterisiert. Mit beiden Zelldesigns konnte erfolgreich konstante Konvektion erzeugt werden, die in stabile Diffusionsschichten an makroskopischen Substratelektroden resultierte. Somit wurde neben dem elektrischen Hochpräzisionsrührer ein zweiter methodischer Ansatz etabliert, welcher zeitunabhängige und reproduzierbare Messungen im Rahmen des amperometrischen SG/TC-Modus ermöglichte.

In den meisten Fällen wird ergänzend zum SG/TC-Modus der konventionelle Feedback Modus eingesetzt, um Komplementärinformationen über die zu untersuchende Oberfläche zu generieren. Für eine bessere Vergleichbarkeit müssen beide Modi mit möglichst identischen experimentellen Parametern angewendet werden. Werden somit SECM-Aufnahmen im neu eingeführten hydrodynamischen SG/TC-Modus aufgezeichnet, so müssen idealerweise auch die Aufnahmen im Feedback Modus unter Bedingungen der forcierter Konvektion durchgeführt werden. Um die Anwendbarkeit des hydrodynamischen Feedback Modus zu überprüfen, wurden innerhalb des zweiten Hauptprojekts die Auswirkungen der durch den elektrischen Hochpräzisionsrührer erzeugten forcierter Konvektion auf den amperometrischen Feedback Modus untersucht. Im Rahmen dieser Grundlagenstudie wurden mit den Dimensionen der UME, dem Substrat zu Spitze Abstand und der Scan Geschwindigkeit die wichtigsten SECM Parameter hinsichtlich ihrer Wechselwirkung mit forcierter Konvektion charakterisiert. Da keine negativen Auswirkungen der Konvektion auf die Bildgebung im Feedback Modus beobachtet wurden, kann der hydrodynamische Feedback Modus in Zukunft für komplementäre Bildgebung eingesetzt werden. Interessanterweise wurde zusätzlich die Performance der SECM-Messungen durch forcierter Konvektion für eine bestimmte Kombination experimenteller Parameter verbessert.

Im dritten Hauptprojekt wurde die Anwendbarkeit von forcierter Konvektion auf biologische Systeme untersucht. Unter Verwendung von PSCs und SECM-Bildaufnahmen

wurden unterschiedlich große Enzym-Spots und eine strukturierte Enzymoberfläche charakterisiert. Analog zum amperometrischen SG/TC Modus wurden stabile Diffusionsschichten von Wasserstoffperoxid erzeugt, welches während der Enzymreaktion von Glucoseoxidase entstand. Eine Enzymstruktur, die ohne forcierte Konvektion auf Grund zeitabhängig wachsender Diffusionsschichten nicht sichtbar war, wurde unter Bedingungen der forcierten Konvektion erfolgreich abgebildet. Im Gegensatz zu eher komplexen Techniken aus der Literatur wurde somit durch das Einbringen von forcierter Konvektion ein praktikabler Ansatz präsentiert, um einen Auflösungsverlust auf Grund diffuser Verbreiterung zu verhindern und zeitunabhängige SECM-Messungen der Enzymaktivität im Kontext des G/C-Modus zu ermöglichen.

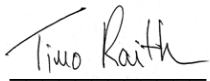
In einem Nebenprojekt wurden konstante Diffusionsschichten an einer makroskopischen BDD-Elektrode mit Hilfe von forcierter Konvektion erzeugt. Während herkömmliche Techniken lediglich Informationen über die gesamte Elektrodenoberfläche liefern, wurde diese unter Verwendung des hydrodynamischen SECM lokal in Bezug auf während der elektrochemischen Sauerstoffentwicklung entstehende reaktive Sauerstoffspezies charakterisiert. Bildaufnahmen im hydrodynamischen SG/TC zeigten die Entwicklung unterschiedlicher reaktiver Sauerstoffspezies an verschiedenen Stellen der BDD-Elektrode. In einem weiteren Nebenprojekt wurde ein im konventionellen Feedback Modus nicht auflösbarer Materialkontrast zwischen zwei leitenden Materialien unter Verwendung von in situ erzeugtem Wasserstoff als Mediatorspezies generiert. In einem dritten Nebenprojekt wurde eine elektrochemische Fließzelle neu konfiguriert, um die amperometrische Detektion in Gegenwart von Luftblasen zu verbessern.

Zusammenfassend wurde das noch junge Feld der forcierter Konvektion innerhalb der elektrochemischen Rasterelektronenmikroskopie hinsichtlich neuer methodischer Entwicklungen, Grundlagenforschung und Anwendung des Konzepts erfolgreich erweitert und somit entscheidend vorangebracht.

Erklärung

Ich habe die vorliegende Arbeit selbstständig verfasst, keine anderen als die angegebenen Quellen und Hilfsmittel benutzt und bisher keiner anderen Prüfungsbehörde vorgelegt. Von den in §27 Abs. 5 vorgesehenen Rechtsfolgen habe ich Kenntnis genommen.

Regensburg, den 29.06.2020

Handwritten signature of Timo Raith in black ink, written in a cursive style.

Timo Raith
Timo Raith